



SCATTERING FROM FINITE BY INFINITE
PERIODIC ARRAYS WITH ARBITRARY
PIECEWISE-LINEAR SLOT ELEMENTS

DISSERTATION

Paul R. Barré, Captain, USAF

AFIT/DSG/ENG/95S-01

DEPARTMENT OF THE AIR FORCE
AIR UNIVERSITY

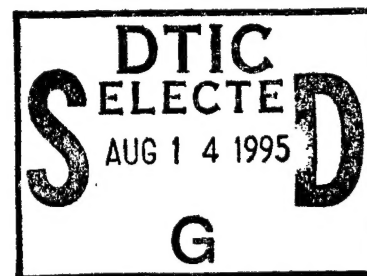
AIR FORCE INSTITUTE OF TECHNOLOGY

Wright-Patterson Air Force Base, Ohio

DTIC QUALITY INSPECTED 8

19950811 052

AFIT/DSG/ENG/95S-01



SCATTERING FROM FINITE BY INFINITE
PERIODIC ARRAYS WITH ARBITRARY
PIECEWISE-LINEAR SLOT ELEMENTS

DISSERTATION

Paul R. Barré, Captain, USAF

AFIT/DSG/ENG/95S-01

Approved for public release; distribution unlimited

SCATTERING FROM FINITE BY INFINITE PERIODIC ARRAYS WITH
ARBITRARY PIECEWISE-LINEAR SLOT ELEMENTS

DISSERTATION

Presented to the Faculty of the Graduate School of Engineering
of the Air Force Institute of Technology

Air University

In Partial Fulfillment of the
Requirements for the Degree of
Doctor of Philosophy

Paul R. Barré, B.S.E.E., M.S.E.E.
Captain, USAF

JUNE, 1995

Accession For	
NTIS CRA&I	<input checked="checked" type="checkbox"/>
DTIC TAB	<input type="checkbox"/>
Unannounced	<input type="checkbox"/>
Justification _____	
By _____	
Distribution /	
Availability Codes	
Dist	Avail and/or Special
A-1	

Approved for public release; distribution unlimited

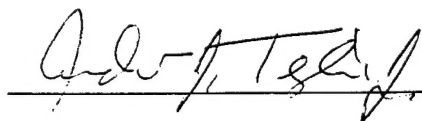
SCATTERING FROM FINITE BY INFINITE
PERIODIC ARRAYS WITH ARBITRARY
PIECEWISE-LINEAR SLOT ELEMENTS

Approved:



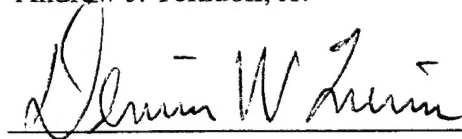
27 JUN 95

Paul Skinner



27 JUN 95

Andrew J. Terzuoli, Jr.



27 JUN 95

Dennis W. Quinn

Accepted:



Robert A. Calico, Jr.
Dean, School of Engineering

Acknowledgements

I wish to extend my sincerest gratitude to one of AFIT's best, Major Paul Skinner, my advisor, for his guidance and support throughout this effort, and for the shining standard that his work ethic has set for me. I also appreciate the helpful advice given by the rest of my committee, Drs Dennis Quinn and Andrew Terzuoli. The support of these three men was invaluable in helping me to accomplish this work.

A "thank you" is also given to Mr Edwin Utt and company at the Wright Lab Multi Spectral Measurement Facility for measuring the backscatter from the FSS samples, and to Dr Errol English and crew at the Mission Research Corporation of Dayton for fabricating the samples.

Special thanks is given to my family and friends for their unending encouragement, and for their patience and understanding during this challenging time in my life.

Paul R. Barré

Table of Contents

	Page
I. Introduction	1-1
II. Analytical Methodology	2-1
Formulation of the Governing Integral Equations	2-2
General Moment Method Solution	2-10
III. Plane Wave Excitation	3-1
IV. Mutual and Self Admittance for Aperture Elements	4-1
Mathematical Representation of Infinite Slot Columns	4-3
Mathematical Representation of Infinite Slot Columns	4-3
Mathematical Representation of Infinite Slot Columns	4-3
Groundplane Shielding and One Sided Admittances	4-5
Filling the Admittance Matrix	4-6
Extension to Infinite Columns	4-6
Periodic Moment Method	4-7
Basis Functions:	4-7
Entire Domain Basis Functions:	4-8
Array Scanning Method	4-14
Validation of Admittance Calculations	4-23
V. Far Zone Scattered Fields	5-1
VI. Results	6-1
VII. Conclusions	7-1
Appendices:	
A. User's Guide	
The FIFEE Input Language	A-1
Introduction	A-1
Syntax	A-2
Symbolic Names	A-2
Data Types	A-3
Constants	A-3
Complex Numbers	A-4
Variables	A-4
Arithmetic Expressions	A-5

Commands	A-6
An Example	A-46
B. Pattern Factors	
Introduction.....	B-1
Piecewise Sinusoidal	B-4
Piecewise Cosinusoidal	B-5
Composite Pattern Factors	B-6
Bibliography	BIB-1

List of Figures

Figure	Page
1.1 Finite by Infinite Frequency Selective Surface with Six Columns of Piecewise-Linear Slot Elements.....	1-7
1.2 Two Slot Arrays Embedded in a Stratified Dielectric Medium Forming a Frequency Selective Surface.....	1-8
2.1 Two Doubly Infinite Groundplanes in Free Space with Arbitrarily Oriented Thin Slots Cut into Them.....	2-3
2.2 Equivalent Scattering Geometry. The M vectors are in the plus or minus	2-6
2.3 A surface S defined by homogenous regions I and II.	2-7
3.1 Slot Mode Excited by External Plane Wave in Region I.....	3-2
3.2 Propagation Direction for an Incident Plane Wave.	3-6
3.3 Stratified Dielectric Medium Bounded by Two Freespace Halfspaces	3-12
3.4 Slotted Groundplane Coated with 2 Slabs, Slots Centered at Origin	3-15
3.5 Slotted Groundplane Coated with 2 Slabs, Slots Centered at $(x,z)=(.28,0)$	3-16
3.6 Excitation Current for Tripole (H-pol).....	3-17
3.7 Excitation Current for Tripole (V-pol).....	3-18
4.1 Equivalent Configuration for Three Slot Arrays: Infinite Columns of Slot Elements are Represented by User Defined Periodic Modes.....	4-3
4.2 Infinite Groundplane with Periodic Slot Elements: Cell structure displayed for illustration of Floquet's Theorem.....	4-11
4.3 General Geometry for Coupling Between Slot Modes in a Stratified Dielectric Medium.....	4-19
4.4 Vertical Slot Geometry: Slot Length=0.67 cm, Slot Width=0.067 cm, $D_x=0.675$ cm, $D_z=1.125$ cm, Frequency=10 GHz	4-25

4.5 Infinite Columns of Vertical Slots: Comparing Real Components of FIFEE, KAHUNA, and PMM Using Geometry in Figure 4.4	4-26
4.6 Infinite Columns of Vertical Slots: Comparing Imaginary Components of FIFEE, KAHUNA, and PMM Using Geometry in Figure 4.4.	4-26
4.7 100 Infinite Columns of Vertical Slots: Comparing Real Components of FIFEE, KAHUNA, and PMM Using Geometry in Figure 4.4.	4-28
4.8 100 Infinite Columns of Vertical Slots: Comparing Imaginary Components of FIFEE, KAHUNA, and PMM Using Geometry in Figure 4.4.	4-29
4.9 Horizontal Slot Geometry: Slot Length=0.75 cm, Slot Width=0.075 cm, Dx=1.125 cm, Dz=0.675 cm, Frequency=10 GHz.	4-30
4.10 Infinite Columns of Horizontal Linear Slots: Comparing FIFEE and PMM Using Geometry in Figure 4.9.	4-30
4.11 Infinite Columns of Slots Rotated 45 Degrees from Horizontal: A Comparison Between FIFEE and PMM Using Geometry of Figure 4.9.	4-31
4.12 Infinite Columns of Linear Slots Rotated 45 Degrees from Horizontal. No Slabs, Two Infinite Halfspaces. Slot Elements According to Figure 4.9.	4-32
4.13 Infinite Columns of Bent Slots: Comparing FIFEE and PMM.	4-33
4.14 100 Infinite Columns of Bent Slots: Comparing FIFEE and PMM.	4-34
5.1 Regions of Interest Defined.	5-2
5.2 Cone of Bistatic Scatter Directions: Dashed lines are forward scatter directions; Solid lines are backscatter directions.	5-4
5.3 Geometry Used in Accounting for the Phase Shift of the Field at the Observation Point.	5-7
5.4 Scattered Fields Radiated by Two Periodic Slot Modes (Trislot): Asymptotic Solution vs Rigorous Solution.	5-11
6.1 Top View of the Radome - 21 columns of Slots on Each Infinite Groundplane with Infinite Dielectrics: Asterisks Designate Each Column of Periodic Slots, Slot Length=0.75 cm, Slot Width=0.075 cm, Dx=0.675 cm, Dz=1.125 cm.	6-2
6.2 Comparison Between FIFEE and KAHUNA: Geometry of 9 Dielectric Slabs and 2 Arrays, with 21 Columns on Each Array.	6-4

6.3 Comparison Between FIFEE, KAHUNA, and Measured Data for FSS #1: No Dielectric Slabs, 16 Columns, Slot Length=1.524cm, Slot Width=0.2286cm, Dx=1.6256cm, Dz=1.778cm, Skewed Grid.....	6-7
6.4 Comparison Between FIFEE and Measured Data for FSS #1.....	6-8
6.5 Illustration of Slot Treatments with Resistive Materials.	6-10
6.6 FSS #2 Configuration.	6-11
6.7 Illustration of Fabrication Anomaly in FSS #2.....	6-14
6.8 Comparison Between FIFEE and Measured Data for FSS #2 at 6 GHz, H-pol: Geometry of 3 Dielectric Slabs, and 1 Array with 49 Slot Columns, Slot Length=0.4cm, Slot Width=0.05cm, Dx=0.52cm, Dz=0.6cm, Skewed Grid.....	6-15
6.9 Comparison Between FIFEE and Measured Data for FSS #2 - 6GHz, Vertical Polarization.	6-16
6.10 Comparison Between FIFEE and Measured Data for FSS #2 - 8 GHz, Horizontal Polarization.	6-17
6.11 Comparison Between FIFEE and Measured Data for FSS #2 at 8GHz, Vertical Polarization.	6-18
A.12 The Spherical Coordinate System Used by FIFEE.....	A-12
A.13 An Example of a Stratified Dielectric Medium.	A-18
A.14 A Loop Composed of 11 Segments and 11 Nodes.	A-20
A.15 Coordinate Transformations in Absolute Coordinates.....	A-28
A.16 Coordinate Transformations in Relative Coordinates. Note: node 20 is defined relative to node 10 and thus node 10 is the center of rotation for node 20.	A-28
A.17 The Grid Structure used by FIFEE.	A-38
A.18 Reference Elements for the Arrays in the FIFEE Example.	A-46
B.1 An Arbitrary Piecewise Linear Current Mode That Contains m Sub Elements on Leg 1 and k Sub Elements on Leg 2	B-2
B.2 Graphical Definitions of the Polarizing Vectors and	B-7

Abstract

A numerical model for analyzing electromagnetic scattering from a planar Frequency Selective Surface (FSS) is developed. The model can represent an FSS with multiple arrays of arbitrary piecewise linear scatterers in a stratified dielectric medium. The FSS's arrays are finite by infinite, accounting for edge effects, where a periodic array element is formed from the piecewise linear connection of thin slots in a groundplane. The stratified dielectric medium is defined as an arbitrary stack of lossless dielectric slabs that sandwich the user defined arrays, simulating an FSS.

The Surface Equivalence theorem is used to construct an equivalent problem based on groundplanes and magnetic current sources. Integral equations based on the equivalent magnetic scattering currents are solved via the moment method. These unknown currents are expanded such that independent modes are defined for each infinite column of an array, where the current fluctuations along each column are defined in terms of a reference element and Floquet's theorem. Individual column contributions are determined using the Array Scanning Method, preserving the plane wave form of the solution. The model has been implemented in a user-friendly computer program, and admittance calculations and scattering predictions have been validated against measured data and appropriately similar FSS codes.

SCATTERING FROM FINITE BY INFINITE PERIODIC ARRAYS WITH ARBITRARY PIECEWISE-LINEAR SLOT ELEMENTS

I. INTRODUCTION

This work concerns itself with electromagnetic scattering from a planar "finite by infinite" frequency selective surface (FSS) due to an incident plane wave. The problem of scattering from such an FSS with arbitrary piecewise-linear slot elements has been solved, and a detailed analysis of the solution is presented in the pages that follow. By having one dimension finite, multiple interactions between the parallel infinite edges can be accounted for. Predicting the effects of such edge terminations is important in any practical design. By addressing piecewise-linear slots of arbitrary shape, the analysis becomes applicable to surfaces with multi-polarization capability. What makes this work unique is that both of these attributes, finite by infinite *and* arbitrary piecewise-linear slot geometries, are part of the problem statement.

The remainder of this chapter will present FSS background material, will highlight past work in the field, and will then give an overview of the work accomplished in this effort. A geometrical description of the problem is also given, including graphical depictions.

An FSS is also referred to as a periodic surface because it is comprised of at least one array of periodically spaced scattering elements. The periodic spacing and the geometric shape of the scattering elements, as well as the number of component arrays, are critical design parameters that control the transmission and reflection characteristics of the surface. These characteristics can be made to vary significantly in relation to the frequency of incident electromagnetic energy. The surrounding media also plays an

important role in defining the surface; the type and thickness of the dielectric slabs sandwiching an array can enhance the array's bandwidth stability for varying incident angles of excitation (1). That is, an FSS with proper dielectric design can provide "frequency filtering" characteristics that are scan independent.

FSS design is an active topic in the antenna and radome world because of this practical ability of the surfaces to filter frequencies. An FSS might be employed as a tuned reflector in a dual frequency antenna, or as a bandpass radome in front of a radar antenna, with applications in such things as aircraft and satellites. For example, the filtering characteristics of an FSS can make it an ideal radome for the antenna of a military aircraft. Such a surface can let signals enter at an antenna's frequency of operation, and remain impenetrable to energy at all other frequencies, thereby making the antenna immune to broad band jamming. An FSS can also be used as a dual-passband dichroic plate in a microwave communications system, e.g., allowing two X-band frequencies to pass while reflecting S-band frequencies. With such uses in high priced systems, it is easy to see why this is such an active research topic. What may not be so intuitive is how an FSS relates to the concept of a filter.

Typically, there are two types of periodic arrays that can comprise an FSS. The first is based on periodically spaced holes cut into a conducting surface, forming an array of aperture (slot) elements. This type is used as a radome. The second type, a dielectric surface embedded periodically with conducting elements such as wires or metal patches, is used as a reflector. Near the resonant frequencies of the array elements, a slot array becomes totally transmissive as if the array were not there, while an array of metallic elements becomes totally reflective, behaving like a solid sheet of metal. Thus, an FSS can be considered as a "space filter"; a slot array corresponds to a bandpass filter, and a wire array corresponds to a bandstop filter (2). And analogous to filter theory, an FSS must have multiple arrays (stages) to obtain a flat response in the pass band or to obtain

rapid attenuation in the stop band. The first type of FSS, the one based on slot arrays, is addressed in this effort, thus allowing bandpass elements to be modeled.

One method used by past scientists to analyze such a slot array first assumed that the groundplane into which the slots were cut was very thin, so as to remove this dimension from the self admittance calculations. Then, the number of rows and columns of a particular element were assumed to be infinite, so that each array was infinitely periodic in two orthogonal directions. Next, the incident wave was assumed to be from the far field (a perfect plane wave), and since the elements were periodic in two directions, the magnitude of the currents on all elements were taken to be identical via Floquet's theorem (3). Only the phase of the currents on the elements differed, and these varied linearly along the two orthogonal directions. Each array in the problem was addressed as a doubly infinite sum of the radiation from the array elements. This approach, however, proved to be computationally expensive. It yielded a double infinite sum of spherical waves which typically converged slowly, and if dielectric slabs were present, the infinite sums of spherical waves hitting their boundaries proved even more cumbersome. Thus, the process of determining the electrical properties of an FSS with multiple arrays embedded in dielectric slabs is difficult to handle in this manner.

In the late 1970's, Munk and associates at the Ohio State University undertook an effort to perform these calculations more efficiently, hoping to improve their radome design capabilities. Their work resulted in the development of a general theory for frequency selective surfaces (4). The highlight of this theory is an approach called the *plane wave expansion method*, which is based on Poisson's Sum Formula. This formula, which relates infinite sums of Fourier transform pairs, is used to transform a doubly infinite sum of spherical waves to a generally faster converging doubly infinite sum of plane waves (plane wave convergence is faster except for observation points extremely close to an array element). Application of this general theory reduces computation time

considerably, more easily accounts for the effects of dielectric layers, and handles thin wire or thin slot array elements of almost arbitrary shape. The major assumptions of this theory are the same as the assumptions made earlier, namely those required by Floquet's theorem. That is, current amplitudes on array elements must be identical and the phase progression from element to element must be linear, corresponding to an infinite incident plane wave or a phased array beaming energy in a certain direction.

In the early 1980's, Henderson applied Munk's theory and developed the Periodic Moment Method (implemented in a computer code named PMM) (2)(22). PMM uses the *method of moments* (5) to apply basis and testing functions to a single reference element, and then, using the known periodicity of the array, applies Floquet's theorem to determine the currents on the rest of the array's elements. This theory, and the accompanying computer model, can analyze multiple infinite arrays of arbitrarily shaped scatterers (piecewise linear) in a stratified dielectric medium. The scatterers can be bent wires in a plane supporting electric currents and/or slots in a conducting plane supporting magnetic currents. The dielectric slabs can be modeled with or without loss. PMM predictions of plane wave transmissions and reflections are very accurate when compared to measured data from an FSS whose arrays have large numbers of rows and columns. But as the number of elements in the composite arrays decrease, FSS edge termination effects become more pronounced; and these effects are ignored by PMM because of the infinite assumptions on array size. Further, measured data from radiating finite phased arrays have shown that sidelobe levels can change dramatically due to edge termination effects. Thus, PMM can only be used as a first order design tool for the fabrication of a radome panel to be mounted in a metallic body, because the code cannot account for the impedance transition between the FSS and the surrounding surface (6:1). If such design work is to be done without having to physically construct and measure an FSS in a trial and error manner, then a design tool must be developed which can predict these edge

effects. However, to fully account for all of the scattering mechanisms of a finite by finite FSS is impractical. Even with the computing power available in today's workstations, such encompassing calculations are too time consuming and too computationally expensive .

Skinner worked out a compromise by implementing a solution (in a computer code called KAHUNA) that provided a mechanism to characterize the scattering from a truncated FSS in a principle plane. He modeled the arrays as being finite in one dimension and infinite in the other, thereby accounting for multiple edge interactions between the parallel infinite edges. This geometry maintains the computational advantage of Floquet's theorem in the infinite dimension, while the edge effects are computed via the moment method in the finite dimension, thereby obtaining solutions much faster than a more direct approach in two finite dimensions. Also, whereas the doubly infinite approach outputs results in the form of plane wave reflection and transmission statistics, the finite by infinite approach can yield scattered field patterns and radar echo widths.

In 1992, Peppler(7) undertook a study to experimentally verify Skinner's implementation, and showed good agreement between the analytical predictions and the measured data. However, there were some significant deviations between the analytical data and the experimental data at higher frequencies. Peppler attributed the differences to elevation grating lobes, which were modeled by Skinner's code, but which would not be measured by the echo chamber's receiving horn due to its finite height. Overall, though, the *main* limitation of Skinner's implementation is that it cannot model surfaces with multi-polarization capability; his model requires all slots to be linear and oriented in the direction of the infinite axis (which is always taken as \hat{z}).

This research overcomes the limitation of Skinner's implementation by including arbitrary piecewise-linear slot elements in the analysis. Skinner's finite by infinite

approach is generalized so that, instead of being limited to z -directed slot elements, two dimensional piecewise-linear slot elements can be modeled. Thus, this implementation can be used as a design tool for an FSS with multi-polarization capability, and allows for the possibility of designing a surface with more than one passband. Also, because slot orientations can take advantage of two dimensions, edge effects can be found in one principal plane, then by rotating the slot elements ninety degrees, edge effects can be found in the other principal plane. For example, to account for the edge effects of an FSS with z -directed slots, run the model for the desired number of columns and request the H-pol scattered field pattern. Then, maintaining the array spacing, define the same slots, but in the x -direction, so that the new configuration can be thought of as the old one rotated 90 degrees. Now request the V-pol scattered field pattern. In this manner, the finite edge effects from all four edges are taken into account.

As part of this effort, a computer model was also developed. Specifically, it can analyze multiple planar arrays of slot scatterers in a stratified dielectric medium, where the arrays are finite by infinite in dimension, where the scatterer's geometrical structure is arbitrary but piecewise linear, and where the dielectric slabs are infinite, homogeneous, and lossless. Figuratively, the scattering elements are formed from thin slots cut into an infinitely thin groundplane, cut in such a way that an overall element shape is formed by the piecewise linear connection of thin slots (see Figure 1.1). The groundplanes extend to infinity past the outer columns of slots. The lossless slabs, together with free space, sandwich the arrays and thereby simulate a frequency selective surface (see Figure 1.2). The model features a user-friendly input language that is based on PMM's input parser. The parser includes built in functions and error messages. It also provides the user with multiple run-time control features, which includes control of the output file format and control of the accuracy desired in the convergence of the infinite sums. Further, element

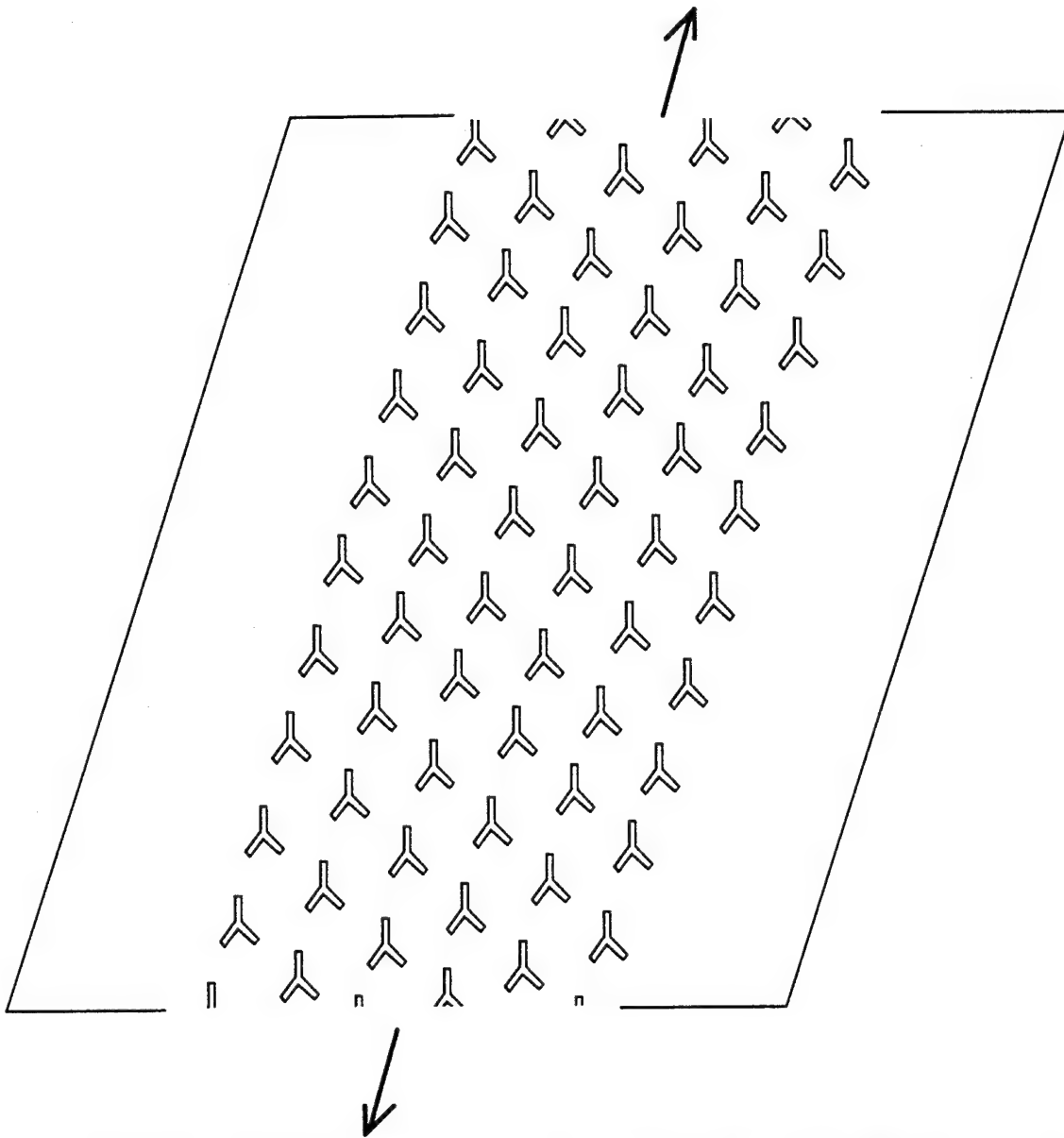


Figure 1 .1 Finite by Infinite Frequency Selective Surface with Six Columns of Piecewise-Linear Slot Elements

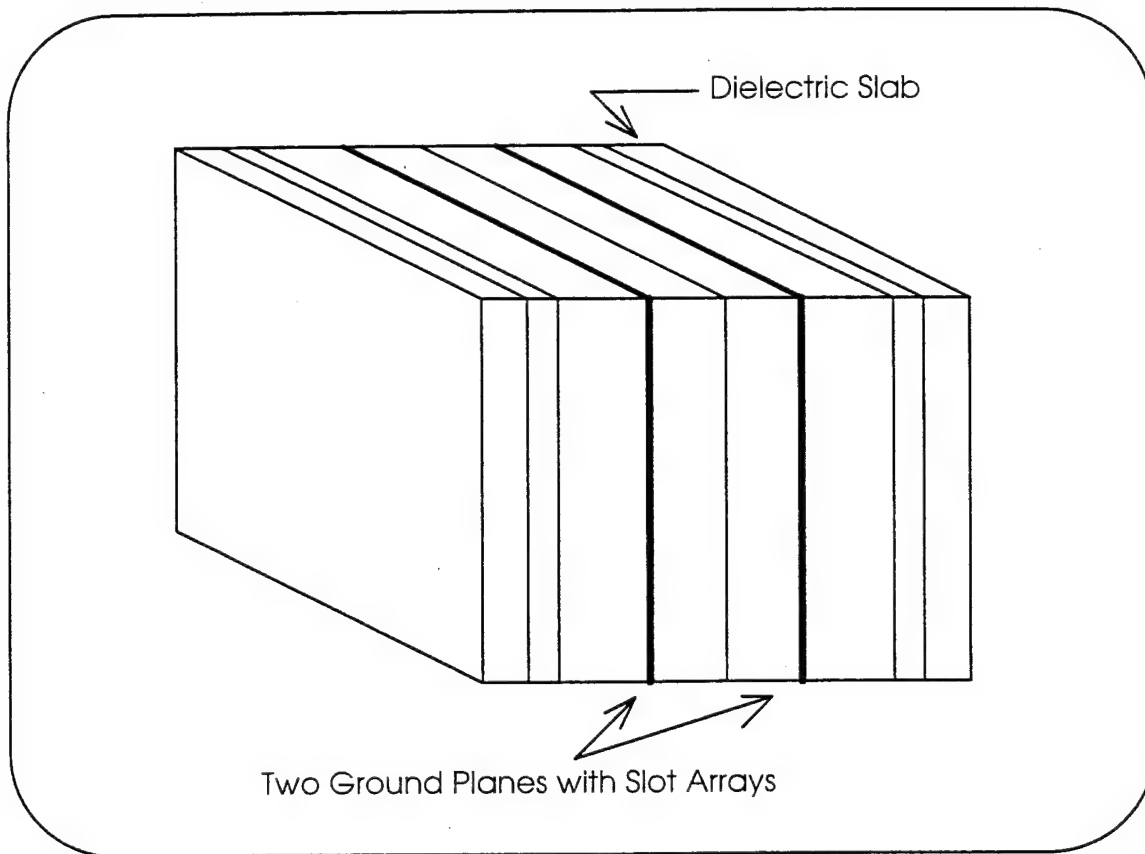


Figure 1.2 Two Slot Arrays Embedded in a Stratified Dielectric Medium Forming a Frequency Selective Surface

shapes can differ between the finite number of columns that comprise an array, and individual columns can be resistively loaded.

In the chapters to follow, the moment method solution to the problem described above is developed. In the next chapter, the overall solution to the problem is developed using two slotted ground planes, and is then stated in matrix (vector) form. Chapter III presents the derivation of the excitation vector entries. Chapter IV extends the analysis of Chapter II to a finite number of infinite columns, and then provides a derivation for the coupling between columns, which is used to form the admittance matrix. The matrix problem is then solved using a "canned" algorithm, yielding the unknown scattering currents. Chapter V derives the far zone fields from the now known scattering currents. Finally, Chapter VI presents numerical results of the complete moment method solution, and compares this to measured data, while Chapter VII summarizes and concludes.

II. ANALYTICAL METHODOLOGY

In this chapter, the general moment method procedure is developed, while the specifics of the solution are described in the remainder of the dissertation. The analysis approach taken is to form integral equations based on equivalent scattering currents for the slots in the groundplanes, and to then solve for these unknown currents using the moment method.

Four major assumptions are made that make the basic problem more tractable, yet detract minimally from the applicability of the analysis. These are: 1. The excitation source is an external plane wave. 2. The array elements are thin slots, where a slot's length is at least about ten times greater than its width. 3. The metal holding the slots has no curvature (all array elements lie in a plane) and the thickness of the metal is negligible. 4. Overlapping piecewise cosinusoidal or sinusoidal basis functions (reference Appendix B) can be used to accurately model the equivalent (filamentary) scattering current induced on a thin slot. The purpose of these assumptions will be explained as they are used in the development of the analytical methodology that follows.

The general solution approach of this dissertation is to use the moment method to capture the characteristics of an FSS's finite dimension, and to use infinite array theory to completely characterize the FSS's other dimension. The approach is described more specifically as follows: First, the governing equations are developed using the surface equivalence theorem (9) on the slots, resulting in integral equations where the unknowns are the slots' equivalent magnetic scattering currents. Next, the *array scanning method* (8) is used in conjunction with the moment method to determine the characteristics of each infinite column of unknown scattering currents. Once the scattering currents are

determined, backward and forward scattered fields are found by asymptotically evaluating the far-zone radiation integrals. This chapter focuses on the basic analytical methodology represented in the first two steps above, namely, defining the equivalent problem and the associated integral equations in the form of a moment method solution. Finding the scattered fields from these currents is addressed in a separate chapter.

Formulation of the Governing Integral Equations.

Figure 2.1 depicts two parallel groundplanes, each with an arbitrarily oriented slot element cut into it. Without loss of generality, this figure is used to develop the governing integral equations used for FSS analysis in this work, where generally each FSS consists of multiple arrays, and each array has a finite number of infinite columns of slot elements. (Only two groundplanes are used in this example to illustrate the theoretical methods - but the methods can be extended to an arbitrary number of slotted planes in a sandwich.) That there is no loss of generality will become apparent when the equations resulting from Figure 2.1 are extended to a more comprehensive configuration in Chapter 4. But for now, the basic problem formulation is presented.

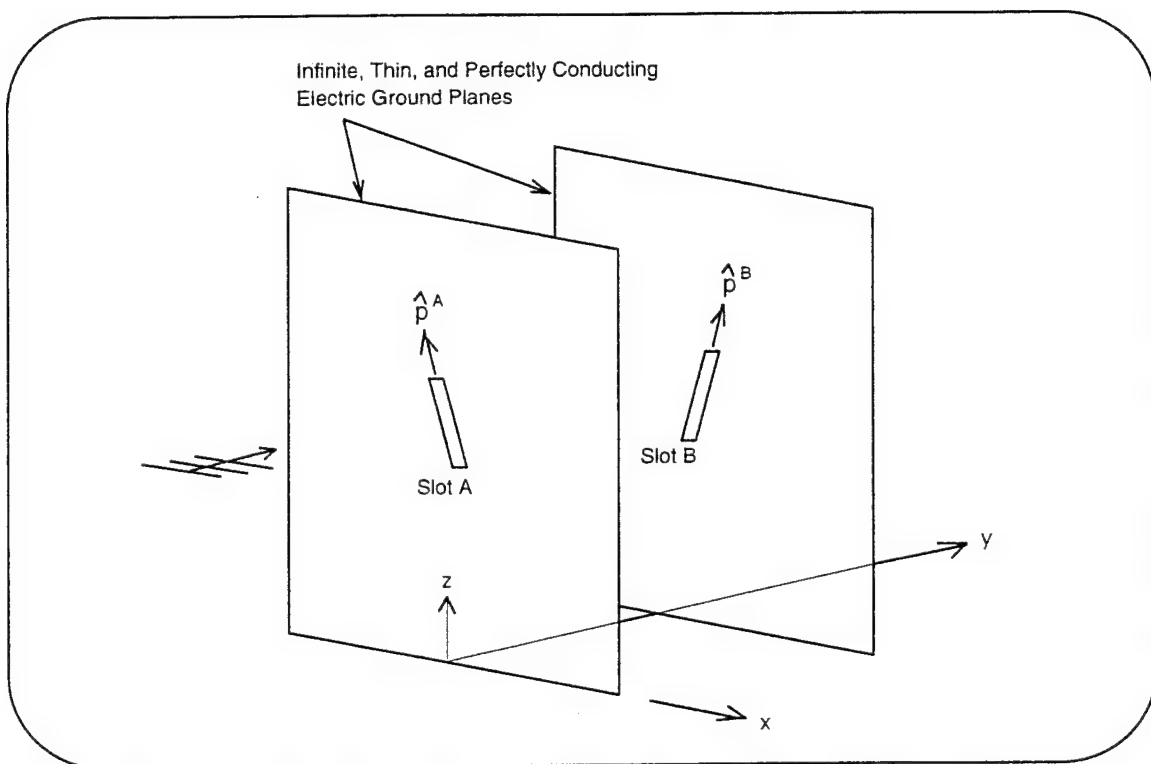


Figure 2.1 Two Doubly Infinite Groundplanes in Free Space with Arbitrarily Oriented Thin Slots Cut into Them

As mentioned in this chapter's introductory paragraph, the surface equivalence theorem is used to fill each array's slot with PEC (perfect electric conductor) material. The scattering sources on the surface of the groundplane due to application of the surface equivalence theorem can be represented by the following equations:

$$\bar{\mathbf{J}}_s^{eq} = \hat{\mathbf{n}} \times \bar{\mathbf{H}}_{orig}|_s \quad (2-1)$$

$$\bar{\mathbf{M}}_s^{eq} = -\hat{\mathbf{n}} \times \bar{\mathbf{E}}_{orig}|_s \quad (2-2)$$

where the "orig" subscript refers to the fields in the original problem, and the "eq" superscript refers to the impressed sources in the equivalent problem. The subscript "s" refers to the closed surface upon which equivalence is based, and " $|_s$ " indicates that the field is evaluated on this surface, S. There is an S for each slot, and each one is defined by the thickness of the PEC plane containing the slot and the two dimensional shape of the slot itself. The theorem requires the volume inside of this surface to be replaced with the same PEC material that formed the conducting plane in the original problem. This action results in a solid (but thin) plane of PEC material, a "groundplane", in the equivalent problem. The closed surfaces are then covered by magnetic currents, which are non-physical mathematical tools used to construct the equivalent problem. These magnetic currents are the scattering sources in the equivalent problem. It is important to remember that equivalent currents must be treated as impressed (source) currents, not as induced currents. Since an impressed electric current on a PEC surface will not radiate, it has no effect, and so there are no equivalent electric current sources to consider ($\bar{\mathbf{J}}_s^{eq} = 0$). Further, no tangential electric fields can exist on the PEC of the original problem. Therefore, by Equation (2-2), there are no equivalent currents existing on those parts of the surface defined by the thickness of the plane in the original geometry. Thus, the only equivalent scattering sources resulting from the application of the theorem are magnetic surface currents that lie infinitesimally close to the (now solid) groundplane,

and lie over the former aperture regions. Summing up, the equivalent problem can be viewed as a conducting plane with magnetic scattering currents on both sides of its surface at the former slot locations.

Figure 2.2 depicts the equivalent scattering geometry with respect to Figure 2.1, although for the sake of illustration, the currents are shown a finite distance away from the groundplanes. The magnetic surface currents are depicted on both sides of the respective groundplane with opposite orientations because the outward normal on one side is in the opposite direction of that on the other (as will be seen in Equations (2-11) and (2-12)). The unit vector \hat{n} represents the outward normal direction for an equivalent surface, the particular surface being denoted by a subscript on \hat{n} . In general, the superscripts on the currents refer to the scattering object, while the subscripts denote the region of space in which the currents are applicable.

Now that the more tractable equivalent problem has been defined, boundary conditions must be applied in order to form the desired integral equations. Four boundary conditions that can be derived from Maxwell's equations follow:

$$\hat{n} \times (\bar{H}_1 - \bar{H}_2) = \bar{J}_s \quad (2-3)$$

$$-\hat{n} \times (\bar{E}_1 - \bar{E}_2) = \bar{M}_s \quad (2-4)$$

$$\hat{n} \cdot (\bar{B}_1 - \bar{B}_2) = m_s \quad (2-5)$$

$$\hat{n} \cdot (\bar{D}_1 - \bar{D}_2) = \rho_s \quad (2-6)$$

where ρ_s and m_s represent the electric and magnetic surface charges on S, respectively. As shown in Figure 2.2, \hat{n} in the above equations is a unit vector normal to S and is directed toward region I, while \bar{J}_s and \bar{M}_s are the electric and magnetic surface currents on S, respectively.

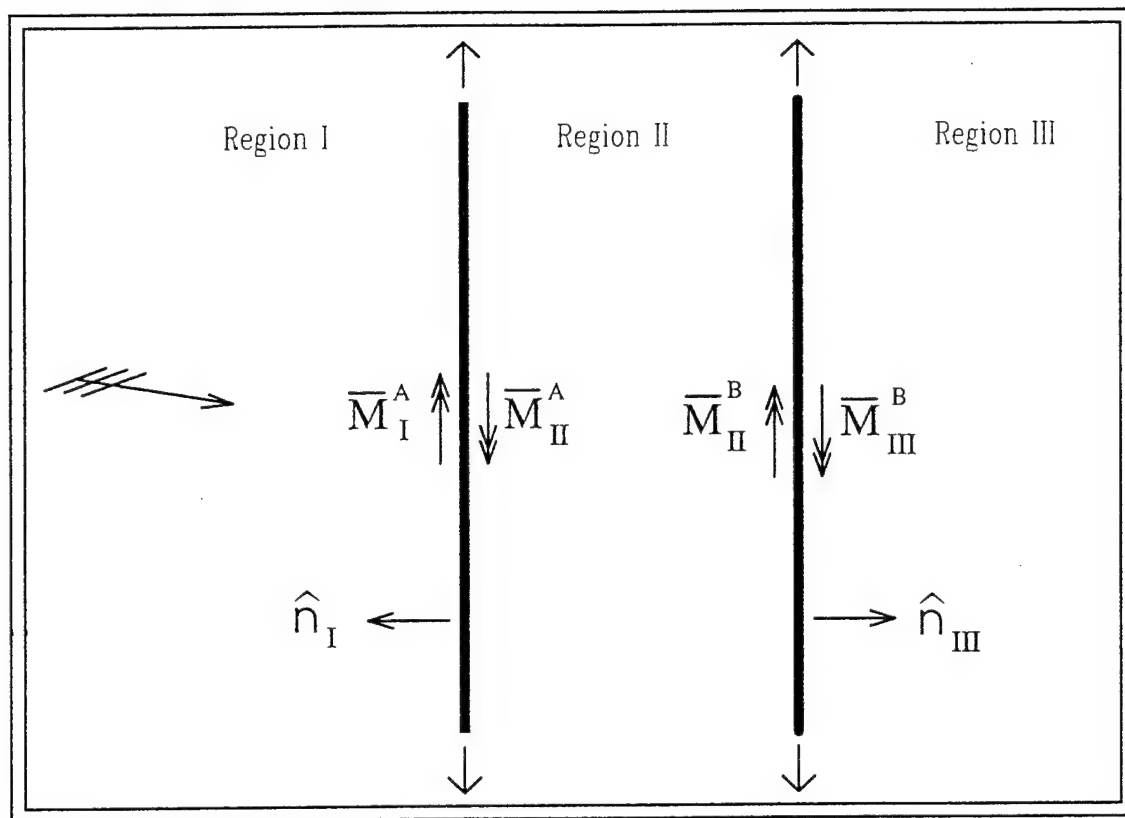


Figure 2.2 Equivalent Scattering Geometry. The \vec{M} vectors are in the plus or minus "p" directions for slots A and B respectively. All regions are free space.

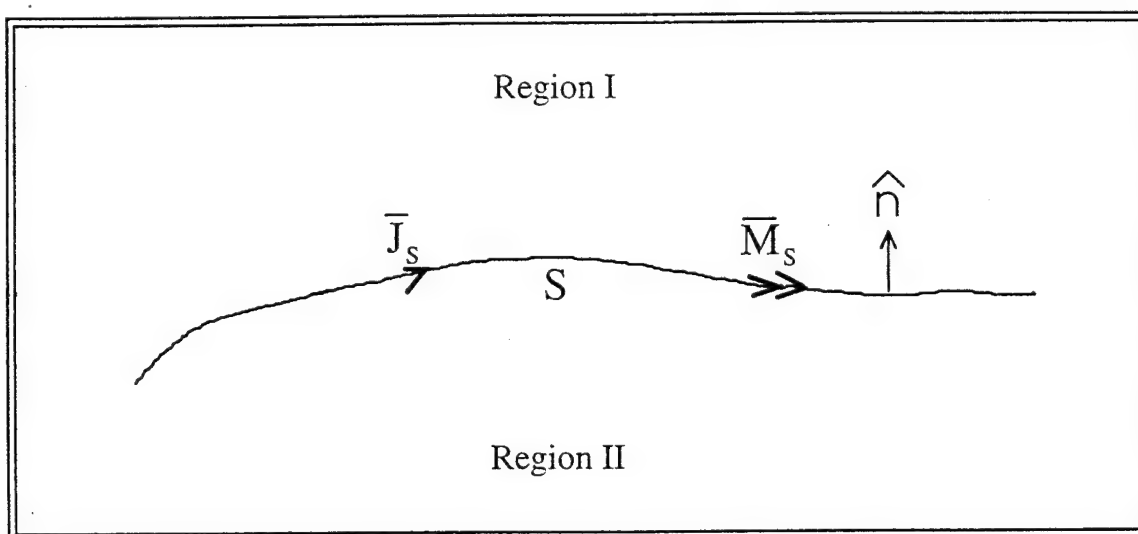


Figure 2.3 A surface S defined by homogenous regions I and II.

For time-harmonic fields, the above boundary conditions are not independent from each other. In fact, in the frequency domain, boundary conditions on tangential $\bar{\mathbf{E}}$ and tangential $\bar{\mathbf{H}}$ form a sufficient set. If the tangential components of the electric and magnetic fields satisfy the boundary conditions, the normal components of the same fields automatically satisfy their appropriate boundary conditions. This is not true in the time domain; and for a static problem, all four boundary conditions are needed (9:27). But, again, only two are needed here.

To apply the first boundary condition, note that $\bar{\mathbf{E}}$ is continuous across the slot in the original problem of Figure 2.1. Thus,

$$\bar{\mathbf{E}}_I^A = \bar{\mathbf{E}}_{II}^A = \bar{\mathbf{E}}^A \quad (2-7)$$

$$\bar{\mathbf{E}}_{II}^B = \bar{\mathbf{E}}_{III}^B = \bar{\mathbf{E}}^B \quad (2-8)$$

and

$$\bar{\mathbf{E}}^A \times \hat{\mathbf{n}}_I = -\bar{\mathbf{E}}^A \times \hat{\mathbf{n}}_{II} \quad (2-9)$$

$$\bar{\mathbf{E}}^B \times \hat{\mathbf{n}}_{II} = -\bar{\mathbf{E}}^B \times \hat{\mathbf{n}}_{III} \quad (2-10)$$

where the minus signs in the above two equations result from the opposite directions of the outward normals. Using Equation (2-2),

$$\bar{\mathbf{M}}_I^A = -\bar{\mathbf{M}}_{II}^A \quad (2-11)$$

and

$$\bar{\mathbf{M}}_{II}^B = -\bar{\mathbf{M}}_{III}^B \quad (2-12)$$

can be derived from the above two equations.

Referring to Figure 2.1, the formulation of the integral equation can be finalized using the second independent boundary condition that the total magnetic field across a particular slot is continuous. Therefore, the H fields in bordering regions must be identical inside the slots where one region meets the other. Thus, based on the equivalent

scattering geometry, a magnetic field continuity equation may be written for points within slot A as follows:

$$\begin{aligned} \hat{\mathbf{n}}_I \times [\bar{\mathbf{H}}_I^{inc} + \bar{\mathbf{H}}_I^{ref} + \bar{\mathbf{H}}_I^{scat}(\bar{\mathbf{M}}_I^A)] \\ = \hat{\mathbf{n}}_I \times [\bar{\mathbf{H}}_{II}^{scat}(-\bar{\mathbf{M}}_I^A) + \bar{\mathbf{H}}_{II}^{scat}(-\bar{\mathbf{M}}_{III}^B)] \end{aligned} \quad (2-13)$$

where Equation (2-11) and Equation (2-12) have been used to remove all explicit references to $\bar{\mathbf{M}}_{II}$. The field $\bar{\mathbf{H}}^{inc}$ is due to the incident plane wave which, as shown in Figure 2.2, is the assumed excitation source originating in Region I and is traveling toward Region II. $\bar{\mathbf{H}}^{ref}$ is the reflected plane wave corresponding to the incident wave hitting the conducting groundplane at the boundary between Regions I and II. Looking ahead, these two terms may be combined together to form a "generalized incident field" such that:

$$\bar{\mathbf{H}}_I^{ginc} = \bar{\mathbf{H}}_I^{inc} + \bar{\mathbf{H}}_I^{ref} \quad (2-14)$$

Similarly, with respect to the field points within slot B, the following magnetic field equation is written:

$$\begin{aligned} \hat{\mathbf{n}}_{III} \times [\bar{\mathbf{H}}_{II}^{scat}(-\bar{\mathbf{M}}_I^A) + \bar{\mathbf{H}}_{II}^{scat}(-\bar{\mathbf{M}}_{III}^B)] \\ = \hat{\mathbf{n}}_{III} \times [\bar{\mathbf{H}}_{III}^{scat}(\bar{\mathbf{M}}_{III}^B)] \end{aligned} \quad (2-15)$$

Equation (2-13) and Equation (2-15) are vector equations involving two surface vector components, one for each of the basis vectors (*not* basis functions) used to represent the two dimensional space of the plane containing the slot. In general, the above two vector equations can be decomposed into four scalar equations, yielding four equations and four unknowns. The four scalar unknowns are represented by the two unknown currents, $\bar{\mathbf{M}}_I^A$ and $\bar{\mathbf{M}}_{III}^B$, each of which is two-dimensional, in general. However, based on the thin slot assumption, the currents in the slot are assumed to be unidirectional in the direction of the slot's major axis, designated by its unit vector $\hat{\mathbf{p}}$; that

is, the current induced due to a slot is represented in one dimension, where the other dimension of possible current flow is assumed negligible. This implies that only two of the four scalar equations are needed to specify the problem. Thus, using the linearity of the radiation operator, $\overline{\mathbf{H}}(-\overline{\mathbf{M}}) = -\overline{\mathbf{H}}(\overline{\mathbf{M}})$; and rearranging terms, the governing equations can be written as:

$$\hat{\mathbf{p}}^A \cdot \overline{\mathbf{H}}_I^{inc} = -\hat{\mathbf{p}}^A \cdot [\overline{\mathbf{H}}_I^{scat}(\overline{\mathbf{M}}_I^A) + \overline{\mathbf{H}}_{II}^{scat}(\overline{\mathbf{M}}_I^A) + \overline{\mathbf{H}}_{III}^{scat}(\overline{\mathbf{M}}_{III}^B)] \quad (2-16)$$

and

$$0 = -\hat{\mathbf{p}}^B \cdot [\overline{\mathbf{H}}_{II}^{scat}(\overline{\mathbf{M}}_I^A) + \overline{\mathbf{H}}_{II}^{scat}(\overline{\mathbf{M}}_{III}^B) + \overline{\mathbf{H}}_{III}^{scat}(\overline{\mathbf{M}}_{III}^B)] \quad (2-17)$$

where each equation is scalar. Equation (2-16) and Equation (2-17) are coupled scalar integral equations where the scattering currents, $\overline{\mathbf{M}}_I^A$ and $\overline{\mathbf{M}}_{III}^B$, compose the unknown integrands that define the $\overline{\mathbf{H}}$ fields. These equations are solved via a moment method based solution.

General Moment Method Solution.

To apply the moment method to Equations (2-16) and (2-17), a set of basis functions must be chosen so that the unknown scattering currents can be discretized. These functions should be as simple as possible so that they are computationally efficient and so that they enhance design insights. But most important, they must be able to accurately represent the anticipated unknown functions that describe the scattering currents for a thin slot.

Representing the desired basis functions as $\phi_n(\overline{\mathbf{R}}')$, the unknown scattering currents are approximated in the following manner:

$$\overline{\mathbf{M}}_I^A \approx \hat{\mathbf{p}}^A \sum_{n=1}^{N_A} V_n^A \phi_n^A(\overline{\mathbf{R}}') \quad (2-18)$$

and

$$\overline{\mathbf{M}}_{III}^B \approx \hat{\mathbf{p}}^B \sum_{n=1}^{N_B} V_n^B \phi_n^B(\overline{\mathbf{R}}') \quad (2-19)$$

The basis functions, $\phi_n(\overline{\mathbf{R}}')$, are dimensionless, while the unknown expansion coefficients, V_n , have the dimension of volts. N_A is the number of basis function *modes* necessary to accurately approximate the scatterer due to slot A, and N_B is the same with respect to slot B. With the moment method, mode lengths based on overlapping piecewise sinusoids or cosinusoids should generally be $\lambda/2$ or less to ensure accurate results. Thus, the electrical size of the object with respect to the wavelength of interest determines how many modes are required.

In the above magnetic current expansions, the current has been discretized and therefore approximated. When substituted back into the governing integral equations, approximation errors are introduced. Using the linearity of the radiation integral, and ϵ to define these approximations errors, the governing equations (with exact equality) are:

$$\begin{aligned} \hat{\mathbf{p}}^A \cdot \overline{\mathbf{H}}_I^{ginc} = & -\hat{\mathbf{p}}^A \cdot \sum_{n=1}^{N_A} V_n^A [\overline{\mathbf{H}}_I^{scat}(\hat{\mathbf{p}}^A \phi_n^A) + \overline{\mathbf{H}}_{II}^{scat}(\hat{\mathbf{p}}^A \phi_n^A)] - \hat{\mathbf{p}}^A \cdot \sum_{n=1}^{N_B} V_n^B \overline{\mathbf{H}}_{II}^{scat}(\hat{\mathbf{p}}^B \phi_n^B) \\ & + \epsilon^A(\overline{\mathbf{R}}, V_1^A, V_2^A, \dots, V_{N_A}^A, V_1^B, V_2^B, \dots, V_{N_B}^B) \end{aligned} \quad (2-20)$$

$$\begin{aligned} 0 = & -\hat{\mathbf{p}}^B \cdot \sum_{n=1}^{N_A} V_n^A \overline{\mathbf{H}}_{II}^{scat}(\hat{\mathbf{p}}^A \phi_n^A) - \hat{\mathbf{p}}^B \cdot \sum_{n=1}^{N_B} V_n^B [\overline{\mathbf{H}}_{II}^{scat}(\hat{\mathbf{p}}^B \phi_n^B) + \overline{\mathbf{H}}_{III}^{scat}(\hat{\mathbf{p}}^B \phi_n^B)] \\ & + \epsilon^B(\overline{\mathbf{R}}, V_1^A, V_2^A, \dots, V_{N_A}^A, V_1^B, V_2^B, \dots, V_{N_B}^B) \end{aligned} \quad (2-21)$$

Note that the error introduced in discretizing the current is a function of the expansion coefficients. To minimize these errors in such a way that its average over the entire structure approaches zero in some sense, the moment method is employed. This technique utilizes testing (or weighting) functions in association with an inner product to

force the errors to vanish. It is important to note that application of the moment method does not lead to the disappearance of error at every point of interest on the produced function, but rather, it forces the boundary conditions to be satisfied in an average sense over the range of the function (9). More specifically, using Harrington's method (5), the errors are forced to vanish by forming an inner product with the testing functions, such that:

$$\int \epsilon^i(\bar{\mathbf{R}}) \cdot \theta_m^i(\bar{\mathbf{R}}) d\bar{\mathbf{R}} = 0 \quad (2-22)$$

Here, i represents slot A or B, and θ_m^i represents the testing functions under summation index m . There must be as many testing functions chosen as there are basis functions, and the index m indicates which testing function is being referenced. The criteria for choosing testing functions is that all m of them must be linearly independent, and it is advantageous to select computationally efficient functions so that the time spent calculating the inner products is minimized. In this manner, applying the moment method efficiently and effectively constrains the outcome of the expansion coefficients, forcing the average error in the discretization approximation to equal zero.

By introducing as many testing functions as there are basis functions, a system of $(N_A + N_B)$ linear equations and $(N_A + N_B)$ unknowns are formed. These equations govern the values of the unknown expansion coefficients, $V_n^{A,B}$, and are written most generally in matrix form as:

$$[\mathbf{I}] = [\mathbf{Y}][\mathbf{V}] \quad (2-23)$$

The entries of the column vector \mathbf{I} represent the electric currents excited in the slots by the generalized incident plane wave and have units of amperes¹ (in the equivalent

¹The units would be *Amps / meter* if the currents were distributed over a surface; but with a thin slot assumption, we treat them as condensed filaments of current along the slot centerline.

problem, these excited currents are more appropriately thought of as the excited magnetic voltages that give rise to the magnetic scattering currents). Note that solving for \mathbf{V} in Equation (2-23) requires inverting the \mathbf{Y} matrix, or some similar routine such as Gaussian elimination. Finding the most efficient routine to perform the inversion was not a concern for this effort, since filling the entries of the \mathbf{Y} matrix is a more time consuming chore by orders of magnitude for typical applications.

Equation (2-23) may be expanded into the following matrix expression:

$$\begin{bmatrix} I_m^A \\ 0 \end{bmatrix} = \begin{bmatrix} Y_{mn_I}^{AA} + Y_{mn_{II}}^{AA} & Y_{mn}^{AB} \\ Y_{mn}^{BA} & Y_{mn_{II}}^{BB} + Y_{mn_{III}}^{BB} \end{bmatrix} \begin{bmatrix} V_n^A \\ V_n^B \end{bmatrix} \quad (2-24)$$

If the slot lengths are longer than approximately one half of the wavelength of the excitation plane wave, then multiple current modes will be needed to accurately model the slots, with each mode being less than 0.5 wavelengths. In such case, the entries of $[\mathbf{Y}]$ will be sub-matrices, and the entries of $[\mathbf{I}]$ and $[\mathbf{V}]$ will be partial column vectors. In Equation (2-24), the entry I_m^A is defined by:

$$I_m^A = \int \hat{\mathbf{p}}^a \cdot \bar{\mathbf{H}}_I^{ginc}(\bar{\mathbf{R}}) \cdot \theta_m^A(\bar{\mathbf{R}}) d\bar{\mathbf{R}} \quad (2-25)$$

and the mathematical definitions for the entries of $[\mathbf{Y}]$ are:

$$Y_{mn_I}^{AA} = - \int \hat{\mathbf{p}}^A \cdot \bar{\mathbf{H}}_I^{scat}(\hat{\mathbf{p}}^A \phi_n^A) \cdot \theta_m^A(\bar{\mathbf{R}}) d\bar{\mathbf{R}} \quad (2-26)$$

$$Y_{mn_{II}}^{AA} = - \int \hat{\mathbf{p}}^A \cdot \bar{\mathbf{H}}_{II}^{scat}(\hat{\mathbf{p}}^A \phi_n^A) \cdot \theta_m^A(\bar{\mathbf{R}}) d\bar{\mathbf{R}} \quad (2-27)$$

$$Y_{mn}^{AB} = - \int \hat{\mathbf{p}}^A \cdot \bar{\mathbf{H}}_{II}^{scat}(\hat{\mathbf{p}}^B \phi_n^B) \cdot \theta_m^A(\bar{\mathbf{R}}) d\bar{\mathbf{R}} \quad (2-28)$$

$$Y_{mn}^{BA} = - \int \hat{\mathbf{p}}^B \cdot \bar{\mathbf{H}}_{II}^{scat}(\hat{\mathbf{p}}^A \phi_n^A) \cdot \theta_m^B(\bar{\mathbf{R}}) d\bar{\mathbf{R}} \quad (2-29)$$

$$Y_{mn_{II}}^{BB} = - \int \hat{\mathbf{p}}^B \cdot \overline{\mathbf{H}}_{II}^{scat} (\hat{\mathbf{p}}^B \phi_n^B) \cdot \theta_m^B(\overline{\mathbf{R}}) d\overline{\mathbf{R}} \quad (2-30)$$

$$Y_{mn_{III}}^{BB} = - \int \hat{\mathbf{p}}^B \cdot \overline{\mathbf{H}}_{III}^{scat} (\hat{\mathbf{p}}^B \phi_n^B) \cdot \theta_m^B(\overline{\mathbf{R}}) d\overline{\mathbf{R}} \quad (2-31)$$

In the above equations, the subscript m denotes both a matrix row and a receiving (or testing) mode; the subscript n denotes both a matrix column and a transmitting (or basis) mode. The "A" and "B" superscripts refer to the respective slots in Figure 2.1, and the Roman numerals refer to the appropriate regions as shown in Figure 2.2. Also, the Y's have the interpretation of mutual and self admittances, with units of mhos; the V's and I's have units of volts and amperes, respectively². Massaging the above equations for the admittance matrices, so that each entry is defined with a minus sign, results in the admittances agreeing with the physical interpretation given by Schelkunoff (10).

Using the formulation where this physical interpretation applies, makes it simple to account for the effects of slots filled with resistive materials. The currents induced on a finite slot array can be viewed as the sum of two currents: the current induced on a similar array of infinite size, and a perturbation current due to the edge effects on the finite array. The idea of filling some slots with thin resistive films is to taper the abrupt change in impedance found at the edge of an array. By resistively loading the columns at and near the edges with progressively larger resistance towards the center of the array, the abrupt change in impedance is smoothed out, and the edge effects are tempered. An analogous situation is scattering from the surface of a finite rectangular plate, where the total induced current can be viewed as the sum of the current predicted by physical optics and a current due to edge diffractions. If the edges of the plate are smoothed (perhaps by

²Units for the admittance matrix terms result from normalization of all basis functions used in generating the inner products. For the magnetic scattering current basis functions, ϕ_n^A and ϕ_n^B , this normalization involves a hidden $1/volt$ factor. This is identical to the normalization procedure used by Skinner (6).

adding resistive card extensions), then the diffractions can be minimized. But a sharp edge or otherwise abrupt termination will maximize the current due to edge diffractions.

To model a resistively loaded slot array using the above matrix equation, all that needs to be done is to add the desired loads in terms of admittances (in parallel) to the self admittance terms of the modes defining the appropriate slots. In the above expressions, $Y_{mn_I}^{AA}$, $Y_{mn_{II}}^{AA}$, $Y_{mn_{II}}^{BB}$, and $Y_{mn_{III}}^{BB}$ represent the self admittance terms for $m=n$. Actually, they represent "one sided" self admittance terms. This distinction begins with the fact that, in the equivalent problem, the incident field only induces scattering currents in the modes of the first array (slot A). The incident wave is seen in Region II only by the relationship between the currents on each side of this first groundplane as defined by Equation (2-11). This first groundplane effectively hides Regions II and III from any direct effect by the incident field. In other words, the groundplanes of the equivalent problem partition the problem such that each region must be analyzed separately. Thus, the need for the "region subscripts" on the Y terms, and the rationale in referring to "one sided" self admittances. This will be explained in more detail in Chapter 4.

The scattering problem is completed by using matrix methods to solve Equation (2-24) for the unknown expansion coefficients in the matrix V . These expansion coefficients were defined in the discretization of the magnetic scattering currents (see Equations (2-18) and (2-19)), and are used to construct an accurate approximation of these currents. Once the magnetic scattering currents are known, radiation integrals are then used to examine the scattered fields associated with these currents. The details are described in Chapter 5.

The solution thus far has been presented in terms of two single slots. Adding a finite number of slots to the problem will not change the method. It only increases the number of modes defined in the sub-matrices above, which would similarly result if more modes were needed because of an electrically large object. The extension to a

"finite by infinite" array does not change the basic moment method procedure, either. First, picture a finite number of slots on an array as just mentioned. Next, expand each slot in the picture into an infinite column of like elements, using a common periodic spacing (in \hat{z}) for all such expansions. Then by defining periodic basis functions which represent single infinite column arrays, the more general configuration can be attacked. This method truncates the testing function so that it is non-zero only on a single element of the column array, and uses the known periodicity to complete the solution.

Because linear independence between modes and computational efficiency are required for both the basis and testing functions, the same type of functions are sometimes used for both. This technique, known as *Galerkin's method*, provides an excellent trade off between accuracy and computational efficiency, and is similar to the method implemented in this effort. But because the testing functions are truncated to exist only on the reference elements, instead of using one on every element in an infinite column (which would lead to infinite numerical entries in the matrices), this implementation cannot be described as Galerkin's method in the strictest sense.

III. PLANE WAVE EXCITATION

In this chapter, expressions are developed for the excitation vector, $[\mathbf{I}]$, which was defined in Chapter II. One of the basic assumptions used in this model is that the excitation source is an external plane wave. This plane wave source originates in Region I (see Figure 2.2), and directly excites all the slot modes on the first groundplane (which separates Regions I and II). Its effects show up in the general matrix equation as $[\mathbf{I}]$ (see Equation (2-23)), whose entries are defined by Equation (2-25).

The geometry depicted below in Figure 3.1 shows a view from the z -axis of a magnetic current mode for a reference slot. Also shown is an arbitrary dielectric slab

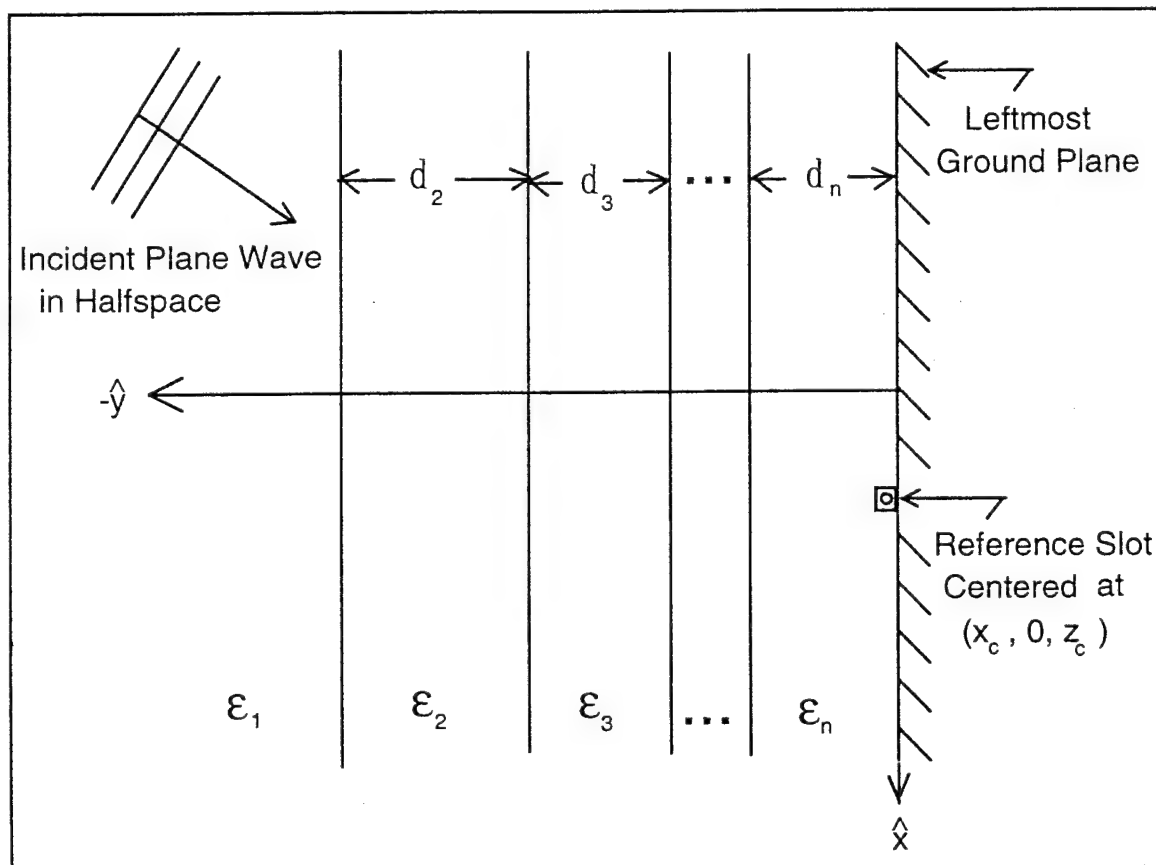


Figure 3.1 Geometry Depicting Slot Mode Excited by an External Plane Wave in Region I.

configuration for Region I, where the infinite half space is considered the first slab. Note that the center of the current mode is arbitrarily located on the groundplane, and that the incident plane wave generally travels from the -y direction to the + y direction.

To characterize the incident wave more specifically, the direction of the incidence in the halfspace may be defined as:

$$\hat{s}_1 = s_{x_1} \hat{x} + s_{y_1} \hat{y} + s_{z_1} \hat{z} \quad (3-1)$$

where the wave in the halfspace is referred to with the subscript 1 because the left halfspace is taken to be the 1st slab.

As the incident wave penetrates a dielectric layer, its polarization vectors are generally changed. The polarization of the incident wave, and all other propagation to be accounted for, can be conveniently handled by decomposing the wave in question into two linear polarizations such that:

$$\bar{H} = H_{\parallel} \hat{n}_{\parallel} + H_{\perp} \hat{n}_{\perp} \quad (3-2)$$

where \hat{n}_{\parallel} and \hat{n}_{\perp} are the directions of linear polarizations. Referring to Figure 3.2, these directions are given by $\hat{n}_{\parallel} = \hat{\eta}$ and $\hat{n}_{\perp} = \hat{\alpha}$. It is convenient to relate the incident field direction's Cartesian components to that of its defining angles α and η . These directional components are:

$$s_{x_1} = -\cos \alpha \sin \eta \quad (3-3)$$

$$s_{y_1} = \cos \eta \quad (3-4)$$

$$s_{z_1} = -\sin \alpha \sin \eta \quad (3-5)$$

where $0^\circ \leq \alpha \leq 180^\circ$ and $-90^\circ \leq \eta \leq 90^\circ$. Further, it is useful to define the polarization directions in terms of the Cartesian components of the incident wave. But since these relations are generally applicable in this problem, not just in the halfspace, the "1"

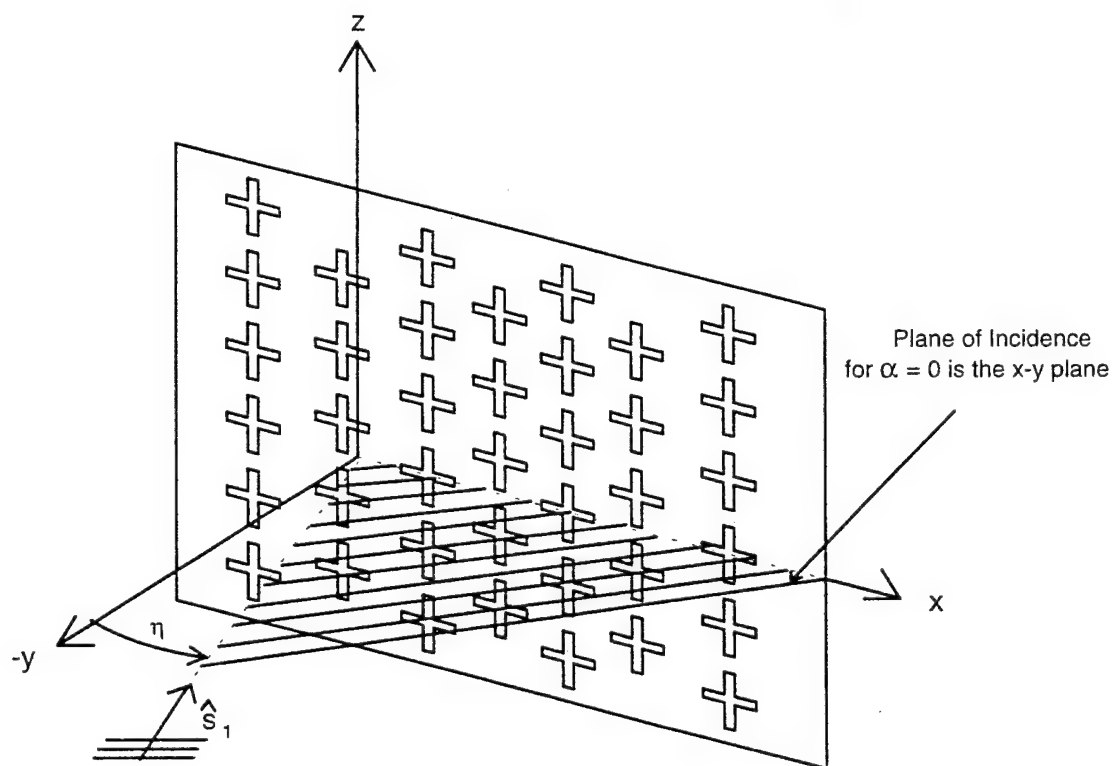
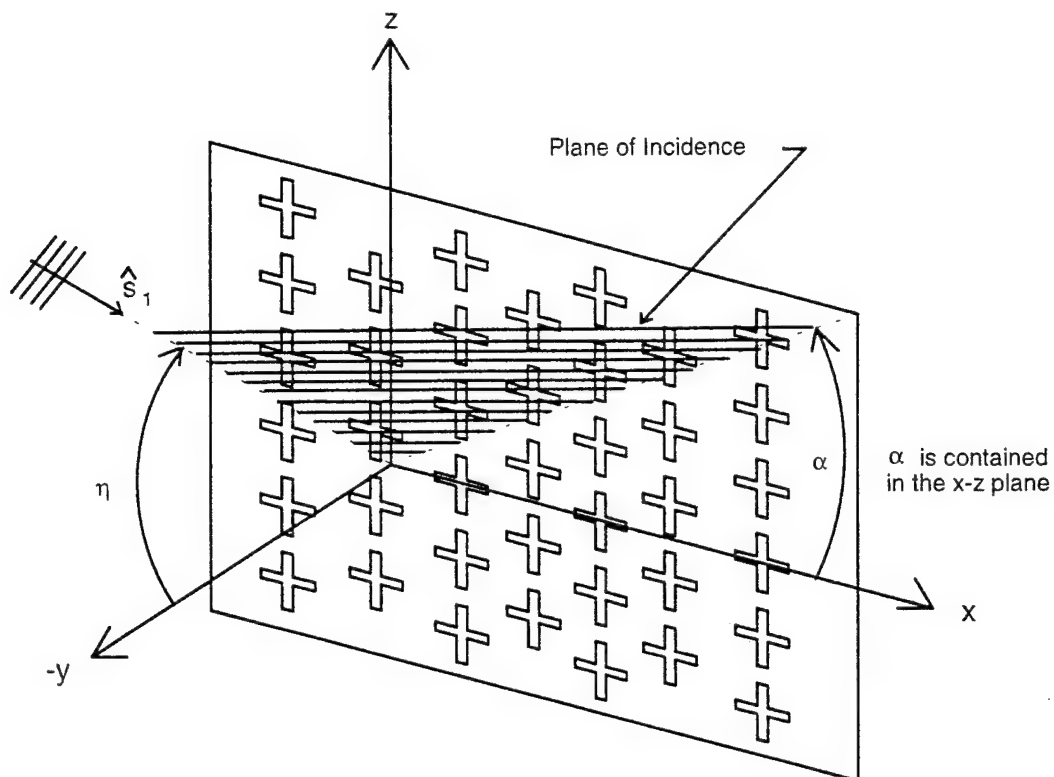


Figure 3.2 Propagation Direction for an Incident Plane Wave.

subscript is dropped and replaced by a more generic one, namely the subscript i . The equations are:

$$\hat{\mathbf{n}}_{\perp i} = -\frac{\hat{\mathbf{y}} \times \hat{\mathbf{s}}_i}{|\hat{\mathbf{y}} \times \hat{\mathbf{s}}_i|} \quad (3-6)$$

$$\hat{\mathbf{n}}_{\parallel i} = \frac{\hat{\mathbf{n}}_{\perp i} \times \hat{\mathbf{s}}_i}{|\hat{\mathbf{n}}_{\perp i} \times \hat{\mathbf{s}}_i|} \quad (3-7)$$

Substituting Equation (3-1) into Equations (3-6) and (3-7), yields:

$$\hat{\mathbf{n}}_{\perp i} = \frac{-s_{z_i} \hat{\mathbf{x}} + s_{x_i} \hat{\mathbf{z}}}{\sqrt{s_{x_i}^2 + s_{z_i}^2}} \quad (3-8)$$

and

$$\hat{\mathbf{n}}_{\parallel i} = \frac{-s_{x_i} s_{y_i} \hat{\mathbf{x}} + (s_{x_i}^2 + s_{z_i}^2) \hat{\mathbf{y}} - s_{y_i} s_{z_i} \hat{\mathbf{z}}}{\sqrt{s_{x_i}^2 + s_{z_i}^2}} \quad (3-9)$$

As the incident wave propagates through the different dielectric layers, its propagation direction refracts. In the i th material, these components can be related to the initial (left halfspace) components as follows:

$$s_{x_i} = s_{x_1} \frac{\beta_1}{\beta_i} \quad (3-10)$$

$$s_{z_i} = s_{z_1} \frac{\beta_1}{\beta_i} \quad (3-11)$$

and

$$s_{y_i} = \sqrt{1 - s_{x_i}^2 - s_{z_i}^2} \quad (3-12)$$

with the positive real root (or -j root) taken for the \hat{y} component. Using the above equations, it can be shown that $\hat{n}_{\perp i} = \hat{n}_{\perp 1}$ for any material i , but in general, $\hat{n}_{\parallel i} \neq \hat{n}_{\parallel 1}$.

Referring to Equation (2-25), the electric current induced in a slot by the incident wave is a function of the "generalized" incident magnetic field at the slot location. Applying Skinner's formulation, where the subscript I indicates Region I, this generalized field (total field in a dielectric clad groundplane with no slots) is:

$$\begin{aligned} \overline{\mathbf{H}}_I^{ginc}(\overline{\mathbf{R}}) = & \phi_{2n} e^{-j\beta_n \overline{\mathbf{R}} \cdot \hat{s}_n} \left[T_{\parallel}^{HE} \left[\overline{\mathbf{H}}_I^{inc}(0, -d_{tot}, 0) \cdot \hat{n}_{\perp 1} \right] \hat{n}_{\perp n} \right. \\ & \left. + \frac{s_{y1}}{s_{yn}} \left[\hat{n}_{\parallel n} - \hat{y}(\hat{y} \cdot \hat{n}_{\parallel n}) \right] \left[\overline{\mathbf{H}}_I^{inc}(0, -d_{tot}, 0) \cdot \hat{n}_{\parallel 1} \right] T_{\perp}^{HE} \right] \end{aligned} \quad (3-13)$$

Several components of the above equation need explaining: First, referencing Figure 3.1, the incident plane wave's magnetic field, $\overline{\mathbf{H}}_I^{inc} = \overline{\mathbf{H}}_I^{ginc} - \overline{\mathbf{H}}_I^{ref}$, is evaluated at the point where the negative y-axis intersects the dielectric boundary created by the halfspace and the first slab, where d_{tot} represents the sum total of the slab thicknesses. The function ϕ_{2n} represents the phase delay from this point to where the y-axis intersects the groundplane, or, in other words, the y component of the delay corresponding to propagation through the Region I dielectric slabs at normal incidence. This delay is formulated as:

$$\phi_{2n} = \prod_{i=2}^n \phi_i = \prod_{i=2}^n e^{-j\beta_i d_i s_{yi}} \quad (3-14)$$

Note that in Region I, as indicated in Figure 3.1, the halfspace has an index of 1, the first slab has an index of 2, and the slab closest to the groundplane has an index of n . Next, let the position vector, $\overline{\mathbf{R}}$, define the point of evaluation for the generalized field. This point lies somewhere on the groundplane at a slot current's location and is given by:

$$\bar{\mathbf{R}} = [x, \hat{x} + z, \hat{z}] + \hat{\mathbf{p}}l = \bar{\mathbf{R}}_r + \hat{\mathbf{p}}l \quad (3-15)$$

where $\bar{\mathbf{R}}_r$ represents the coordinates of the current mode's reference node ("terminal node" in PMM vernacular), and $\hat{\mathbf{p}}$ is the direction of the linear slot piece of interest, whose length is l . Finally, the two T factors, T_{\perp}^{HE} and T_{\parallel}^{HE} are polarized functions that give the effective transmission from the halfspace boundary to the dielectric slab nearest the groundplane, accounting for an infinite geometric series of plane wave bounces within the slab closest to the groundplane. These T factors carry the HE superscript to indicate that they transform the magnetic field scattered by the slot source into an electric field. To transform from H to E is a matter of convenience since the scattered fields are to be determined in the far zone. Based on the assumptions previously made, the E and H fields in the far zone are orthogonal and are related in magnitude by the intrinsic impedance of the medium. So it is sufficient to explicitly find the solution in terms of only one of these fields. The E field is chosen because Skinner's solution is in that form, and his code is used to validate the accuracy of numerical calculations in this model's code. The T factor equation is:

$$T^{HE} = \frac{2 \prod_{m=2}^n [1 + \Gamma_{m-1,m}]}{\prod_{m=2}^n [1 - \Gamma_{m,m-1} \Gamma_{m,m+1}^{eff} e^{-j2\beta_m d_m s_{ym}}]} \quad (3-16)$$

In the denominator above, n is the number of slabs in Region I. When m equals n , the effective reflection coefficient, $\Gamma_{m,m+1}^{eff}$, is simply the Fresnel reflection coefficient (with polarization dependence suppressed) for the boundary created by the n th slab and the groundplane. It should be noted that Equation (3-16) applies to both the perpendicular and parallel polarization terms as introduced above; the polarization symbols have been suppressed for convenience. To apply them, just place the applicable polarization symbol

on all Γ references on the right hand side of the equation. The Γ references represent reflection coefficients. The Γ 's without superscript are ordinary Fresnel reflection coefficients which are derived on the assumption that two unbounded halfspaces form the boundary of interest, while those Γ 's with the "eff" superscript are effective reflection coefficients.

The concept of effective reflection coefficients (and effective transmission coefficients) has been covered thoroughly by other authors (4:App D)(2:12-15)(6:76). A brief discussion, along with the appropriate equations, are given here for completeness.

Henderson (2:12) defines an effective reflection coefficient for a particular interface as the ratio between the total wave reflected from the boundary and the total wave incident upon the boundary. To make the point by comparison, a Fresnel reflection coefficient assumes the boundary is formed by two infinite halfspaces so that any wave transmitted through the boundary of interest is never reflected back, while the effective reflection coefficient does not make this assumption, but, rather, accounts for the initial reflection and also reflections on other boundaries due to transmissions through all boundaries present. Consider Figure 3.3. For waves incident from the left direction and traveling in the $-\hat{y}$ direction, the general effective reflection and transmission coefficients for the m th slab are, respectively:

$$\Gamma_{m-1,m}^{eff} = \frac{\Gamma_{m-1,m} + \Gamma_{m,m+1}^{eff} e^{-j2\beta_m d_m s_{ym}}}{1 - \Gamma_{m,m+1}^{eff} \Gamma_{m,m-1} e^{-j2\beta_m d_m s_{ym}}} \quad (3-17)$$

$$\tau_{m-1,m}^{eff} = \frac{1 + \Gamma_{m-1,m}}{1 - \Gamma_{m,m+1}^{eff} \Gamma_{m,m-1} e^{-j2\beta_m d_m s_{ym}}} \quad (3-18)$$

For waves incident from the right direction and traveling in the $+\hat{y}$ direction, the indices or the effective reflection and transmission coefficients are reversed as follows:

$$\Gamma_{m+1,m}^{eff} = \frac{\Gamma_{m+1,m} + \Gamma_{m,m-1}^{eff} e^{-j2\beta_m d_m s_{ym}}}{1 - \Gamma_{m,m-1}^{eff} \Gamma_{m,m+1} e^{-j2\beta_m d_m s_{ym}}} \quad (3-19)$$

$$\tau_{m+1,m}^{eff} = \frac{1 + \Gamma_{m+1,m}}{1 - \Gamma_{m,m-1}^{eff} \Gamma_{m,m+1} e^{-j2\beta_m d_m s_{ym}}} \quad (3-20)$$

The above expressions are valid for E or H fields. The type of field described by the chosen expression is determined by the type of Fresnel coefficient used in its construction; if the Fresnel coefficients are referenced to the E field, then the resulting effective coefficient is referenced to the E field (and similarly for the H field).

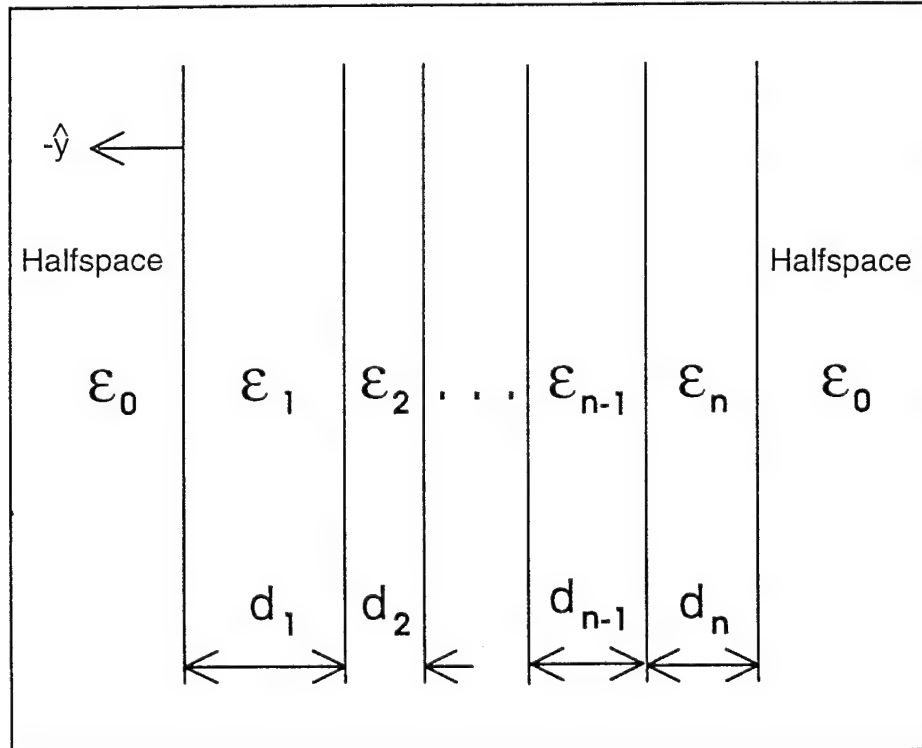


Figure 3.3 Stratified Dielectric Medium Bounded by Two Freespace Halfspaces

Now, back to finding the electric current excited in a slot by the incident plane wave. Substituting Equation (3-13) into Equation (2-25), yields:

$$I^A = \int_a^b \phi_{2n} e^{-j\beta_n [\bar{\mathbf{R}}_r + \hat{\mathbf{p}}l] \cdot \hat{\mathbf{s}}_n} \left[T_{\parallel}^{HE} \left[\bar{\mathbf{H}}^{inc}(0, -d_{tot}, 0) \cdot \hat{\mathbf{n}}_{\perp 1} \right] \frac{\hat{\mathbf{p}} \cdot (-s_{z_n} \hat{\mathbf{x}} + s_{x_n} \hat{\mathbf{z}})}{\sqrt{s_{x_n}^2 + s_{z_n}^2}} \right. \\ \left. + \frac{\hat{\mathbf{p}} \cdot (-s_{x_n} s_{y_1} \hat{\mathbf{x}} + s_{y_1} s_{z_n} \hat{\mathbf{z}})}{\sqrt{s_{x_n}^2 + s_{z_n}^2}} \left[\bar{\mathbf{H}}^{inc}(0, -d_{tot}, 0) \cdot \hat{\mathbf{n}}_{\parallel 1} \right] T_{\perp}^{HE} \right] I^{test}(l) dl \quad (3-21)$$

where $\hat{\mathbf{p}}$ is again the direction of the slot element segment of length l , a and b are the endpoints of this element, and $I^{test}(l)$ represents the testing function shape that is used to form the inner product for the moment method. Recall that it is assumed that piecewise (co)sinusoidal basis functions can be used to accurately model the actual current induced on a thin slot, and further that the chosen testing functions are of shapes that are similar to the basis functions (cosinusoidal/sinusoidal).

If a periodic slot mode is composed of more than one piecewise linear segment, then the above integral is performed with respect to each to each segment and the results of these integrations are then added to obtain the overall solution for the slot mode. Assuming now this more general case of multiple segments, Equation (3-21) may still be simplified by applying Munk's (4) pattern factor definitions, which he used in the plane wave expansion of fields from doubly-infinite arrays. Let the mode of interest be composed of m piecewise linear segments, and let the subscript κ denote one of these segments, with $\hat{\mathbf{p}}$ indicating the direction of that segment. Equation (3-21) then becomes:

$$I^A = \phi_{2n} e^{-j\beta_n \bar{\mathbf{R}}_r \cdot \hat{\mathbf{s}}_n} \left[T_{\parallel}^{HE} P'_{\perp, n} \left[\bar{\mathbf{H}}^{inc}(0, -d_{tot}, 0) \cdot \hat{\mathbf{n}}_{\perp 1} \right] \right. \\ \left. + \frac{s_{y_1}}{s_{y_n}} T_{\perp}^{HE} P'_{\parallel, n} \left[\bar{\mathbf{H}}^{inc}(0, -d_{tot}, 0) \cdot \hat{\mathbf{n}}_{\parallel 1} \right] \right] \quad (3-22)$$

where polarized pattern factors are defined such that:

$$P_{\parallel n}^r = \sum_{\kappa=1}^m P_{n,\kappa}^r \hat{\mathbf{p}}_{\kappa} \cdot \hat{\mathbf{n}}_{\parallel n} \quad (3-23)$$

$$P_{\perp n}^r = \sum_{\kappa=1}^m P_{n,\kappa}^r \hat{\mathbf{p}}_{\kappa} \cdot \hat{\mathbf{n}}_{\perp n} \quad (3-24)$$

where the superscript r indicates that the basic pattern factor for the mode of interest is of the receiving type, whose general equation with respect to slab n and segment κ is given by:

$$P_{n,\kappa}^r = \int_a^b I^{test}(l) e^{-j\beta_n l \hat{\mathbf{p}}_{\kappa} \cdot \hat{\mathbf{s}}_n} dl \quad (3-25).$$

A more thorough discussion of pattern factors and the associated testing current shapes is given in Appendix B.

In the computer program implementation of this model, the plane of incidence is limited to the x-y plane. Looking back on Figure 3.2, this restriction effectively defines the angle α as zero. Under this scenario, the incident plane wave's z-component of propagation is zero ($\hat{\mathbf{s}}_z = 0$), and the linear polarization directions simplify such that:

$$\hat{\mathbf{p}}_{\kappa} \cdot \hat{\mathbf{n}}_{\perp i} = \hat{\mathbf{p}}_{\kappa} \cdot \frac{s_{x_i}}{\sqrt{s_{x_i}^2}} \hat{\mathbf{z}} = \text{sgn}(s_{x_i}) \hat{\mathbf{p}}_{\kappa} \cdot \hat{\mathbf{z}} \quad (3-26)$$

$$\hat{\mathbf{p}}_{\kappa} \cdot \hat{\mathbf{n}}_{\parallel i} = \hat{\mathbf{p}}_{\kappa} \cdot \left[\frac{-s_{x_i} s_{y_i} \hat{\mathbf{x}} + s_{x_i}^2 \hat{\mathbf{y}}}{\sqrt{s_{x_i}^2}} \right] = -\text{sgn}(s_{x_i}) s_{y_i} \hat{\mathbf{p}}_{\kappa} \cdot \hat{\mathbf{x}} \quad (3-27)$$

making the expressions for the polarized pattern factors more compact, and thereby simplifying Equation (3-21) even further. Note that $\hat{\mathbf{p}}_K$ has no y component.

In an effort to demonstrate that the above equations have been implemented correctly in the associated computer model, called FIFEE (Finite by Infinite: Fss with Edge Effects), two scenarios were set up. The data generated from the resulting calculations are compared in the plots that follow with data from Henderson's model, PMM, and Skinner's model, KAHUNA.

The first scenario creates a groundplane with two z -directed slots: one slot is centered at the origin and the other slot is centered at $x = 0.28$ centimeters. The groundplane has two dielectric layers before it. The slab closest to the groundplane has a relative dielectric constant of 4 and a thickness of 0.2 times the wavelength in this medium. The second slab has a relative dielectric constant of 2 and its thickness is also 0.2 times the medium's wavelength. The operating frequency is 10 GHz, and each slot is 0.75 cm long. Their testing currents are defined by piecewise sinusoids (reference Appendix B), and the slot interiors are defined with an effective dielectric constant of 4 (for the purpose of defining the PWS shape). The excitation currents were computed for both slots by KAHUNA and FIFEE. These currents are shown as a function of η in Figures 3.4 and 3.5. The perfect agreement between the two predictions indicates the implementation for the new FIFEE code is correct.

Excitation Current for z-Directed Slot at Origin, 10 GHz, TE_z, 2 Slabs in Region I

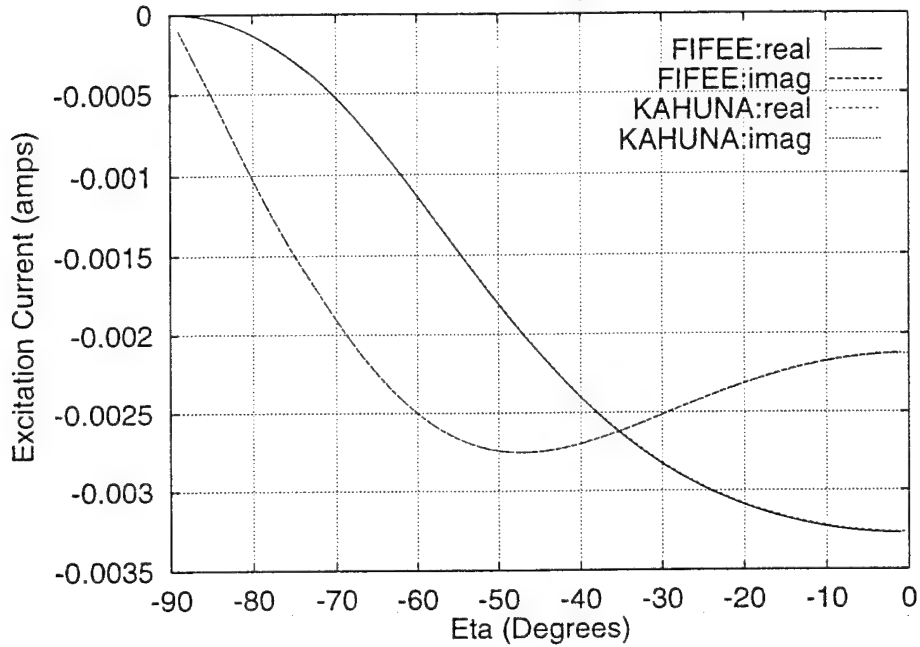


Figure 3.4 Slotted Groundplane Coated with 2 Slabs with Slot Length = $\lambda_3/2$, Slot Width = $\lambda_3/20$, $\epsilon_e = \epsilon_3 = 4\epsilon_1$, $\epsilon_2 = 2\epsilon_1$, $d_3 = 0.2\lambda_3$, $d_2 = 0.2\lambda_2$, $\alpha = 0$.

Excitation Current for z-Directed Slot at $(x,z)=(0.28,0.0)$ cm, 10 GHz, TE_z, 2 Slabs in Region I

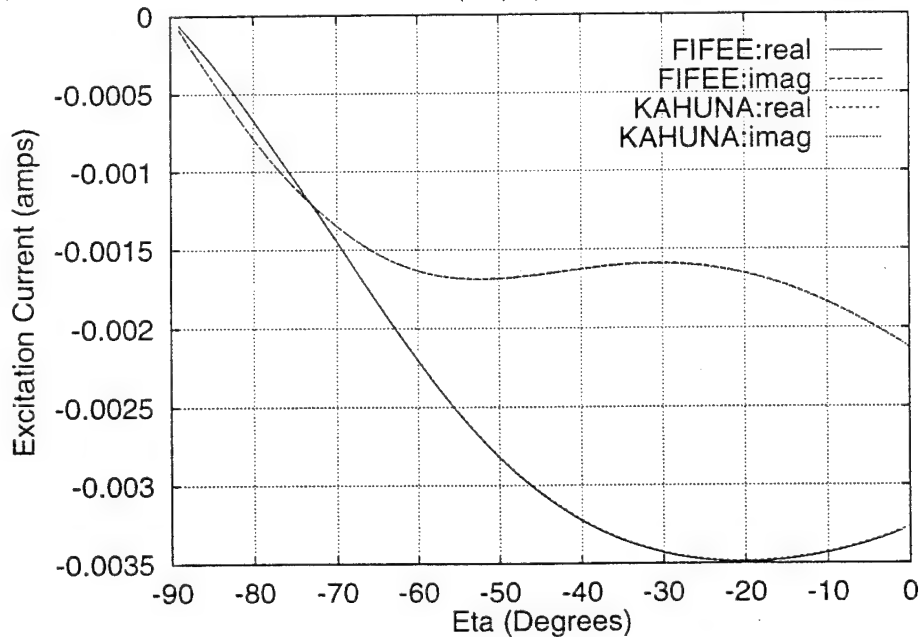
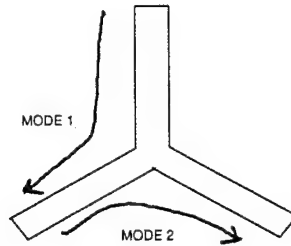


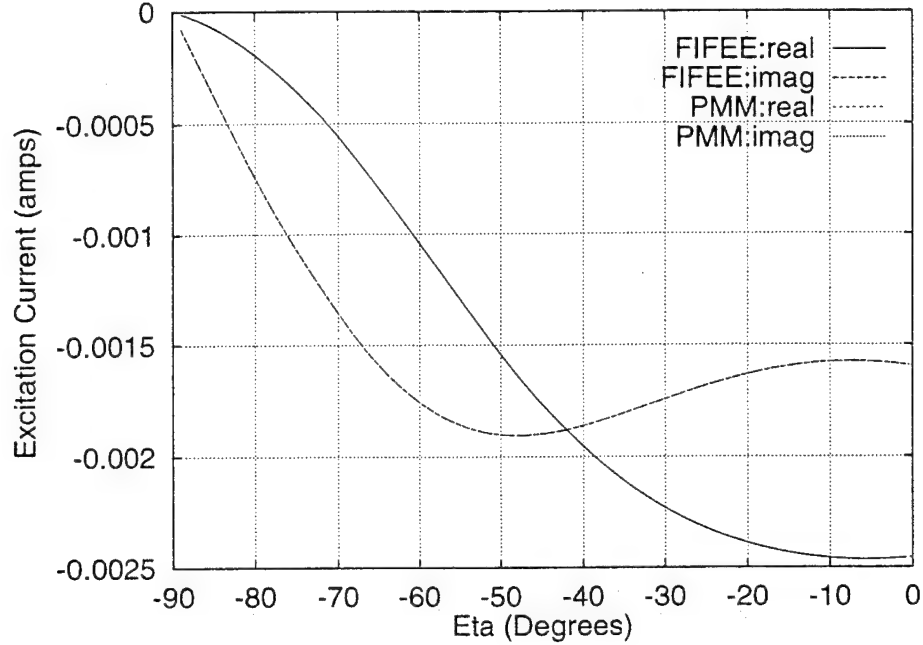
Figure 3.5 Slotted Groundplane Coated with 2 Slabs with Slot Length = $\lambda_3/2$, Slot Width = $\lambda_3/20$, $\epsilon_e = \epsilon_3 = 4\epsilon_1$, $\epsilon_2 = 2\epsilon_1$, $d_3 = 0.2\lambda_3$, $d_2 = 0.2\lambda_2$, $\alpha = 0$.

The second scenario is the same as the first except that, instead of two z-directed slots, one trislot configuration is centered at $(x, z) = (0.1, 0.1)$ centimeters. Each trislot leg is $\lambda_3/4$ in length, and the trislot's modes are oriented in the following manner:



Figures 3.6 and 3.7 show the excitation current results as calculated by FIFEE and PMM for the TE_z (H-POL) and the TM_z (V-POL) cases, respectively. Again, the perfect agreement between the two predictions indicates that the implementation for FIFEE is correct.

TEz, Mode 1 Excitation Current for Trislot Centered at (x,z)=(0.1,0.1)cm, 10 GHz, 2 Slabs in Region I



TEz, Mode 2 Excitation Current for Trislot Centered at (x,z)=(0.1,0.1)cm, 10 GHz, 2 Slabs in Region I

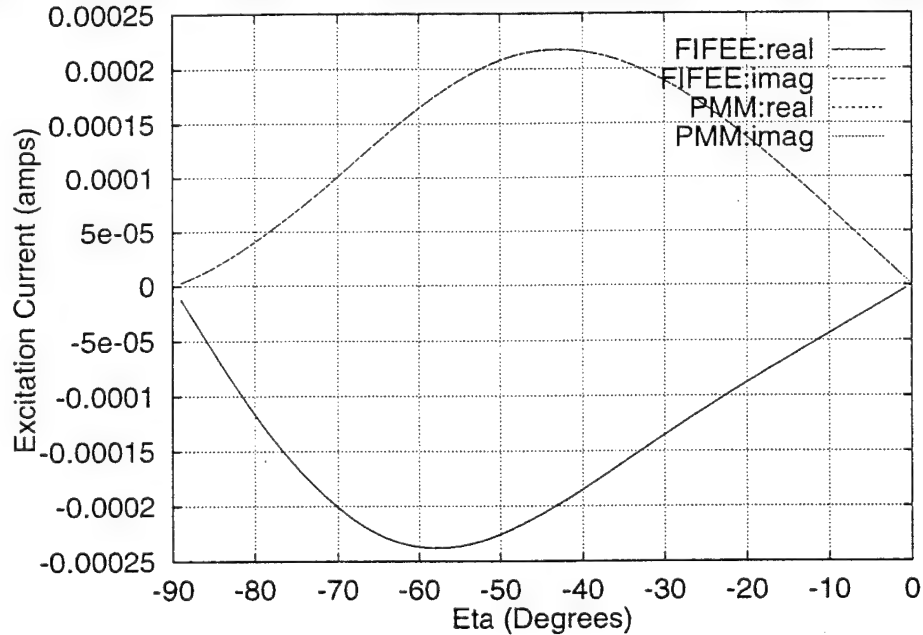
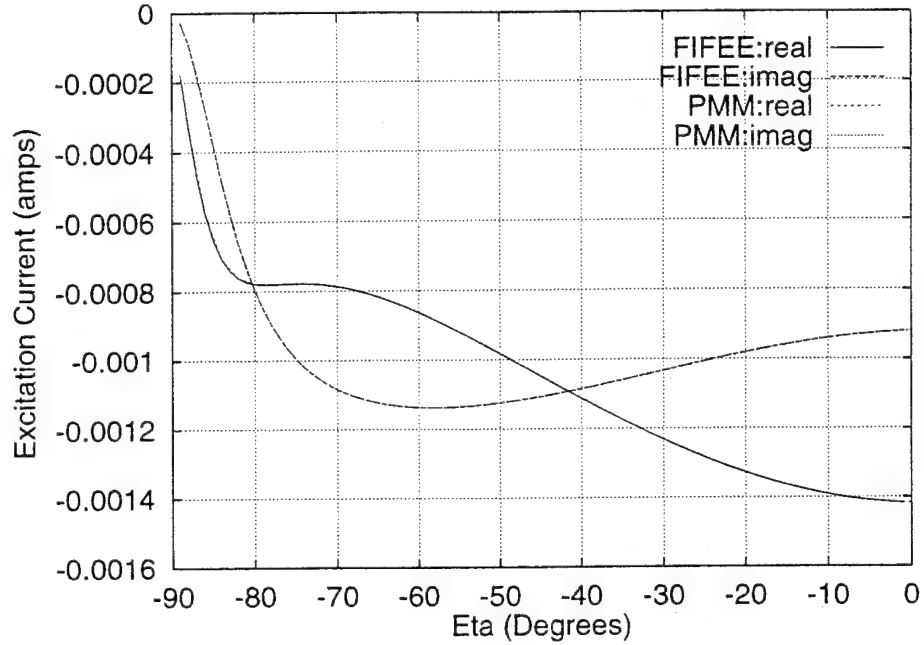


Figure 3.6 TEz with $\epsilon_e = \epsilon_3 = 4\epsilon_1$, $\epsilon_2 = 2\epsilon_1$, $d_3 = 0.2\lambda_3$, $d_2 = 0.2\lambda_2$, $\alpha = 0$.

TMz, Mode 1 Excitation Current for Trislot Centered at (x,z)=(0.1,0.1)cm, 10 GHz, 2 Slabs in Region I



TMz, Mode 2 Excitation Current for Trislot Centered at (x,z)=(0.1,0.1)cm, 10 GHz, 2 Slabs in Region I

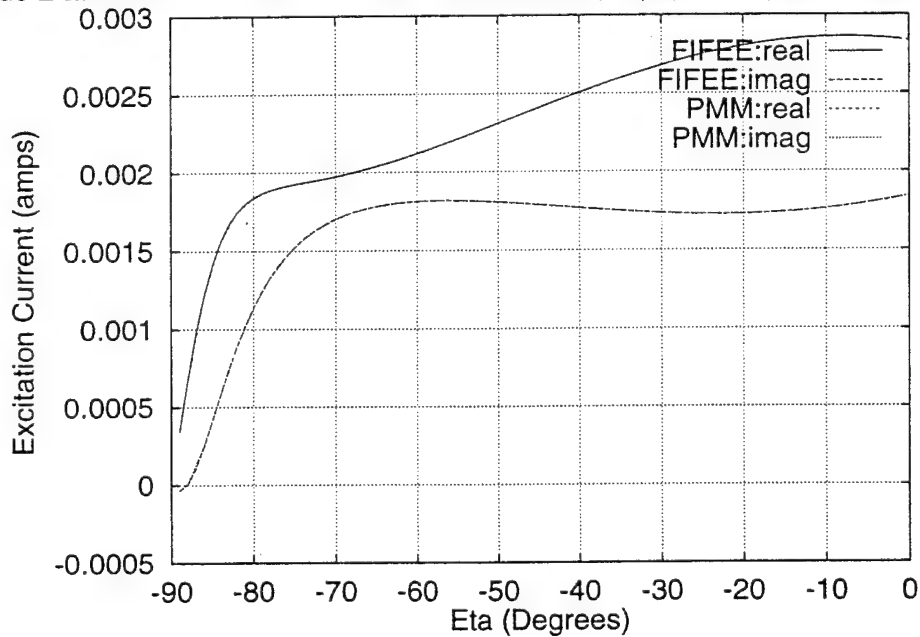


Figure 3.7 TMz, $\epsilon_e = \epsilon_3 = 4\epsilon_1$, $\epsilon_2 = 2\epsilon_1$, $d_3 = 0.2\lambda_3$, $d_2 = 0.2\lambda_2$, $\alpha = 0$.

IV. MUTUAL AND SELF ADMITTANCES FOR THIN APERTURE ELEMENTS

This chapter focuses on the self and mutual admittances presented in Equation (2-24) of Chapter 2. Here, expressions are developed which fully define the numerical calculations necessary for determining the individual entries of such an admittance matrix.

Looking back to Chapter 2, it can be noted that Equation (2-24) was obtained using the simplistic geometries pictured in Figures 2.1 and 2.2, which contain the geometry of the original problem and the "equivalent problem" geometry, respectively. Both of these figures depict a configuration that consists of two "arrays", with each "array" composed of only one slot column, and with each slot column composed of only one slot (the single slot can be visualized as a slot column having an inter-element spacing that approaches infinity). However, the FIFEE computer model is designed such that each slot column has an infinite number of identical slot elements, with a constant inter-element spacing. The more simplistic geometry of Chapter 2 was only used for the purpose of clarity in illustrating the general formulation of the solution, and was done without loss of generality. As will be discussed, generalizing the geometry of Chapter 2 such that each slot is now an infinite slot column is mathematically easy. Further, it does not change the overall form of the solution. That is:

$$[\mathbf{I}] = [\mathbf{Y}][\mathbf{V}] \quad (4-1)$$

is maintained as the applicable equation, where $[\mathbf{I}]$ is still a column vector representing the excitation of the generalized incident plane wave, $[\mathbf{V}]$ is still the desired solution vector, a column vector representing the unknown expansion coefficients of the moment method, and $[\mathbf{Y}]$ is still the admittance matrix. With respect to the general form of the

solution, the subtle difference is that now the dimensions of $[\mathbf{Y}]$ as a square matrix depend upon the total number of slot columns in the problem, rather than on the total number of individual slots. With these things in mind, and with the thought of developing the admittance equations in such a way as to give the reader more insight into the nature of the solution, the more representative geometry of Figure 4.1 is presented.

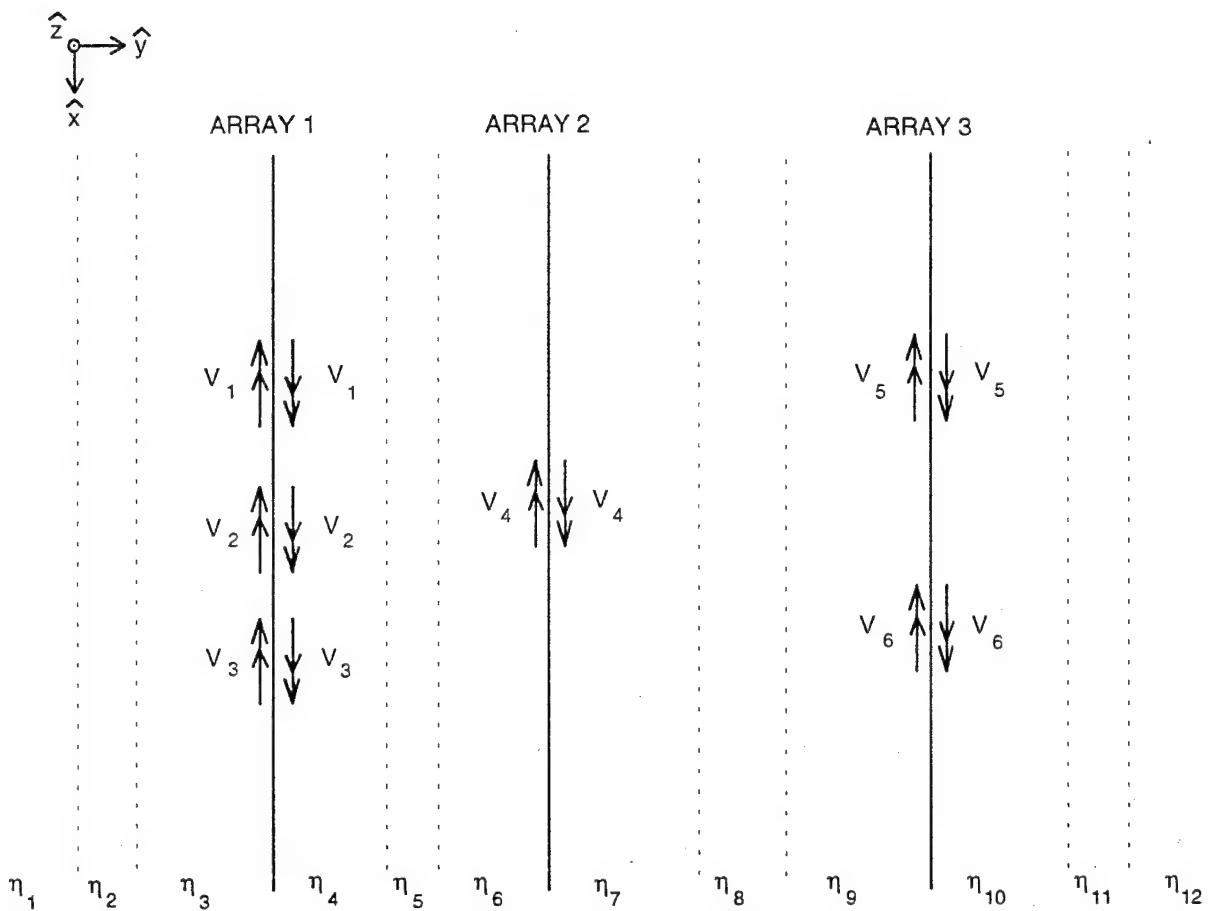


Figure 4.1 Equivalent Configuration for Three Slot Arrays: Infinite Columns of Slot Elements are Represented by User Defined Periodic Modes

Mathematical Representation of Infinite Slot Columns

In the example geometry of Figure 4.1, there are three slot arrays embedded in twelve dielectric slabs. Each slot array is considered to be composed of slots cut into a doubly infinite, infinitely thin, and perfectly conducting groundplane. The groundplane locations are depicted by solid lines; for example, the groundplane for the first array is depicted by the solid line separating slabs 3 and 4. The first slot array has three infinite columns of slots cut into it. The second array has one infinite slot column (column 4), and the third array has two infinite slot columns (columns 5 and 6). The view in Figure 4.1 is such that the infinite slot columns would extend into and out of the page. The inter-element spacing for each column is arbitrary but periodic (with identical periodicity in each column), and the inter-column spacing is arbitrary but fixed (for this illustration the exact values of these spacings are not important). Worth noting, however, is that the first and last slabs (slabs 1 and 12, respectively) can be considered as infinite halfspaces.

Figure 4.1 has been presented in the "equivalent problem" format. Thus, using Schelkunoff's surface equivalence theorem for perfect electric conductors (PECs), each slotted groundplane was wrapped in a Huygen surface and the volume inside of this surface was filled with PEC material, effectively filling in the slots in the groundplane (10). Also, the surfaces on both sides of the groundplane at the previous slot locations have been impressed with equivalent magnetic scattering currents (impressed *electric* currents cannot radiate from a PEC surface). The magnetic currents on opposite sides of a particular slot have the same magnitude, but are opposite in direction due to the opposite directions of the Huygen surface normals at these locations. Thus, each infinite slot column is represented in the equivalent problem by two infinite columns of impressed magnetic current sources, one on each side of the associated groundplane. Referring to Figure 4.1, the relative location of these infinite columns of equivalent

currents are shown as a double headed arrows, and the view is such that the columns extend into and out of the page; and although the figure depicts them to be a further away, these currents are mathematically placed an infinitely small distance away from their respective groundplane.

Groundplane Shielding and One Sided Admittances:

The matrix

equation for the solution of the configuration in Figure 4.1 is described as follows:

$$\begin{bmatrix} I_1 \\ I_2 \\ I_3 \\ 0 \\ 0 \\ 0 \end{bmatrix} = \begin{bmatrix} Y_{11} & Y_{12} & Y_{13} & Y_{14} & 0 & 0 \\ Y_{21} & Y_{22} & Y_{23} & Y_{24} & 0 & 0 \\ Y_{31} & Y_{32} & Y_{33} & Y_{34} & 0 & 0 \\ Y_{41} & Y_{42} & Y_{43} & Y_{44} & Y_{45} & Y_{46} \\ 0 & 0 & 0 & Y_{54} & Y_{55} & Y_{56} \\ 0 & 0 & 0 & Y_{64} & Y_{65} & Y_{66} \end{bmatrix} \begin{bmatrix} V_1 \\ V_2 \\ V_3 \\ V_4 \\ V_5 \\ V_6 \end{bmatrix} \quad (4-2)$$

The solution vector entries of $[V]$ have units of electric volts, the excitation vector entries of $[I]$ have units of amperes, and the units of the entries in $[Y]$ are mhos. Note that the bottom three entries in $[I]$ are zero. This is due to the fact that while the generalized incident field induces electric currents I_1 , I_2 , and I_3 in Array 1, the other arrays are not directly excited by this field; they are shielded by the groundplane associated with Array 1. In a similar manner, the groundplane of the second array shields Array 3 from Array 1; thus, the admittance terms representing interactions between Array 1 and Array 3 are identically zero, as shown in Equation (4-2).

Another effect of this "groundplane shielding" is that the interactions between columns on the same array are calculated in two stages: first between columns on the left hand side of the groundplane, and then between columns on the right hand side. The intermediate result of a particular "hand side" can be referred to as a "one sided

admittance". One sided admittances are added in parallel to get the complete mutual admittance between slot columns. That is, the desired result is obtained as follows:

$$Y_{xy} = Y_{xy}^{right} + Y_{xy}^{left} . \quad (4-3)$$

If the problem is such that the geometry is symmetric with respect to a particular groundplane, then for that groundplane $Y_{xy}^{right} = Y_{xy}^{left}$.

Filling the Admittance Matrix: Now that one sided admittances have been introduced, the general procedure used to fill in the entries of $[Y]$ is discussed. The arrays are processed from right to left, from Array #1 to Array #3. First, processing Array #1, the one sided admittances for the left side of this array are calculated, then the one sided admittances for the right side are obtained. Only columns associated with the array being processed (Array #1) are used in these calculations. These one sided admittances are then added together to obtain Y_{11} , Y_{12} , Y_{13} , Y_{22} , Y_{23} , and Y_{33} . Due to reciprocity, Y_{11} , Y_{12} , Y_{22} , Y_{13} , Y_{23} , and Y_{33} is a diagonally symmetric matrix and, thus, it is not necessary to calculate $[Y]$. Next, the mutual admittances are calculated between the columns on the right hand side of Array #1 and those columns on the left hand side of Array #2, yielding Y_{14} , Y_{24} , and Y_{34} , and thereby completing the processing of the first array. The same scheme is then applied to the second array, using one sided admittances to obtain Y_{44} , and then obtaining Y_{45} and Y_{46} . Finally, since there are no arrays to the right of Array #3, only one sided admittances are used to find the remaining non-zero entries of Y_{11} , Y_{12} , Y_{22} , Y_{13} , Y_{23} , and Y_{33} , namely Y_{55} , Y_{56} , and Y_{66} . This completes the description of the upper layer of logic used to fill Y_{11} , Y_{12} , Y_{22} , Y_{13} , Y_{23} , and Y_{33} . Still, the extension to infinite slot columns needs to be addressed so that these entries can be calculated.

Extension to Infinite Columns: The implementation concept for an infinite column of slots with finite slot periodicity is now broached by describing how an infinite slot column is defined in the FIFEE input file. Recall that the slotted elements that compose a particular infinite slot column are assumed to be identical to each other, in both shape and size. Also, since these elements are assumed to be periodic, they differ only in their spatial position in the column, which, according to Figure 4.1, would be characterized by a difference in their z coordinates. Since this spacing is known, the entire column can be geometrically specified by describing the structure of just one of these elements, henceforward referred to as the *reference element*. The physical structure of a reference element is limited to the piecewise linear connection of an arbitrary number of thin slots. Once the physical structure is decided upon, FIFEE requires the user to take the additional step of defining the mode structure (moment method) used to represent the equivalent scattering currents.

Periodic Moment Method: The moment method is a numerical technique that is commonly used to solve the integral equations developed from electromagnetic boundary conditions. Rather than solving such an equation only at discrete points on a structure, and risking that the boundary conditions are not satisfied between these points, this technique uses an inner product to force the average error over the entire structure to zero. Inherent in this approach is the use of a known basis set to construct approximations to the desired unknown functions. In the case at hand, the unknown functions are the equivalent magnetic scattering currents on the structure. This process of constructing approximations is referred to as "expanding the current with a set of basis functions", or, "with a set of modes".

Basis Functions: There are three criteria for a set of basis functions:

1. They must be able to accurately model the actual unknown current distribution,
2. They must be computationally efficient, and
3. They must be linearly independent.

Because these functions are used to construct a resemblance of the actual current, it is not wise to use basis functions that have smoother properties than that of the anticipated unknown. Rather, choosing basis functions that have properties similar to the unknown function will maximize the accuracy of the solution. Although this implies that a prior knowledge of the unknown function is required, the degree of this requirement depends on which class of basis function is used. Of the many possible sets of basis functions, there are generally two classes: *entire domain functions*, which exist over the entire domain of the function to be modeled, and *subdomain functions*, which are non zero for only part of the domain of the function to be modeled (9).

Entire Domain Basis Functions: The entire domain approach has the advantage that, when the user has prior knowledge of the function to be modeled, and uses this knowledge to choose a good basis set, an accurate solution may be found with far fewer calculations than would be required with subdomain functions. It is commonly known that the current on a dipole has primarily a sinusoidal distribution, and that the current at the ends of the dipole go to zero. Therefore, it makes sense to attempt using piecewise sinusoids (PWS) or piecewise cosinusoids (PWC) as the entire domain basis functions to predict scattering from dipoles or thin slots (via reciprocity). Because PWS and PWC basis functions are also computationally efficient and form linearly

independent sets (they meet the other two criteria), such attempts have already been made by other researchers. It is now common knowledge that these entire domain modes are indeed effective with respect to modeling the scattering from dipoles and thin slots; that is, as long as the mode lengths are never much larger than a half of a wavelength. When the nature of the function to be modeled is unknown, however, entire domain basis functions generally cannot provide accurate solutions.

Sub Domain Basis Functions: In cases where prior knowledge of the unknown function (current) is limited, the subdomain approach is most effective. This method involves segmenting the element into non-overlapping pieces (segments), and then defining the modes in conjunction with the endpoints of these pieces. For example, overlapping modes can be applied such that each mode spans two of these segments and such that the number of modes is always one less than the number of segments. This will result in having the endpoints of a given mode corresponding to the terminals of its neighboring modes, which leads to smoother approximations while still using a minimum number of modes. But that is not the only benefit of overlapping modes: properties of the basis set that are needed to deal with the ends of the structure (such as a current going to zero at the ends of a dipole) do not restrict the accuracy in the calculations of the middle segments (which might not go to zero). When using subdomain modes, the current on each mode is solved separately, and superposition is used to combine all of the answers into a single solution. Thus, there is a larger computational price to pay for implementing modes in this manner.

The Basis Set: Although FIFEE requires the user to define the mode structure, she provides the freedom to choose either the entire domain or the subdomain approach for defining modes on a reference element. This option is provided because, if the element to be modeled is electrically small enough, there is a significant

computational advantage to representing it (or its major piecewise linear segments) with a single mode. In order to effectively implement both of these approaches, prior knowledge of the unknown currents is required in order to select an appropriate basis set. Since FIFEE only deals with thin slot elements, as per the discussion above, PWC and PWS basis functions were chosen as the constructs. With these basis functions in mind, the user must specify the coordinates of the end points and of the terminals of all the modes deemed necessary to represent each reference element. The desired periodicity, dz , is also required from the user in order to completely define the geometry of the infinite columns. One additional note about user responsibilities is: In order to preserve the thin slot assumption, dielectric layers that lie next to a groundplane must be thicker than one fourth of the array's slot width. With the above information provided, and employing the fact that all propagation in a problem will be handled in the form of plane waves, FIFEE applies Floquet's theorem and extends the definition of each mode associated with a reference element out to infinity.

Floquet's Theorem: The essence of Floquet's theorem is that when an infinite periodic array is illuminated by a plane wave, the resulting scattered fields are also periodic. Refer to the cell structure in Figure 4.2. Assuming plane wave illumination, Floquet's theorem predicts that the fields in each cell will be identical except for a linear phase shift due to a common reference point. To put it another way, note the dots in the top part of the slots in cells $y+1$ and $y+2$. The theorem predicts that the field at the dot in cell $y+2$ is the same as the field in cell $y+1$ except for a phase shift, and that in general, the fields repeat themselves along the length of the column.

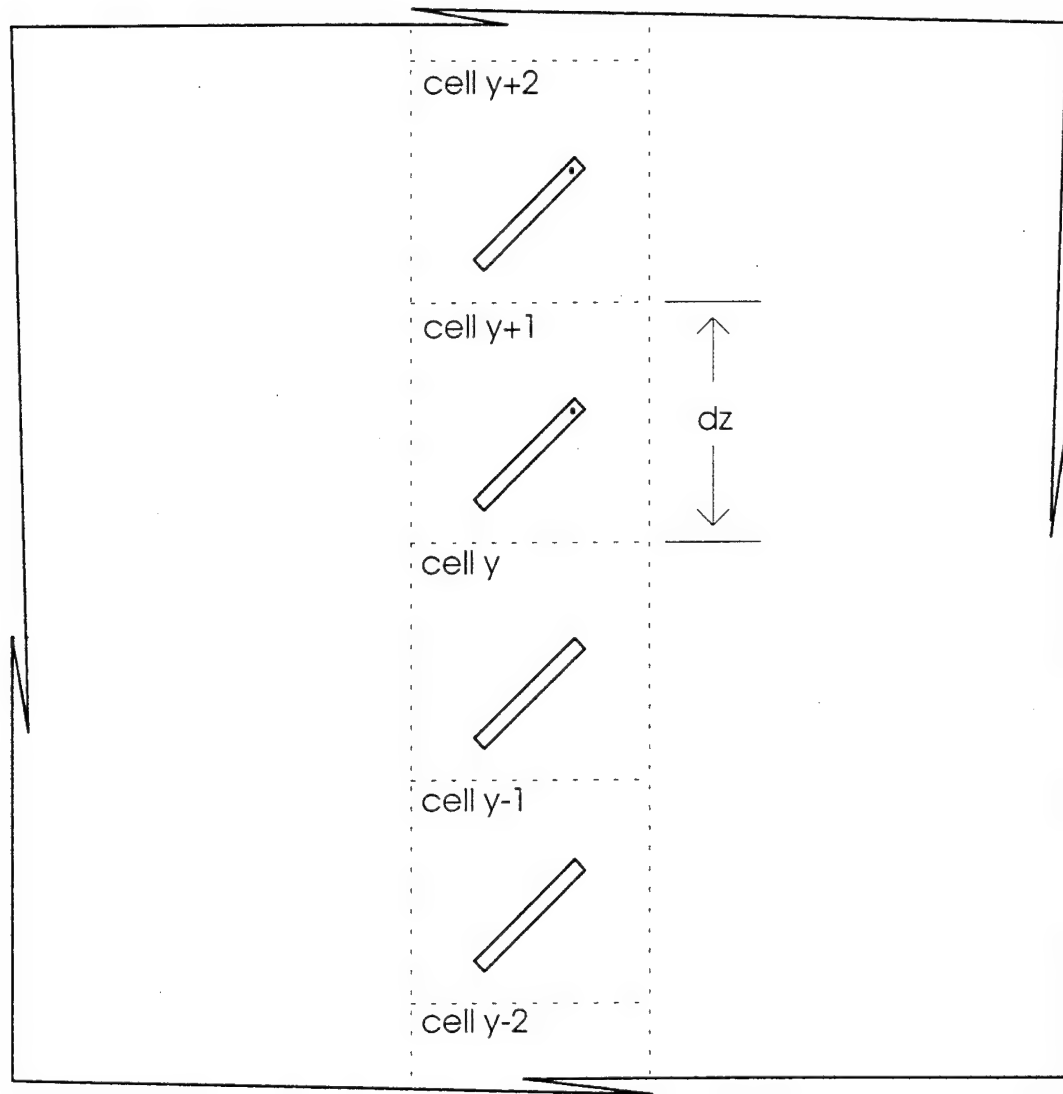


Figure 4.2 Infinite Groundplane with Periodic Slot Elements: Cell structure for infinite column of linear slots displayed for illustration of Floquet's theorem.

More explicitly, if $\overline{\mathbf{M}}(\overline{\mathbf{R}}_y)$ is the value of the current related to a specific location in the slot of cell y , then the value of the currents in other cells at the same location in their respective slot is given by:

$$\overline{\mathbf{M}}(\overline{\mathbf{R}}_{y+m}) = \overline{\mathbf{M}}(\overline{\mathbf{R}}_y) e^{-j\beta m \cdot dz \cdot s_z} \quad (4-4)$$

where the $\bar{\mathbf{R}}$'s are position vectors. The exponential in Equation (4-4) is referred to as the Floquet phase factor. Note that the phasing is linearly dependent on the z translation, which is represented by $m \cdot dz$ (s_z is a constant associated with incident direction of the plane wave). Therefore, once the currents associated with the modes of a reference element are known, periodicity is used to construct the currents at any desired location along the column. That is, by letting the basis functions cycle with the same periodicity as the cells, the Floquet phase factor can be used in conjunction with these basis functions to construct the appropriate approximation for the scattering current due to any cell along the infinite column. Thus, periodic basis functions are defined, and are used to extend the definitions of each reference element to that of an infinite columns. Mathematically, an infinite summation from $-\infty$ to ∞ is used to process the "cells" of the periodic basis functions associated with each infinite column. In this manner, the single slot geometry of Chapter 2 is extended to a geometry of infinite slot columns. This particular implementation of the moment method is referred to as the Periodic Moment Method.

It should be noted that each column's reference element is represented in the moment method calculations by one or more magnetic current modes, and that the number of modes used in a successful representation depends on the electrical size of the element and the manner in which the piecewise linear slots are connected. In cases where more than one mode is used, the definition of each of these modes is extended to an infinite periodic column of like modes. In this manner, the geometry of a particular infinite column of elements is actually modeled in the code by using multiple periodic modes, each of which can be considered as an infinite radiating column. The discussion above has implied that the notation Y_{ab} represents the mutual admittance (or self admittance for $a=b$) between two infinite slot columns a and b in a slotted groundplane geometry. If the slots in the column are linear with a length that is roughly less than $\lambda/2$, then when the moment method is applied, only one periodic mode is needed to model the

magnetic scattering current associated with the column. In this case, Y_{ab} is a number to be calculated. In general, however, more than one periodic mode is needed to model a slot column's current because of the electrical size of the reference element or because this element is composed of more than one linear segment. In this case, Y_{ab} is a matrix whose entries are the admittance values between all the modes that define both columns. Thus, if column "a" is defined using two modes and column "b" is defined using three, then Y_{ab} is a 5x5 matrix whose entries represent the mutual and self admittances for the 5 infinite columns of periodic modes (5 infinite radiating columns) used to represent columns "a" and "b".

Truncated Testing Functions: It was mentioned earlier that the moment method uses inner products to force the average error to zero over the entire structure to be modeled. These inner products are formed between periodic basis functions and other entities called testing functions. In order to calculate the mutual coupling between two infinite columns of modes, it is convenient to consider one as the transmitting column and the other as the receive column. More particularly, let the transmitting column be represented by a periodic basis function, and consider the testing function as a mathematical instrument to represent the receive column. Then, the desired mutual coupling is nothing more than the inner product between the testing function and the field radiated by the infinite basis function.

To form a clear picture of the analysis, it is helpful to imagine every element of the transmitting column radiating to the reference element of the receive column. In the spatial domain, the more distant a transmitting element is from the reference element, the more negligible the coupling effect of its radiation is. Thus, there is a point where the outer terms of this infinite sum of radiating fields can be neglected, leading to a finite, yet accurate, sum. Using this method, or a similar method in the spectral domain, the

coupling between the infinite column and the reference element of the receive column can be calculated. Then, if the receive column is also periodic with the same periodicity as the transmitting column, the Floquet phasing factor can be used to determine the mutual coupling sensed over its entire length. This can be done because, since both columns are infinite with the same periodicity, any receive element is an equally valid reference element. That is, no matter which element is chosen as the reference element, the coupling result will be the same, and this function will vary periodically over the receive column according to the Floquet phase factor. Thus, by restricting all columns of all arrays to having the same inter-element spacing, the reference element cell of any receive column (and its associated non-periodic modes) is the only cell that need be considered.

One way to view this implementation is to picture the testing function modes as non-zero for the reference element only, rather than being infinitely periodic as in the case of the basis functions. This perspective gives rise to the idea of a "truncated testing function". One last note is worth mentioning. At some point in the calculations, a given column will play the role of a receiver and, at another point, that of a transmitter. Thus, the same reasons that led to a choice of basis functions also apply to choosing the testing functions. As a result, in this model, PWS are always used as testing functions.

Array Scanning Method

The last section stated the need to determine the radiation from a transmitting periodic column mode, with the objective being to determine the mutual coupling between two infinite column modes. For coupling between such modes in a stratified dielectric medium, the classical approach would first determine the Green's function that meets the boundary conditions for all of the interfaces. Even when this function is found,

which is no simple task since the computer code must allow an arbitrary number of dielectric slabs and groundplanes, the resulting Sommerfeld integrals will be highly oscillatory. The computational expense to solve such integrals to any degree of accuracy is extreme. As an alternative to this approach, Skinner (6) successfully employed a completely rigorous formulation called the Array Scanning Method (ASM) to calculate the mutual coupling between infinite columns of \hat{z} oriented linear slot elements. This method is adopted here to account for coupling between the modes of arbitrary, yet piecewise linear, planar slot elements.

Although the ASM does avoid Sommerfeld integrals, it also produces an integral that becomes singular at times. These singularities have the physical interpretation of being resonances associated with surface wave formations in the dielectric slabs. Mathematically, they occur when the denominator of a T factor goes to zero. FIFEE addresses this difficulty by inserting a slight loss tangent for the \hat{y} components of plane wave propagation in each dielectric layer. In this manner, the formerly singular terms are finely integrated to accurately capture the now finite peaks of the "singularity".

To explain the ASM, consider the following: The total magnetic vector potential of a doubly-infinite array of Hertzian dipole sources (with periodic spacing) may be written in the form of an exponential Fourier series as

$$\bar{dA} = \sum_{q=-\infty}^{\infty} \bar{dA}_q e^{-jq\beta D_x s_x} \quad (4-5)$$

\bar{dA}_q represents the coefficients in the series, and also has the interpretation of being the total magnetic vector potential due to the q th infinite column of sources. Put another way, the doubly infinite array is composed of an infinite number of infinite columns, and \bar{dA}_q represents the potential of the infinite column identified by the index q . In the above equation, β is the wave number, D_x is the periodic spacing between the infinite

columns of the doubly infinite array, and s_x is the x component of the propagation direction of the incident plane wave. The unit vector depicting plane wave propagation is fully given by:

$$\hat{s} = s_x \hat{x} + s_y \hat{y} + s_z \hat{z} \quad (4-6)$$

Note that for \hat{s} to maintain its unit vector definition and for its components to be real valued (corresponding to propagation in real space), the components of \hat{s} have the following restriction:

$$-1 \leq s_x, s_y, s_z \leq 1 \quad (4-7)$$

Using the Fourier method, the vector potential for any of these columns, that is, for the q th column, is given by

$$d\bar{A}_q = \frac{1}{T} \int_{-T/2}^{T/2} (d\bar{A}) e^{jq\beta D_x s_x} ds_x \quad (4-8)$$

where the period of the Fourier series is

$$T = \frac{\lambda}{D_x} \quad (4-9)$$

Choosing the reference element of the doubly infinite array such that it resides in the $q=0$ column, the magnetic vector potential of this single column of sources is

$$d\bar{A}_0 = \frac{D_x}{\lambda} \int_{\frac{-\lambda}{2D_x}}^{\frac{\lambda}{2D_x}} (d\bar{A}) ds_x \quad (4-10)$$

where the integrand is the total vector potential from the complete doubly infinite array of sources. Thus, the magnetic vector potential from a single periodic column of sources can be derived from a doubly infinite array that is composed of an infinite number of

these columns. That is, for a doubly infinite array with a given inter-element spacing for its columns and some arbitrary, but constant, inter-column spacing, the vector potential due to a single column of this array can be derived from the vector potential of the entire array using Equation (4-16).

Although Equation (4-16) is written for magnetic vector potentials, it is generically representative of the ASM. Completely analogous results can be derived for Hertzian arrays of slots by using equivalent magnetic current sources and the electric vector potential. Also, because the integration in Equation (4-16) is with respect to the plane wave parameter s_x , spatial integrals and spatial derivatives can freely be moved in and out of this integration; they have no effect on the integration with respect to s_x .

Thus, integration can be used to extend the above results from Hertzian elements to slots or dipoles of finite length. And the curl operator can be used to find the fields of single columns. Similarly, since the desired mutual coupling is obtained from the inner product of the field radiated by a periodic basis function and of the testing function, Equation (4-16) can be extended for admittances. To do so, let Y_0 be the admittance between a transmitting column mode and the truncated testing mode of the receive element. And, constructing a doubly infinite planar array using this column mode and an inter-column spacing of D_x , let Y be the admittance between this doubly infinite array and the same truncated testing mode of the receive element. Then,

$$Y_0 = \frac{D_x}{\lambda} \int_{\frac{-\lambda}{2D_x}}^{\frac{\lambda}{2D_x}} Y ds_x \quad , \quad (4-11)$$

where λ is the wavelength in the dielectric slab abutting the groundplane (and the associated transmitting mode). This dielectric slab is the same region for which the s_x parameter is valid. In this application, D_x is chosen to be $\lambda/2$ such that the limits of integration become -1 and 1, which are the limits of s_x for this component of propagation

to exist in real space (see Equation (4-7)). Substituting this value of D_x into Equation (4-11) yields

$$Y_0 = \frac{1}{2} \int_{-1}^1 Y ds_x \quad . \quad (4-12)$$

By solving for Y_0 , the mutual (or self) admittance between two infinite columns of magnetic current modes can be found. This is a straightforward procedure once the admittance Y from the doubly infinite planar array is known. Before the equation for Y is presented, consider the geometry of Figure 4.3. The small circle labeled with a "t" and located next the first groundplane represents the transmitting mode. The center of the reference cell for this transmitting mode is located at the position vector

$$\bar{\mathbf{R}}^t = x_t \hat{x} + b_{m-1} \hat{y} + z_t \hat{z} \quad . \quad (4-13)$$

The small square labeled with an "r" and located to the left of the second groundplane represents the receiving mode. The terminals of the receiving mode is located at the position vector

$$\bar{\mathbf{R}}^r = x_r \hat{x} + b_n \hat{y} + z_r \hat{z} \quad (4-14)$$

Figure 4.3 shows the case where the receiving mode is located to the right of the transmitting mode, and as such, $R_y^r = b_n$. For cases where the receive mode is located on the same groundplane as the transmitting mode, R_y^r is modified so that the position vector is given by

$$\bar{\mathbf{R}}^r = x_r \hat{x} + b_{m-1} \hat{y} + z_r \hat{z} \quad (4-15)$$

or in the self admittance case, by

$$\bar{\mathbf{R}}^r = x_r \hat{x} + (b_{m-1} + a) \hat{y} + z_r \hat{z} \quad (4-16)$$

where a is one fourth of the width of the thin slot segments that compose the reference element, in accordance with the thin slot assumption.

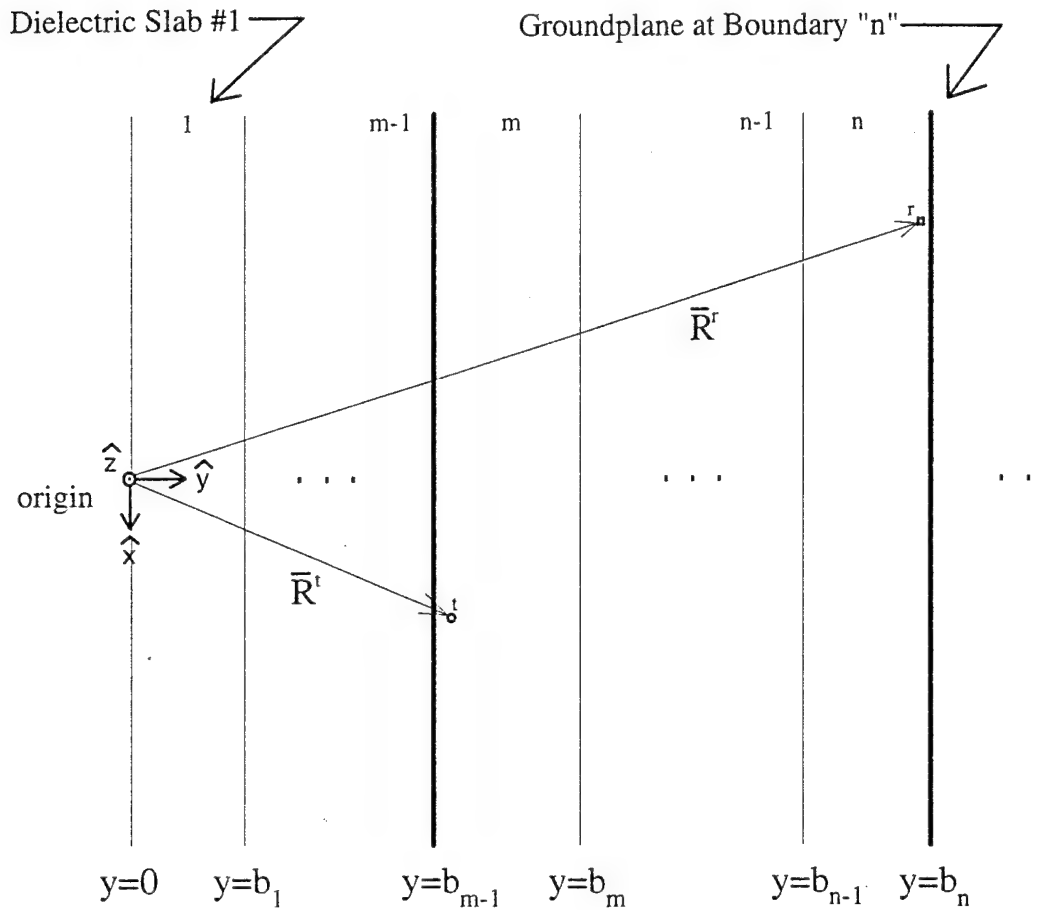


Figure 4.3 General Geometry for Coupling Between Slot Modes in a Stratified Dielectric Medium

The mutual impedance between doubly infinite planar arrays of dipoles was derived by Munk (4), with the resulting expression consisting of a doubly infinite sum of plane waves. Thus, the mutual admittance Y between doubly infinite planar arrays of

slots can be obtained as a spectrum of plane waves by applying duality to Munk's result, which yields:

$$Y = \frac{Y_m}{2D_{x_i}D_{z_i}} \sum_{k=-\infty}^{\infty} \sum_{n=-\infty}^{\infty} e^{-j\beta_i(b_m\hat{y}-\bar{\mathbf{R}}^t)\hat{\mathbf{r}}_i} e^{-j\beta_r(\bar{\mathbf{R}}^r-b_{n-1}\hat{y})\hat{\mathbf{r}}_r} \quad (4-17)$$

$$* \Phi_{m,n} \left[\frac{P'_{\perp,m} P'_{\perp,n} T_{\perp,m,n}}{r_{y_n}} + \frac{r_{y_m}}{r_{y_n}} \frac{P'_{\parallel,m} P'_{\parallel,n} T_{\parallel,m,n}}{r_{y_n}} \right]$$

There are several parameters in Equation (4-17) that need clarification. Y_m is the intrinsic admittance of the dielectric slab closest to the transmitting mode. D_{x_i} is the inter-column spacing, and D_{z_i} is the column inter-element spacing, both with respect to the doubly infinite transmit array. β_i and β_r are the wave numbers in the dielectric slabs closest to the transmitting and receiving modes, respectively. The unit vectors $\hat{\mathbf{r}}_i$ and $\hat{\mathbf{r}}_r$ give the directions of the plane waves in the slabs closest to the transmitting and receiving modes, respectively. The general form for these unit vectors is:

$$\hat{\mathbf{r}} = \left(s_x + \frac{k\lambda}{D_x} \right) \hat{\mathbf{x}} + r_y \hat{\mathbf{y}} + \left(s_z + \frac{n\lambda}{D_z} \right) \hat{\mathbf{z}} \quad (4-18)$$

where r_y normalizes the unit vector and is chosen with the -j square root for evanescent plane waves (for imaginary square root). That is,

$$r_{y_i} = \sqrt{1 - r_{x_i}^2 - r_{z_i}^2} \quad , \quad (4-19)$$

where the subscript i represents t or r , respectively. Note that, as described in Chapter 3, this implementation of FIFEE requires the plane of incidence to be the x - y plane. Since $s_z = -\sin\alpha \sin\eta$, and $\alpha = 0$ when the x - y plane is the plane of incidence, Equation (4-18) can be re-written as

$$\hat{r} = \left(s_x + \frac{k\lambda}{D_x} \right) \hat{x} + r_y \hat{y} + \frac{n\lambda}{D_z} \hat{z} . \quad (4-20)$$

Propagation directions in the other dielectric layers are found by applying the following two equations:

$$r_{x_i} = r_{x_t} \frac{\beta_t}{\beta_i} \quad (4-21)$$

$$r_{z_i} = r_{z_t} \frac{\beta_t}{\beta_i} \quad (4-22)$$

Note that r_{y_i} does not have a similar relation but must be found from Equation (4-19).

Looking back to Equation (4-17), the parameter $\phi_{m,n}$ accounts for the phase delay from groundplane "m" to groundplane "n", and is given by:

$$\phi_{m,n} = \prod_{i=m}^n e^{-j\beta_i d_i \hat{r}_{y_i}} \quad (4-23)$$

where d_i represents the thickness of the appropriate dielectric slab. The P 's again represent pattern factors, and are the same as those addressed in Chapter 3 and Appendix B. The T factors again account for the complete transition of the fields through the dielectric layers, except for the associated phase delay, which is accounted for by Equation (4-24). However, because the geometry being considered is more general in this section, the form of the T factors is also more general (compared to the last chapter). The T factors are obtained via the following equation:

$$T_{m,n} = \frac{2 \left[1 + \Gamma_{n,n+1}^{eff} e^{-j2\beta_n (b_{n\theta n} - R_y') r_{y_n}} \right]}{\left[1 - \Gamma_{m,m-1}^{eff} \Gamma_{m,m+1}^{eff} e^{-j2\beta_2 d_2 r_{y_2}} \right]} \tau_{m,n}^{eff} \quad (4-24)$$

The above equation applies to both parallel and perpendicular polarizations; to solve for a given polarization, it is only necessary to place the appropriate polarization symbol on all

Γ and τ references which occur on the right hand side of the equation. In Equation (4-24), b_{right} refers to the boundary to the right of the receiver's location. This definition is made general to account for the other two scenarios not shown in Figure 4.3, but which are referenced in Equations (4-15) and (4-16). With respect to the geometry that is shown in Figure 4.3, the receiver is taken to be just to the left of $y = b_n$, an infinitely small distance away. Thus, $b_{right} = b_n$. Therefore, in this case, the exponential term associated with b_{right} goes to one, since R'_y also equals b_n . When the receive mode is located on the same groundplane as the transmit mode, the boundary to the right (with respect to Figure 4.3) is $y = b_m$. Note that there are two possible definitions for R'_y in this case. Also to be noted for this case is that the effective transmission coefficient (the τ on the far right of the above equation) is identically one. Although the effective transmission coefficients were discussed and defined in Chapter 3, it is worth noting that

$$\tau_{m,n}^{eff} = \tau_{m,m+1}^{eff} \tau_{m+1,m+2}^{eff} \cdots \tau_{n-1,n}^{eff} \quad (4-25)$$

Now that Equation (4-17) has been clarified, it is substituted into Equation (4-16), where D_{x_t} has been set equal to $\lambda_t/2$, with the result being:

$$Y_0 = \frac{Y_m}{2D_{z_t}\lambda_t} \sum_{k=-\infty}^{\infty} \sum_{n=-\infty}^{\infty} \int_{-1}^1 e^{-j\beta_t(b_m\hat{y}-\bar{R}')\hat{r}_t} e^{-j\beta_r(\bar{R}'-b_{n-1}\hat{y})\hat{r}_r} \quad (4-26)$$

$$* \phi_{m,n} \left[\frac{P'_{\perp,m} P'_{\perp,n} T_{\perp,m,n}}{r_{y_n}} + \frac{r_{y_m}}{r_{y_n}} \frac{P'_{\parallel,m} P'_{\parallel,n} T_{\parallel,m,n}}{r_{y_n}} \right] ds_x$$

The above equation defines the numerical calculations necessary for determining the individual entries of the admittance matrix. The integral associated with the inner product of the basis function and the testing function is buried inside the pattern factors, and the dependence on k and n is buried inside the \hat{r} vectors.

Validation of Admittance Calculations

To verify that the FIFEE is correctly calculating the column to column admittance data, the following numerical experiment was performed for several geometrical configurations. A finite by infinite array is constructed by applying a constant inter-column spacing, D_x , to a finite number of infinite columns, say 50. Next, the one-sided self admittance is calculated for the first column, and then the one-sided mutual admittance is sequentially calculated between the first column and every other column, proceeding from column 2 to column 50. All the geometrical configurations considered consisted of one groundplane in a symmetrical dielectric sandwich; thus, the one-sided scan admittances data was then multiplied by two to obtain the total admittance data. Each data point, which was collected at increasing integral multiples of D_x , was then spatially multiplied by the appropriate Floquet phase factor, with this phase factor being linearly dependent on $m \cdot D_x$, with m representing the column number. This data, when added sequentially from 1 to 50, forms a partial sum, whereas an infinite number of columns would need to be added to construct the infinite series associated with this partial sum. Since PMM models an infinite number of infinite columns, its calculated value for the self admittance of such a doubly infinite array should be equal to the infinite series just described. This numerical experiment uses the partial sum in conjunction with an algorithm designed to accelerate the convergence of infinite sums. That is, the partial sum is used as input to an algorithm that predicts the convergence of the related infinite sum. Thus, if FIFEE is calculating the admittance data correctly, the acceleration of her partial sum will compare favorably with the PMM data described above. Also, to expand the validation methodology, the same infinite sum acceleration technique was applied to Skinner's model, KAHUNA, for added comparison on the linear slot cases.

Two different algorithms are used here to accelerate partial sum convergence (two, in order to ensure correct implementation of the concept). One is based on the Fejer kernel, which is a simple triangular windowing function, and the other is Shanks' transformation. Both are discussed thoroughly in Appendix A of Skinner's dissertation (6). Shanks' transformation generally gives quick convergence on a series which oscillates about some convergence point, which is a characteristic of an infinite array problem in the spatial domain; spectral domain sums tend to converge monotonically. As will be seen, better results are achieved with Shanks' transformation, particularly at high scan angles where the calculations are more sensitive and, generally, a larger partial sum is needed to obtain a specified accuracy.

The geometry shown in Figure 4.4 was used for the first experiment. For FIFEE and KAHUNA, 50 infinite slot columns were defined on the array groundplane. For PMM, its reference element for a double infinite array was defined accordingly. The calculations described above were made at one degree increments of scan angle (scanning in the x - y plane). The real components of the results are plotted in Figure 4.5, while the imaginary components are given in Figure 4.6.

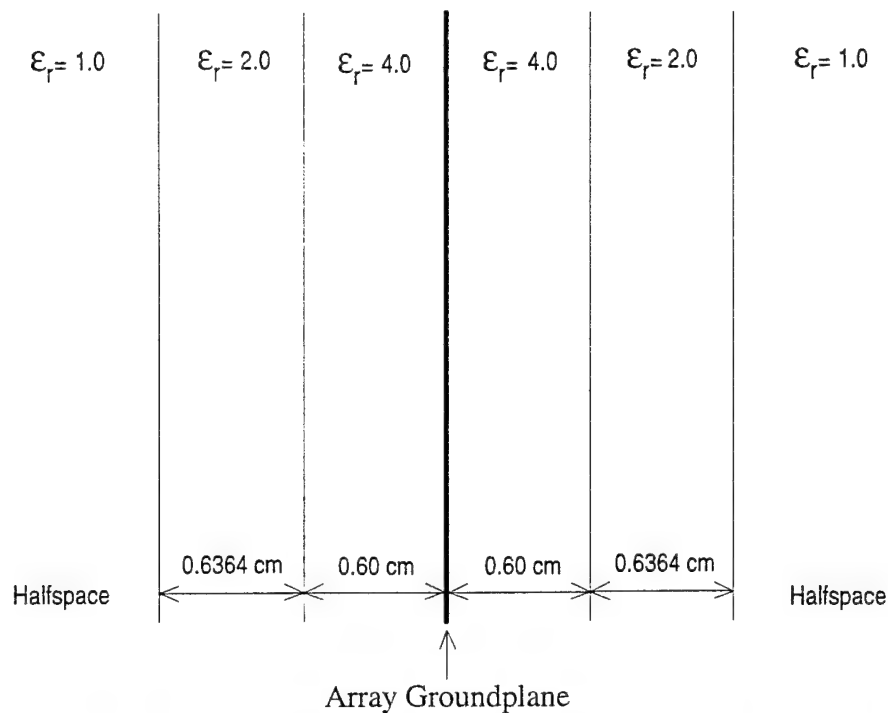


Figure 4.4 Vertical Slot Geometry: Slot Length=0.67 cm, Slot Width=0.067 cm, Dx=0.675 cm, Dz=1.125 cm, Frequency=10 GHz.

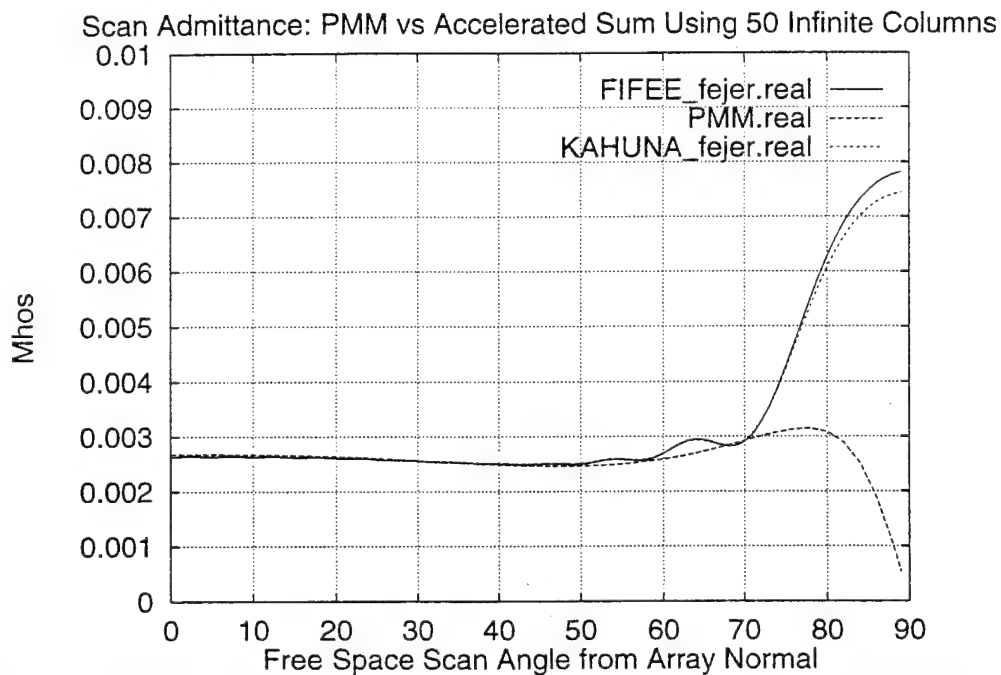


Figure 4.5 Infinite Columns of Vertical Slots: Comparing Real Components of FIFEE, KAHUNA, and PMM Using Geometry in Figure 4.4.

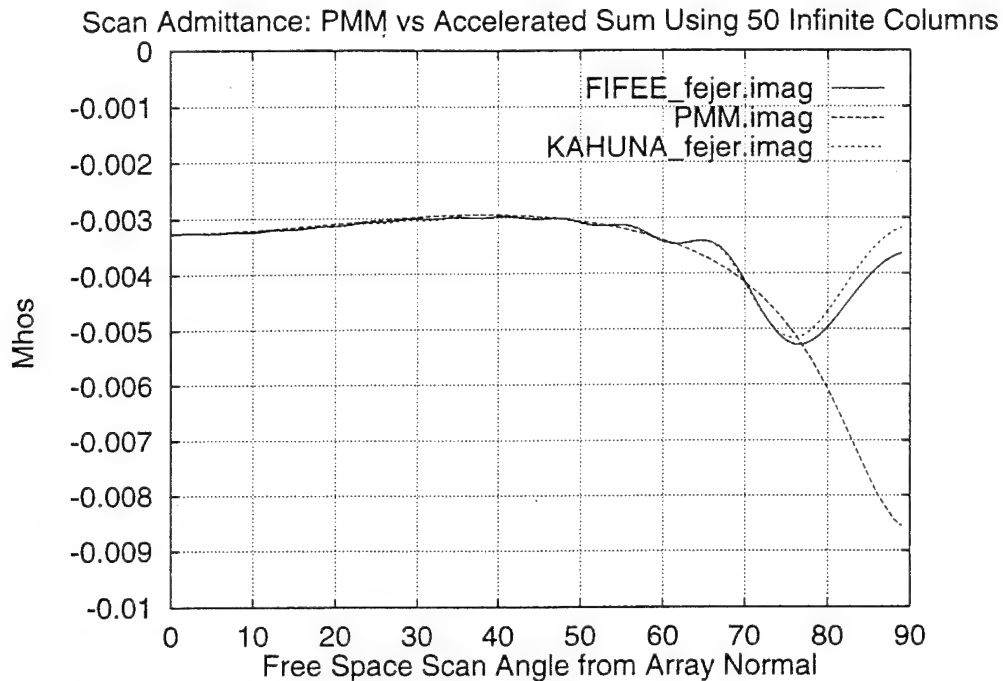


Figure 4.6 Infinite Columns of Vertical Slots: Comparing Imaginary Components of FIFEE, KAHUNA, and PMM Using Geometry in Figure 4.4.

Note that there is a high correlation between the results of FIFEE and KAHUNA for all scan angles, while there is excellent agreement between all three codes for the lower scan angles. This gives confidence that FIFEE is calculating the admittance data correctly for vertical polarization, and that she is also correctly handling multiple slab geometries.

To demonstrate that the calculations involved in this method of comparison are more sensitive at higher scan angles, thereby requiring larger partial sums to achieve the same accuracy, this experiment was repeated using 100 columns. The results are shown in the following two figures, where it can be seen that the agreement has indeed improved at the higher angles. Also, Shanks' transformation was implemented on the FIFEE data to demonstrate its superior convergence properties for these types of series. Because it leads to a significantly higher correlation with the PMM data, the Shanks' transformation will be the sole acceleration routine used in the remainder of this chapter.

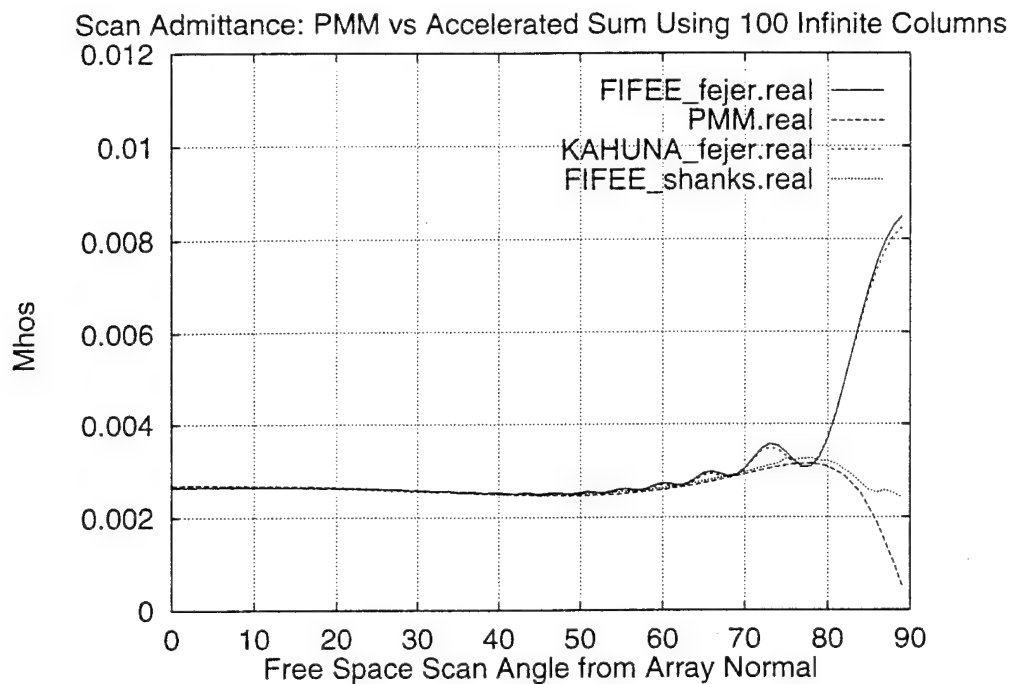


Figure 4.7 100 Infinite Columns of Vertical Slots: Comparing Real Components of FIFEE, KAHUNA, and PMM Using Geometry in Figure 4.4.

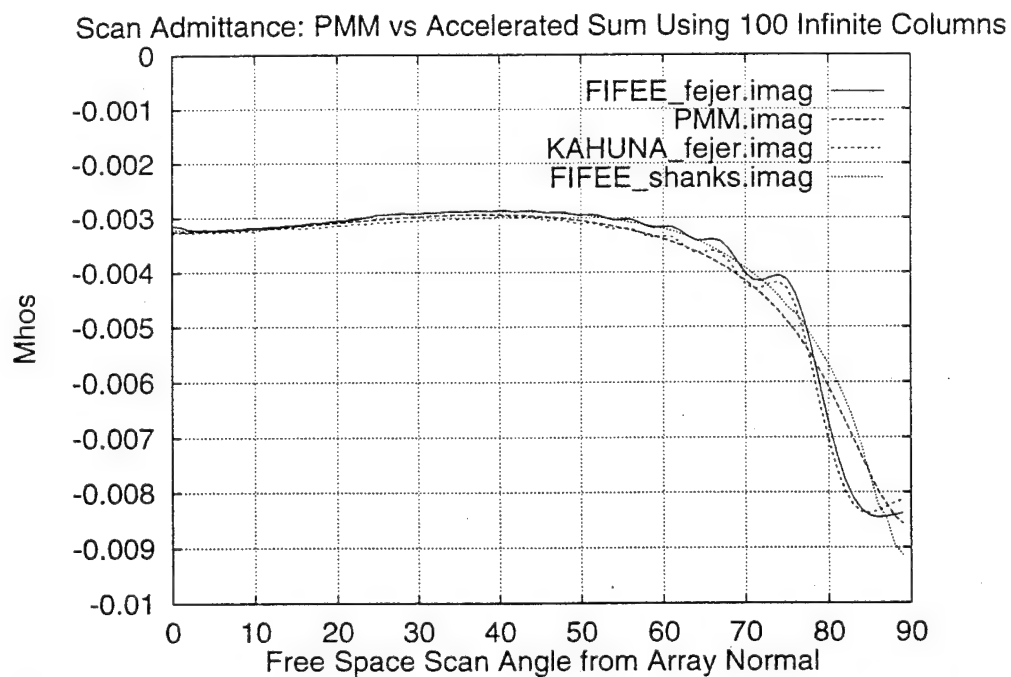


Figure 4.8 100 Infinite Columns of Vertical Slots: Comparing Imaginary Components of FIFEE, KAHUNA, and PMM Using Geometry in Figure 4.4.

The next set of calculations was performed on an almost identical geometry, except that, instead of vertical slots, horizontal slots were used. The geometry is shown in Figure 6.6. The purpose of exploring this configuration is to demonstrate that FIFEE is calculating the admittance data correctly for vertical polarization. This time, only 50 column to column mode admittances were spatially added with \hat{x} directed Floquet phasing factors (before sum acceleration). As can be seen in Figure 4.10, there is excellent agreement between this method and results from the PMM code, where the doubly infinite plane wave expansion method is used.

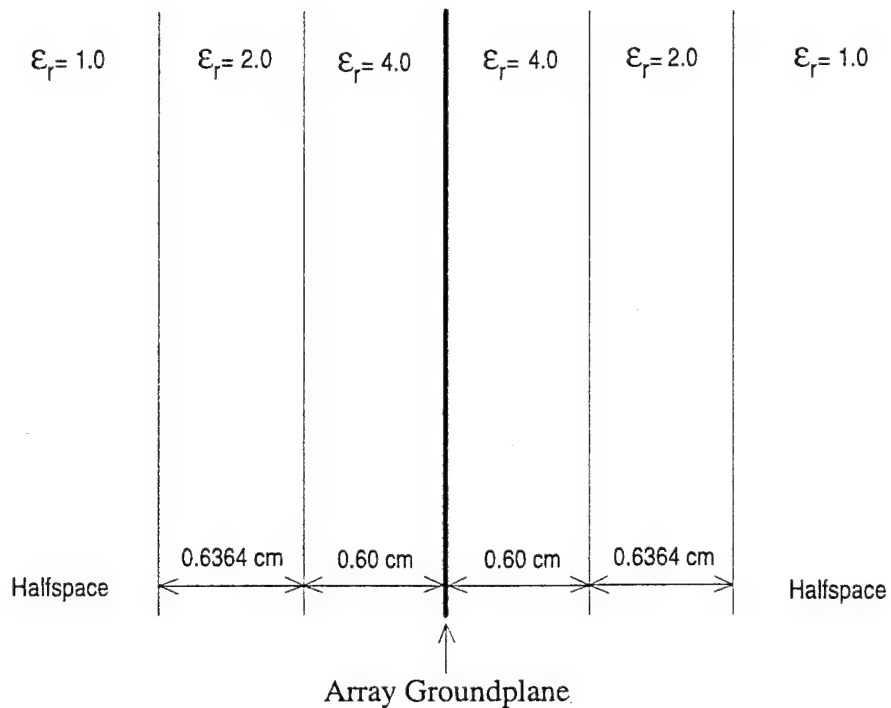


Figure 4.9 Horizontal Slot Geometry: Slot Length=0.75 cm, Slot Width=0.075 cm, Dx=1.125 cm, Dz=0.675 cm, Frequency=10 GHz.

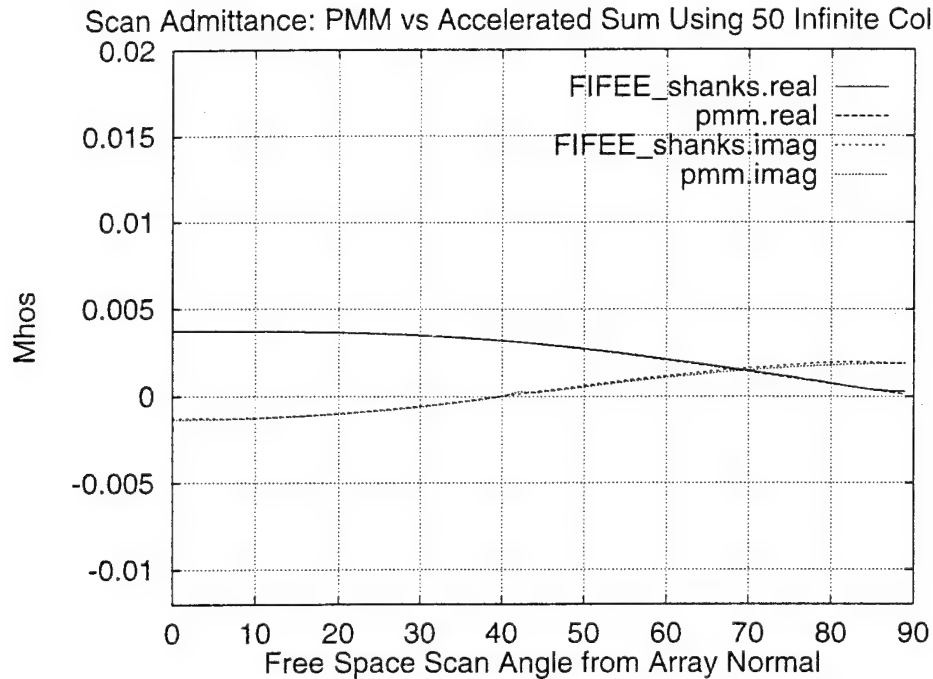


Figure 4.10 Infinite Columns of Horizontal Linear Slots: Comparing FIFEE and PMM Using Geometry in Figure 4.9.

The next configuration that was explored was identical to the horizontal slot example (above), except that the slots were rotated forty five degrees counterclockwise to vertical. This demonstration is aimed at showing that FIFEE is decomposing dual polarized elements into the correct horizontal and vertical components. The results are shown in Figure 4.11. Again, the predictions match most favorably, with only minor deviations being at high scan angles, which could be improved by using more columns.

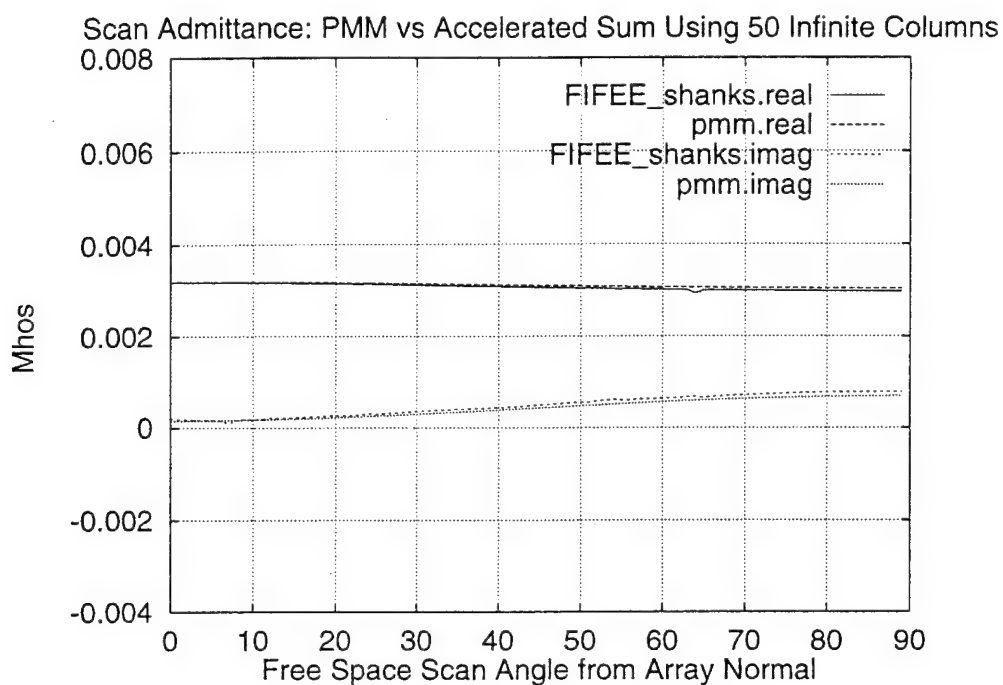


Figure 4.11 Infinite Columns of Slots Rotated 45 Degrees from Horizontal: A Comparison Between FIFEE and PMM Using Geometry of Figure 4.9.

The next configuration is the same as the previous one, except that the dielectric slabs closest to the array are extended out to infinity, so that the slotted array is now sandwiched by two halfspaces, each with a relative dielectric constant of 4.0. The double slab configuration was removed to show that FIFEE is generating correct data for minimal dielectric configurations. The results for this run are shown in Figure 4.12.

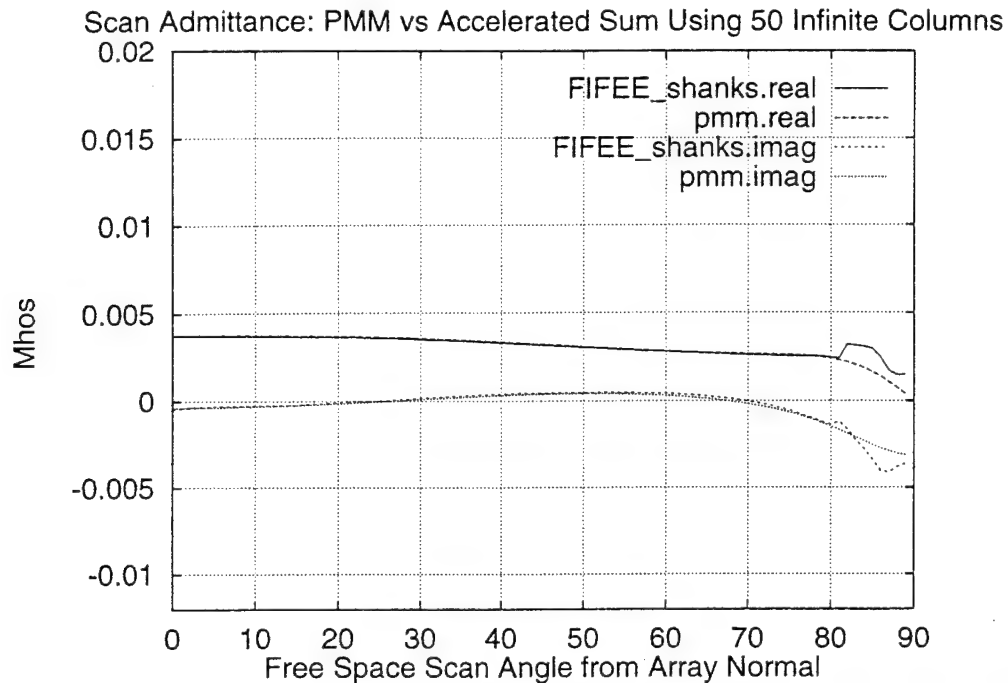


Figure 4.12 Infinite Columns of Linear Slots Rotated 45 Degrees from Horizontal. No Slabs, Two Infinite Halfspaces. Slot Elements According to Figure 4.9.

The previous illustrations were all examples of linear slots. To demonstrate that FIFEE handles bent modes correctly, the configuration of the last example was modified such that the top half of the 45 degree slots were bent to vertical. Also for this occasion, the double slab sandwich was re-installed, with each slab having a thickness of 0.1 times the wavelength in the slab (this form of input tested out a feature of the input parser - its ability to handle user defined variables in the input file). The results for 50 such columns (as just described) are given in Figure 4.13, where it is compared to PMM data. Again, there is a high correlation between the two, with the only deviations coming at the highest of scan angles. Figure 4.14 shows results for when the number of columns in the FIFEE input file is increased to 100. As expected, the agreement at the higher scan angles was improved.

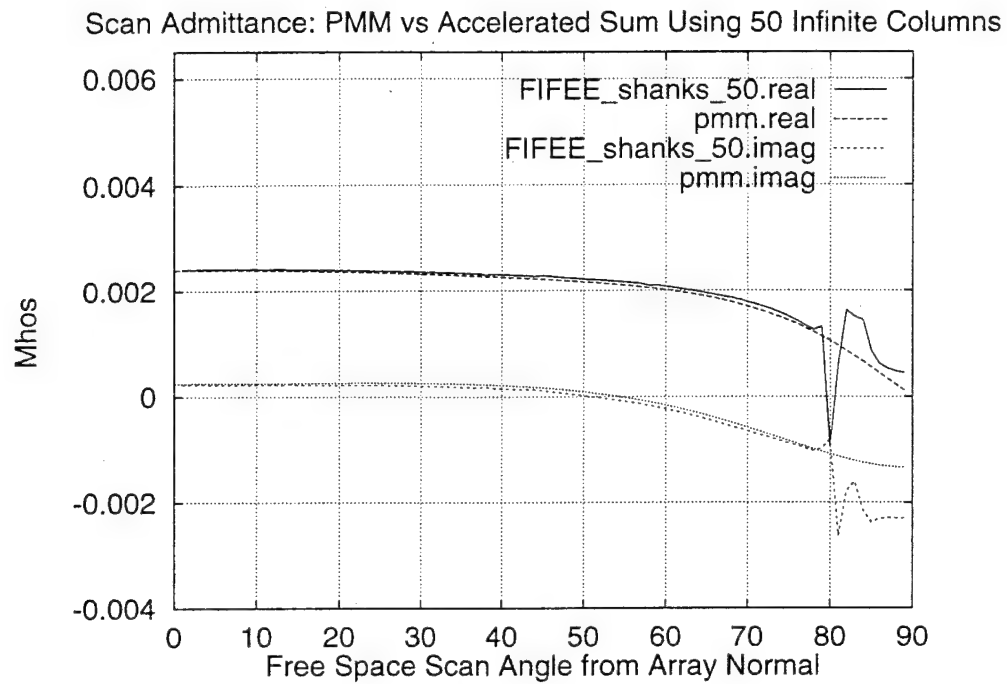


Figure 4.13 Infinite Columns of Bent Slots: Comparing FIFEE and PMM.

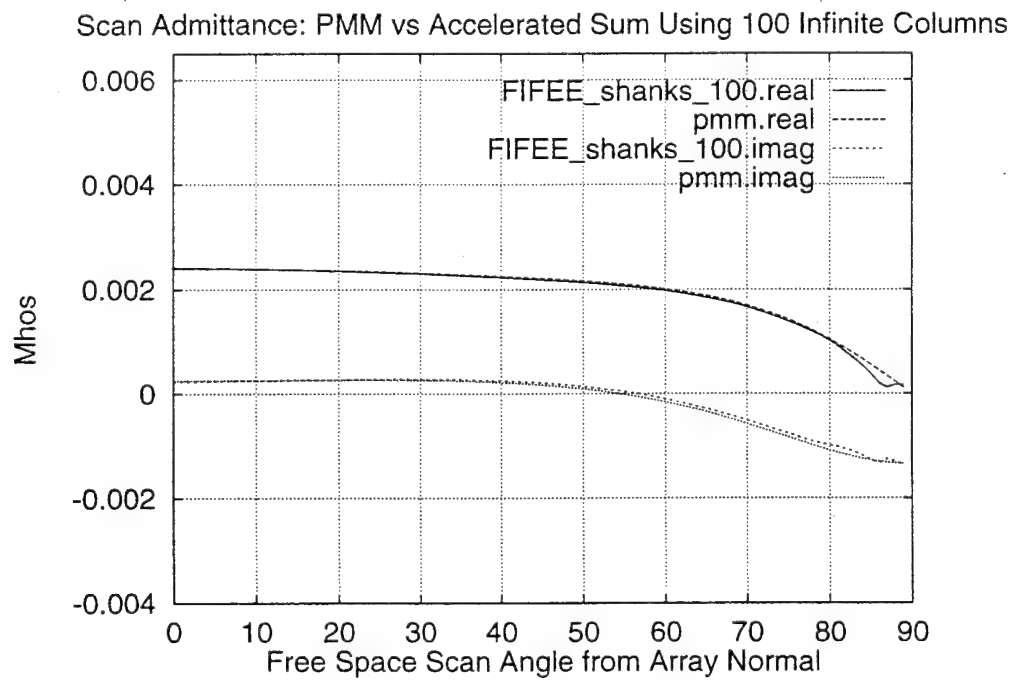


Figure 4.14 100 Infinite Columns of Bent Slots: Comparing FIFEE and PMM.

The previous set of data runs successfully tested all of the major code components of FIFEE that deal with calculating the admittance matrix. This includes calculation of the T factors, of the pattern factors, and of plane wave phasing. These runs also indicate that the truncations of the infinite sums are being performed accurately. The bottom line is that the admittance calculations performed by FIFEE can be used to generate confident scattering predictions.

V. FAR ZONE SCATTERED FIELDS

Now that the moment method solution for the equivalent magnetic scattering currents of an FSS has been obtained, it is desired to obtain the far zone scattered fields of these currents. In this chapter the far zone field equation is derived, and is shown to be applicable for both forwardscattered and backscattered fields. For backscattered fields, the far zone equation accounts for a magnetic scattering current on the left hand side of the first groundplane (array) radiating through an arbitrary number of dielectric layers and into the far field of Region I. Superposition can then be used to sum up the fields from each current mode, resulting in the backscatter (or back hemisphere of bistatic scattering) of the incident plane wave. The results can be used to determine the echo width at various angles of incidence, thereby obtaining the data necessary to create plots of the monostatic field patterns. By inputting the values of the currents on the right hand side of the last array into the same far zone equation, plots of the forward scattered (or transmitted) field pattern in Region III can be obtained in a similar manner. Reference Figure 5.1 for a graphical definition of the regions, and recall that FIFEE can handle an arbitrary number of arrays.

Figure 5.2 depicts an incident plane wave propagating in the \hat{s}_1 direction. The subscript 1 refers to the left halfspace, which is considered the 1st slab. Also shown is a representation of a cone of bistatic scatter directions for the main lobe of a periodic column of trislots. This scatter cone is analogous to the edge diffraction cone postulated by Keller (21:165-168). If the spacing of the column elements is such that elevation grating lobes exist, each such lobe will have an associated cone of scattering; but they are generally nonexistent when $D_z < \lambda_1$ and are definitely absent when $D_z < \lambda_1/2$. FIFEE does not concern herself with such secondary scattering when calculating the scattered field pattern because, for a monostatic scattering situation in the far field, a receiving

antenna of finite size will only receive the main lobe; the scattering directions of any elevation grating lobes will cause any real world energy associated with such lobes to pass above or below the receive element.

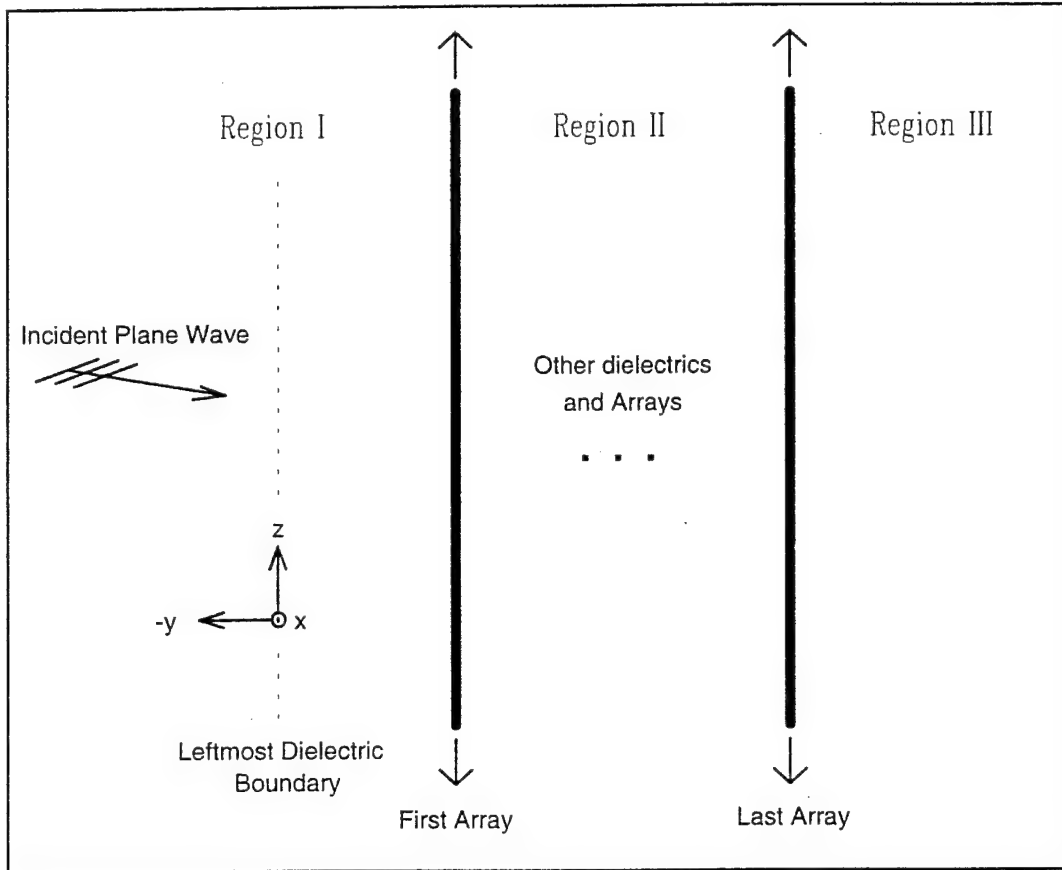


Figure 5.1 Regions of Interest Defined.

Mathematically, s_{z_1} is the parameter that determines the conic angle, and does so according to the law of diffraction. This fact can be made more clear by recalling from Chapter 3 that

$$\hat{s}_1 = s_{x_1} \hat{x} + s_{y_1} \hat{y} + s_{z_1} \hat{z}, \quad (5-1)$$

and from Chapter 4 that s_{z_1} is used to account for the Floquet phasing between the reference element of a particular infinite column and every other element in that column. Thus, the chosen direction for the incident wave, \hat{s}_1 , defines the quantity s_{z_1} , which in

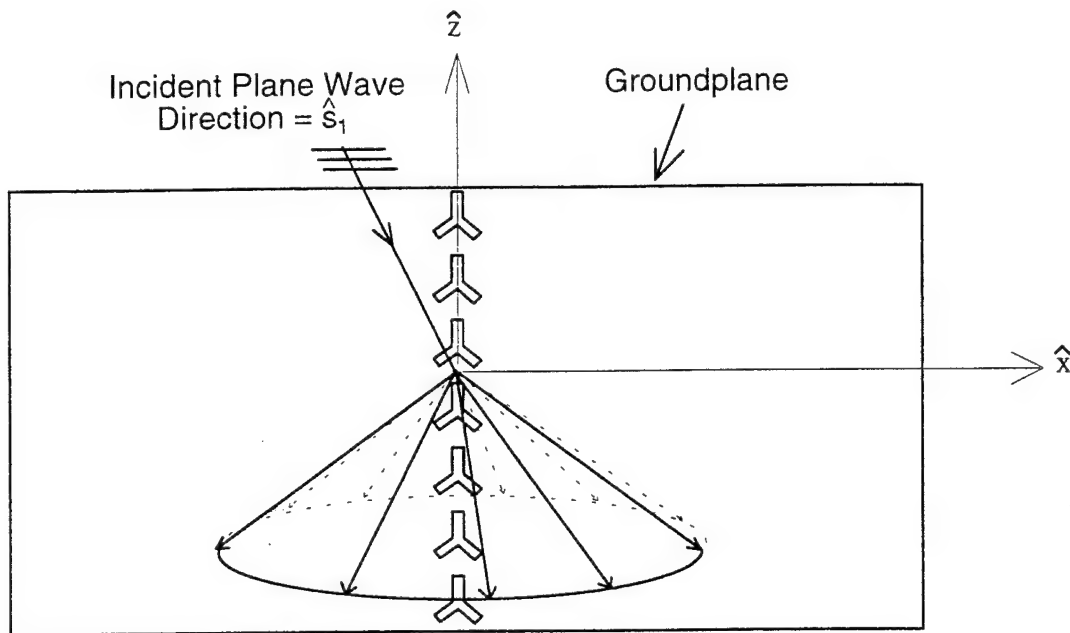


Figure 5.2 Cone of Bistatic Scatter Directions For a Periodic Column of Slots:
Dashed lines are forward scatter directions; Solid lines are backscatter directions.

turn is used to define the periodic basis functions of each column, upon which the resulting moment method solution is dependent.

Based on the dependencies discussed in the previous paragraph, it can be seen that the scattered field directions, and thus their associated expressions, are dependent on the same s_{z_1} that defines the incident plane wave. Approaching the derivation of the far zone scattered field equation with this in mind, the value of s_{z_1} that is to define the periodic basis functions of the scatterer in question must also be used in the derivation at hand. Thus, the only directions in which the far zone scattered fields are valid are the \hat{s}^{scat} directions, where

$$\hat{\mathbf{s}}^{scat} = s_x^{scat} \hat{\mathbf{x}} + s_y^{scat} \hat{\mathbf{y}} + s_{z_1} \hat{\mathbf{z}} \quad (5-2)$$

and where s_x^{scat} and s_y^{scat} are real valued numbers satisfying the normalization of $\hat{\mathbf{s}}^{scat}$. The different combinations of s_x^{scat} and s_y^{scat} that satisfy Equation (5-2) identify the different directions embodied in the cone of scattering. It should be noted that this *cone of scattering* approach is valid only in the asymptotic limit of the far zone, and that, in general, the scattered fields may be evaluated at any point in space*.

As described in Chapter 3, FIFEE assumes that the plane of incidence is the x - y plane. With respect to the spherical coordinate system shown in Figure 3.2, this assumption requires the angle α to equal zero. Substituting this value of α into Equation (3-5) shows that s_{z_1} is always zero under this restriction, in which case monostatic backscatter can be obtained by choosing

$$\hat{\mathbf{s}}^{scat} = -\hat{\mathbf{s}}_1 = -s_{x_1} \hat{\mathbf{x}} - s_{y_1} \hat{\mathbf{y}} \quad (5-3)$$

Focus now on the Region I geometry. Consider that M slot modes exist on the surface of the leftmost groundplane and that this groundplane is coated with an arbitrary number of dielectric slabs. Also, assume that the reference element for the m th slot mode is centered at

$$\bar{\mathbf{R}}_m = x_m \hat{\mathbf{x}} + z_m \hat{\mathbf{z}} \quad (5-4)$$

Using the Array Scanning Method, the scattered field from the infinite m th column mode is

$$\bar{\mathbf{E}}_m = \frac{D_x}{\lambda_g} \int_{\frac{-\lambda_g}{2D_x}}^{\frac{\lambda_g}{2D_x}} \bar{\mathbf{E}}_m^{\infty 2} ds_{x_g} \quad (5-5)$$

* At a finite distance from the array, calculations to include the grating lobe radiation should be considered.

where the subscript g refers to the slab closest to the groundplane, and where $\bar{E}_m^{\infty^2}$ denotes the radiation from an imagined doubly-infinite array of slots. In this imagined array, each infinite column of elements is identical to the m th column mode except in its x -location. The inter-column spacing for this array, D_x , is arbitrary, yet determines each column's x -location. By choosing

$$D_x = \lambda_g/2 \quad (5-6)$$

when implementing this method, azimuthal grating lobes will be nonexistent (for the integrand in Equation (5-5)).

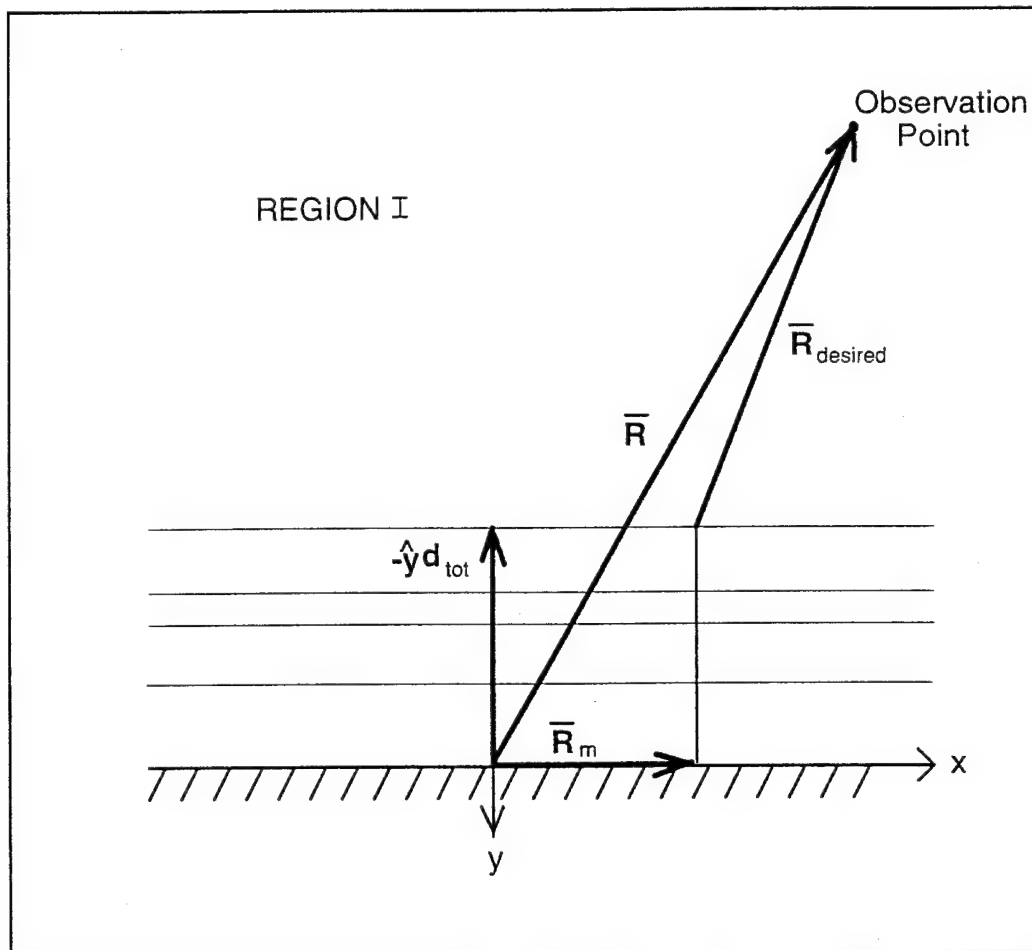


Figure 5.3 Geometry Used in Accounting for the Phase Shift of the Field at the Observation Point.

Referring to the geometry in Figure 5.3 and using the methods of Munk(4), the integrand in Equation (5-5) can be defined as follows:

$$\overline{\mathbf{E}}_m^{\infty 2} = -\frac{V_m}{2D_x D_z} \sum_{k=-\infty}^{\infty} \sum_{n=-\infty}^{\infty} \frac{e^{-j\beta_1(\overline{\mathbf{R}}-\overline{\mathbf{R}}_m+\hat{\mathbf{y}}d_{tot})\cdot\hat{\mathbf{r}}_{1,-}}}{r_{y_g}} \phi_{2g} \left[P'_{\parallel} T_{\perp}^{HE} \hat{\mathbf{n}}_{\parallel} - \frac{r_{y_g}}{r_{y_1}} P'_{\perp} T_{\parallel}^{HE} \hat{\mathbf{n}}_{\perp_1} \right] \quad (5-7)$$

where again the subscript g represents the slab closest to the groundplane, where the subscript 1 represents the left halfspace, and where the notation of Munk is employed by using $\hat{\mathbf{r}}_{1,-}$ to denote the backscattered direction in the left halfspace (slab #1). Note that when $k=n=0$, $\hat{\mathbf{r}}_{1,-}$ is another name for the far zone scattered field direction, $\hat{\mathbf{s}}^{scat}$. Using this notation, plane wave directions in the slab closest to the groundplane are defined by

$$\hat{\mathbf{r}}_{g,-} = \left(s_{x_{g,-}} + \frac{k\lambda_g}{D_x} \right) \hat{\mathbf{x}} - r_{y_{g,-}} \hat{\mathbf{y}} + \left(s_{z_{g,-}} + \frac{n\lambda_g}{D_z} \right) \hat{\mathbf{z}}. \quad (5-8)$$

where the square root for $r_{y_{g,-}}$ is positive real for propagating waves, and negative imaginary ($-j$ root) for evanescent waves. Plane wave directions can be found in the remaining layers of Region I by using Equations (3-10) through (3-12) to obtain the refracted $\hat{\mathbf{x}}$ and $\hat{\mathbf{z}}$ components. Also note that in Equation (5-7)

$$(\overline{\mathbf{R}} - \overline{\mathbf{R}}_m + \hat{\mathbf{y}}d_{tot}) = \overline{\mathbf{R}}_{desired} \quad (5-9)$$

is used to account for the phase shift of the scattered field at the observation point with respect to the point at which it leaves the dielectric slab ($\overline{\mathbf{R}}_{desired}$ is defined graphically in Figure 5.3). As described in Chapter 3, the P terms denote the pattern factors, the T terms denote the "magnetic to electric T Factors", the unit vectors $\hat{\mathbf{n}}$ are the polarization state vectors, and ϕ_{2g} is the phase delay due to plane wave propagation through the dielectric layers.

The pattern factors in Equation (5-7) are for the magnetic fields radiated by the transmitting slots in the dielectric slab closest to the groundplane. The T factors will transform these magnetic fields to the appropriate electric fields in the halfspace. Thus, Equations (5-5) and (5-7) can be used to find the m th slot mode's scattered electric field anywhere in the left halfspace. However, for the far field, only the k, n terms of the doubly-infinite sum that represent propagating plane waves need be considered — those k, n combinations that yield a real value for $r_{y_{1,-}}$. But the interest here is even more restrictive, that being the desire to find the far field of the main elevation lobe of the m th column mode. Therefore, the only applicable plane wave term in Equation (5-7) is the $k = n = 0$ term.

Implementing Equations (5-5), (5-6), and (5-7) in this fashion, the far zone field from the m th periodic column mode is:

$$\bar{E}_{m,fz} = -\frac{V_m}{2\lambda_g D_z} \int_{-1}^1 \frac{e^{-j\beta_1(\bar{R}-\bar{R}_m+\hat{y}d_m)\cdot\hat{r}_{1,-}}}{r_{y_f}} \phi_{2g} \left[P'_{\parallel} T_{\perp}^{HE} \hat{n}_{\parallel} - \frac{r_{y_1}}{r_{y_f}} P'_{\perp} T_{\parallel}^{HE} \hat{n}_{\perp_1} \right]_{k=n=0} ds_{x_1} \quad (5-10)$$

The integrand in Equation (5-10) becomes more and more oscillatory as the observation point is moved farther and farther away from the slot, making the numerical implementation of this equation very costly.

However, a practical solution can be implemented by using the method of stationary phase to perform an asymptotic evaluation of the integral. Applying this method to Equation (5-10) yields:

$$\bar{E}_{m,fz} \approx \frac{V_m}{2D_z} \sqrt{\frac{j}{\rho\lambda_1}} e^{-j\beta_1\rho} e^{j\beta_1\bar{R}_m\cdot\hat{s}^{stat}} \phi_{2g} \left[P'_{\parallel} T_{\perp}^{HE} \hat{n}_{\parallel} - \frac{r_{y_1}}{r_{y_f}} P'_{\perp} T_{\parallel}^{HE} \hat{n}_{\perp_1} \right]_{k=n=0}^{stat.pha.pt} \quad (5-11)$$

where

$$\rho = \sqrt{(x - x_m)^2 + (y + d_{tot})^2}. \quad (5-12)$$

The stationary phase point, x , is identified by the s_{x_g} value that solves the following equation:

$$x = \frac{d_g s_{x_g}}{\sqrt{1 - s_{x_g}^2}} + \frac{d_{g-1} \left(\frac{\beta_g}{\beta_{g-1}} \right) s_{x_g}}{\sqrt{1 - \left(\frac{\beta_g}{\beta_{g-1}} s_{x_g} \right)^2}} + \dots + \frac{d_2 \left(\frac{\beta_g}{\beta_2} \right) s_{x_g}}{\sqrt{1 - \left(\frac{\beta_g}{\beta_2} s_{x_g} \right)^2}} + \frac{(y - d_{tot}) \left(\frac{\beta_g}{\beta_1} \right) s_{x_g}}{\sqrt{1 - \left(\frac{\beta_g}{\beta_1} s_{x_g} \right)^2}} \quad (5-13)$$

Since the observation point is extremely far from the slot, the following approximation can be made:

$$s_{x_g} (stat. pha. pt.) \approx \frac{\beta_1}{\beta_g} \sin \eta \quad (5-14)$$

where η identifies the angle of incidence in the x - y plane ($\alpha = 0$) as discussed in Chapter 3.

A numerical experiment was made to compare the results of Equations (5-10) and (5-11) in order to ensure that the stationary phase evaluation was implemented correctly. The experiment was configured as follows: The reference slot for an infinite column of trislots was centered at the origin, with two dielectric slabs covering the associated groundplane. The slab closest to the groundplane had a relative dielectric constant of 4 and a thickness of $0.2\lambda_1$. The second slab had a relative dielectric constant of 2 and a thickness of $0.2\lambda_2$. The operating frequency was 10 GHz, each of the three trislot legs was $\lambda_1/4$ in length ($= 0.375$ cm), and the two modes for the trislot were defined as shown below. The basis function was defined by a piecewise sinusoid with an effective relative dielectric constant of 4. The results for both polarization states are plotted in Figure 5.4. The high correlation between the two methods of solution indicates a successful stationary phase implementation. Although the data differs appreciably for

$80^\circ < \eta < 90^\circ$, this is a numerical difficulty that can be alleviated by sampling the integrand more finely.

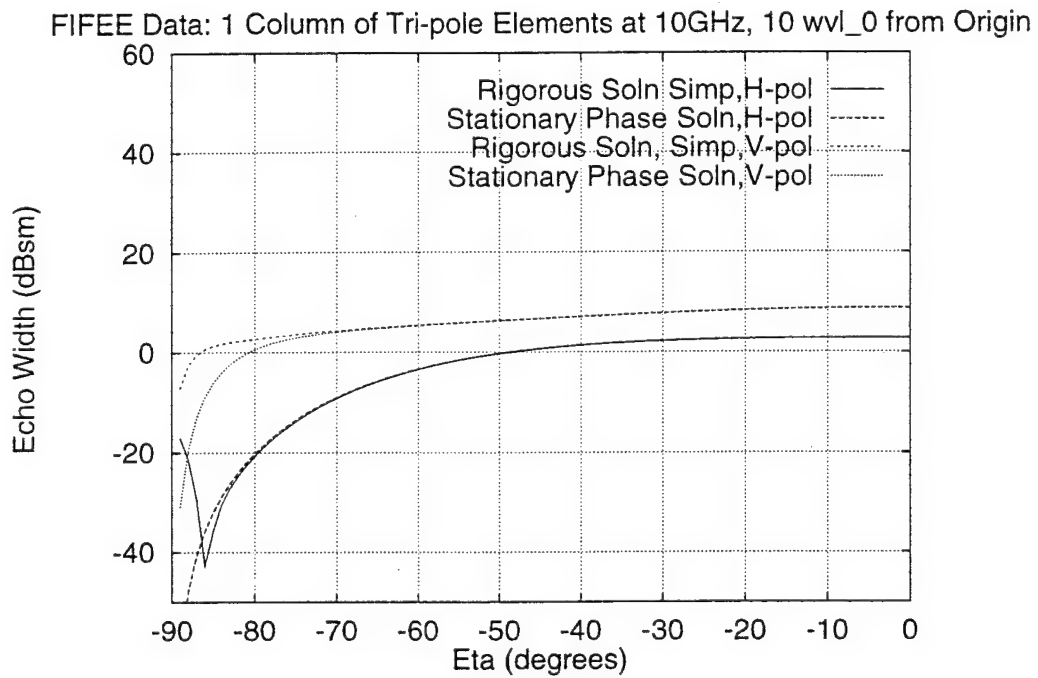
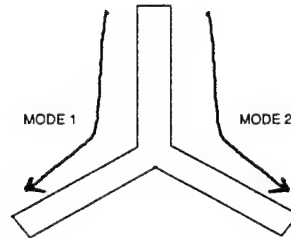


Figure 5.4 Backscattered Fields Due to Infinite Column of Trislots (Two Periodic Slot Modes) with a Double Slab Geometry.

VI. RESULTS

This chapter brings together the mathematical methods that were developed in the previous chapters in order to demonstrate the accuracy of the electromagnetic scattering predictions resulting from such analysis. For those readers who skip right to the results section, the analysis procedure that was implemented (a computer model called FIFEE) is a moment method based solution that determines scattering from finite by infinite slot arrays, where the slots are planar, thin, and piecewise linear, but otherwise arbitrary. FIFEE can also account for an arbitrary number of dielectric slabs in the problem geometry. All the results generated by this model are for plane wave excitation where the direction of incidence lies in the $\alpha=0$ plane (see Figure 3.2). The basis functions used are periodic piecewise sinusoids or piecewise cosinusoids (defined along individual slot columns), the choice being left to the user. The testing functions are always piecewise sinusoids. Appendix A describes the syntax of the commands that are used to construct the input file.

In this chapter, several geometries are considered by FIFEE from which backscatter patterns are generated. These results are compared to the that of another computer model (KAHUNA) and also to measured data in order to validate the methodology described within this dissertation. Also, FIFEE's ability to selectively load individual columns resistively, which can reduce sidelobe levels on scattering patterns, is demonstrated.

The first geometry considered is a radome design using periodic surfaces. This geometry is a reproduction from Skinner's dissertation (6), and is shown in Figure 6.1. The top view is such that one is looking down the \hat{z} axis; the arrays are contained in an x - z plane. There are nine dielectric slabs counting the halfspaces, and two slot arrays with twenty one columns of slots on each array. Each slot column is periodic in \hat{z} , and each slot is linear and in the \hat{z} direction so that only horizontal polarization is of interest. The selected frequency is 10 GHz.

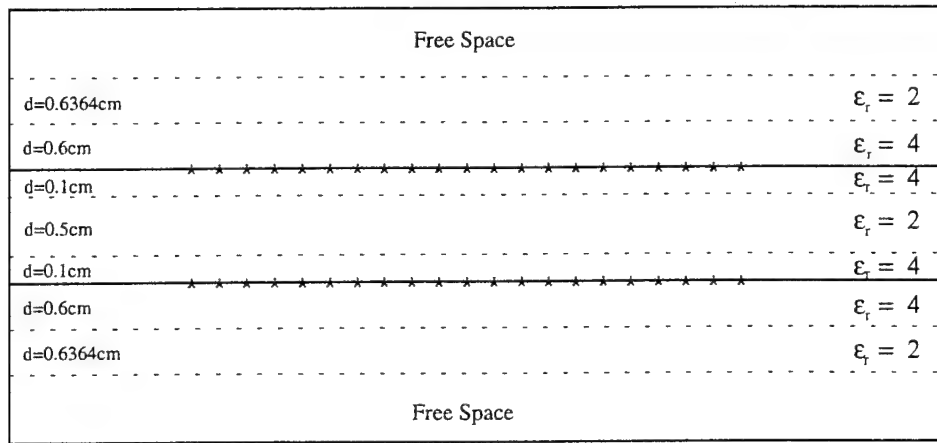


Figure 6.1 Top View of the Radome - 21 Columns of Slots on Each Infinite Groundplane with Infinite Dielectrics: Asterisks Denote Columns of Periodic Slots, Slot Length=0.75cm, Slot Width=0.075cm, $D_x=0.675$ cm, $D_z=1.125$ cm.

Skinner's computer model KAHUNA is used to create the data for graphical comparison. Both FIFEE and KAHUNA used one periodic piecewise sinusoidal mode for each slot column (entire domain approach). The resulting backscatter patterns are shown in Figure 6.2, and the excellent agreement between the two codes is further proof that the analysis in this dissertation has been implemented correctly. Although this is somewhat of a restrictive case in that only horizontal polarization is examined, it does demonstrate a capability to handle multiple arrays and an arbitrary number of dielectric slabs. The pattern factors, the T factors, the one sided admittances, the Array Scanning

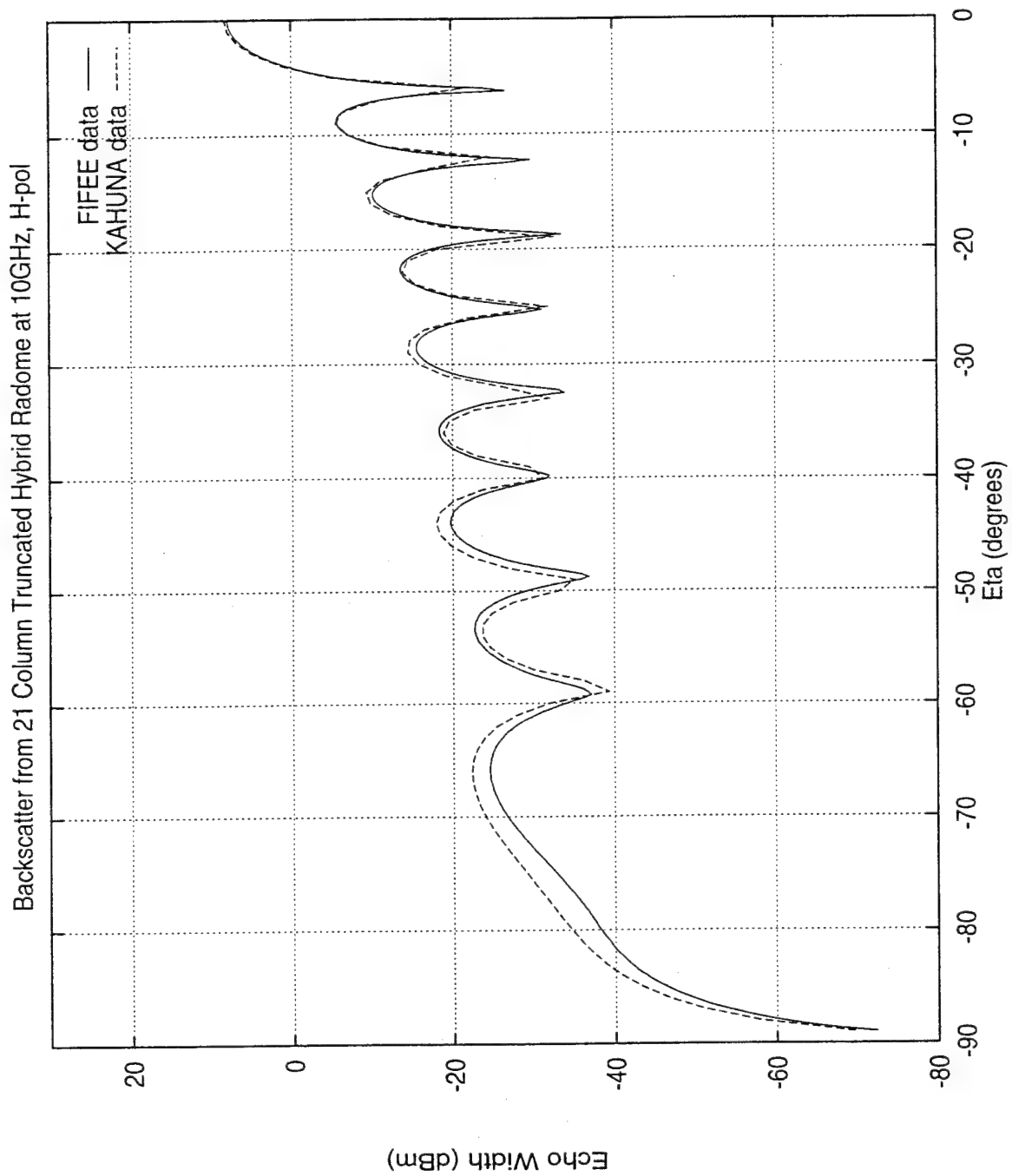


Figure 6.2 Comparison Between FIFEE and KAHUNA: Geometry of 9 Dielectric Slabs and 2 Arrays, with 21 Columns on Each Array.

Method, the excitation due to the incident wave, and the calculation of the scattered fields due to the equivalent magnetic scattering currents were all implemented so as to allow the user flexibility in specifying the geometry. The number of columns on each array, the number of segments in the elements that compose these columns, and the number of arrays and slabs themselves are only limited by the computer resources at hand, not by the code. The results in Figure 6.2 demonstrate the successful integration of the above mentioned mathematical tools into this generalized approach.

The next geometry considered is referred to as FSS #1, and consists of only one array (slotted groundplane) sandwiched by two infinite halfspaces of freespace. The array has 16 infinite columns of linear slots where the slots are \hat{z} directed; each slot length is 1.524 centimeters and the width is 0.2286 centimeters; the inter-column spacing is $D_x=1.625$ centimeters, and the inter-element spacing on a column is $D_z=1.778$ centimeters. Also, the grid is skewed (see the *Skewed Grid* command in Appendix A).

FSS #1 was fabricated into a physical sample by the Mission Research Corp of Dayton, Ohio. This physical approximation was made by truncating the infinite columns to 14 inches in height; these columns were cut into a rectangular sheet of copper foil which was then mounted on an annulus. [For the remaining data plots in this chapter, when comparing to measured data, the FIFEE output is converted from echo width to echo area by using $L = 14$ " in the following formula:

$$\sigma_{3D} = \sigma_{2D} \cdot \frac{2L^2}{\lambda} \quad (6-1)$$

resulting in RCS data.] The resulting circular disk (with the slotted columns in the center) was taken to the Advanced Compact Range at Wright Labs where the Signature Technology Office (WL/XPN) performed radar cross section measurements on it. The FSS sample (circular disk) was mounted on a copper clad, teardrop shaped test body.

The test body had a hollow interior which was filled with absorber material in an effort to isolate the backscatter effects to that of the FSS sample. The process used to calibrate the horizontal and vertical polarization data utilized vector background subtraction, and is given by the following equation:

$$\sigma_{tgt}(\omega, \alpha) \text{ dBsm} = \left| \frac{E_{tgt}(\omega, \alpha) - E_{tgtbkg}(\omega, \alpha)}{E_{sph}(\omega) - E_{sphbkg}(\omega)} \right|^2 * \sigma_{exact\ sph}(\omega) \quad (6-2)$$

where;

E_{tgt} is the measured field of the target and the test body, at frequency ω and angle α .

E_{tgtbkg} is the measured field of the chamber with only the test body, at frequency ω and angle α . In this case the FSS target was replaced with a copper clad circular disk, this disk having the same dimensions as the target so that it fit the test body with the same contour as the FSS target.

E_{sph} is the measured field of the 8" diameter reference sphere at frequency ω and is independent of angle α .

E_{sphbkg} is the measured field of the chamber with the sphere mount, at frequency ω and is independent of angle α .

$\sigma_{exact\ sph}$ is the Mie Series solution to the backscatter of a sphere at frequency ω and is independent of angle α .

The FSS #1 data measured for an incident plane wave at a frequency of 12 GHz is shown in Figure 6.3, along with predictions for this configuration by FIFEE and KAHUNA. Both FIFEE and KAHUNA used three piecewise sinusoidal modes to represent each linear slot. For this plot and the other measured data plots that follow, the angle 0° corresponds to grazing incidence and the angle 90° corresponds to normal

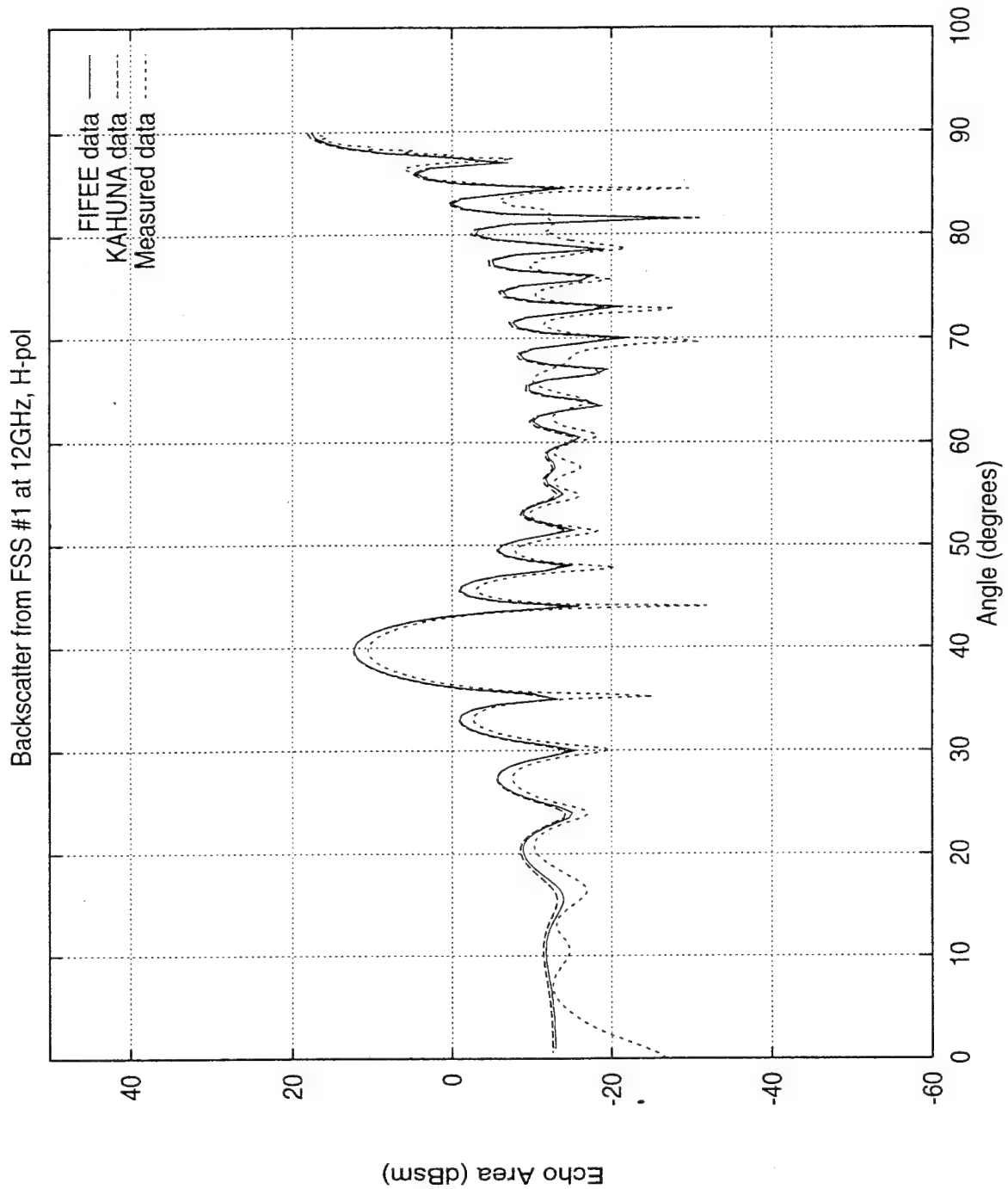


Figure 6.3 Comparison Between FIFEE, KAHUNA, and Measured Data for FSS #1: No Dielectric Slabs, 1 Array with 16 Columns, Slot Length=1.524cm, Slot Width=0.2286cm, Dx=1.6256cm, Dz=1.778cm, Skewed Grid.

incidence to the FSS/test body configuration. The FIFEE and KAHUNA results are in excellent agreement with each other, and their lobing structures agree well with the measured data, although there is a difference of two to six dB between the peak levels of the lobes. This could be the result of energy "rattling" back to the radar in the measured data case. This phenomena would be due to the non-perfect absorber that filled the cavity of the test body.

Next, Figure 6.4 shows the "FIFEE versus measured data" results for FSS #1 at 9.5 GHz. Only one mode was used to model each reference element. Lowering the frequency seems to have resulted in less of a difference between the peak levels of the lobes, such that the two results compare most favorably.

As mentioned at the end of Chapter 2, FIFEE provides a feature that allows the user to resistively load individual columns of an array (see the ZLOAD command in Appendix A). This makes it possible to account for the effects of slots filled with resistive materials. More specifically, when this feature is used, FIFEE places a complex valued shunt impedance load across the slot centers of the respective column. As a demonstration of this feature, Figure 6.5 has been included. The data labeled as "Tapered Resistive Treatment" placed 100 ohms on the slots in columns one and sixteen, 200 ohms on columns two and fifteen, 300 ohms on columns three and fourteen, and 400 ohms on columns four and thirteen. The data labeled as "Resist.200 Treatment" placed 200 ohms on columns one through four and thirteen through sixteen. It can be seen that the tapered approach (which was not an optimized design) reduced the edge effects more, as evidenced by having the same lobing structure as the "200" case, but with peak lobe levels about 5 dB down on average.

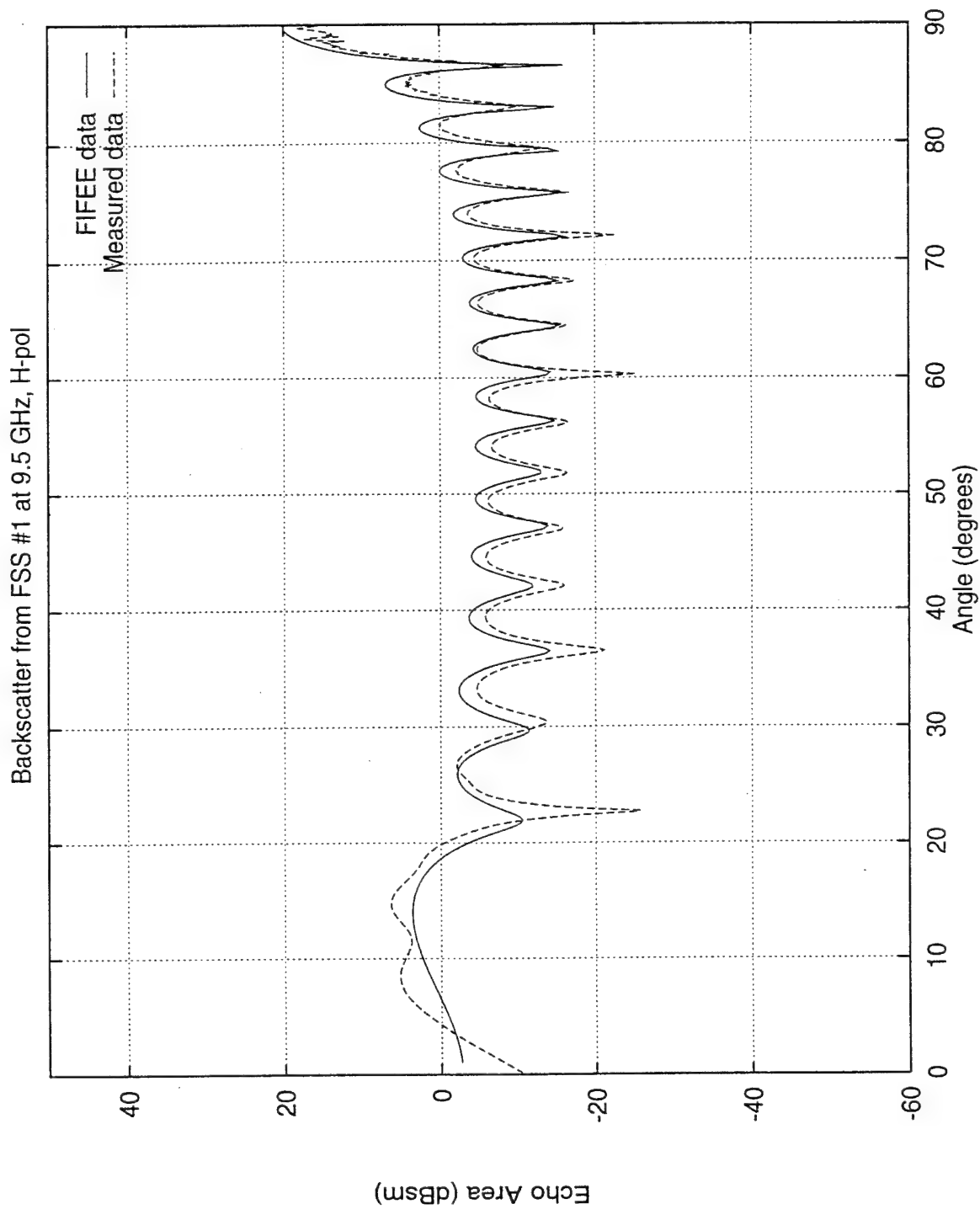


Figure 6.4 Comparison Between FIFEE and Measured Data for FSS #1.

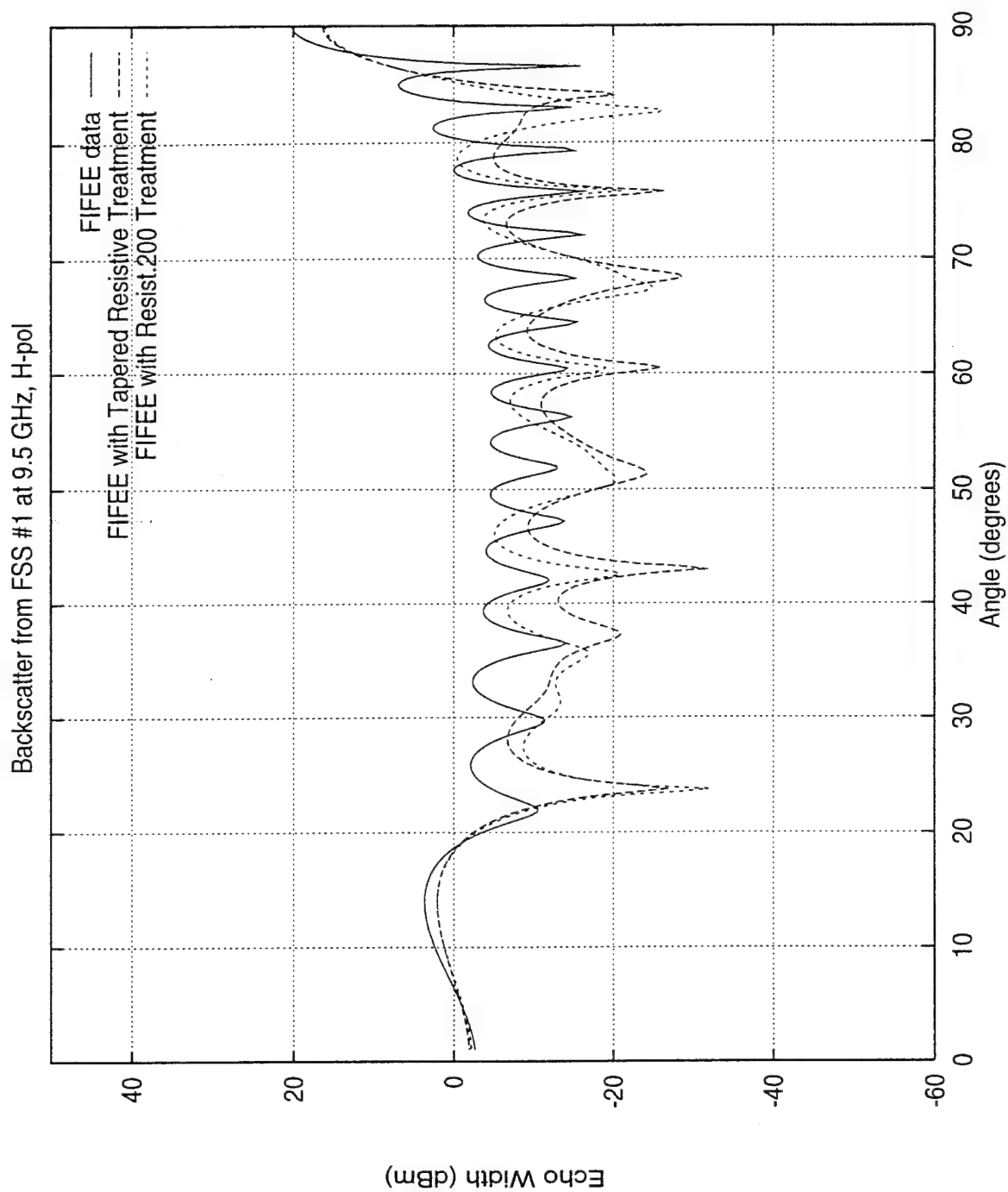


Figure 6.5 Illustration of Slot Treatments with Resistive Materials.

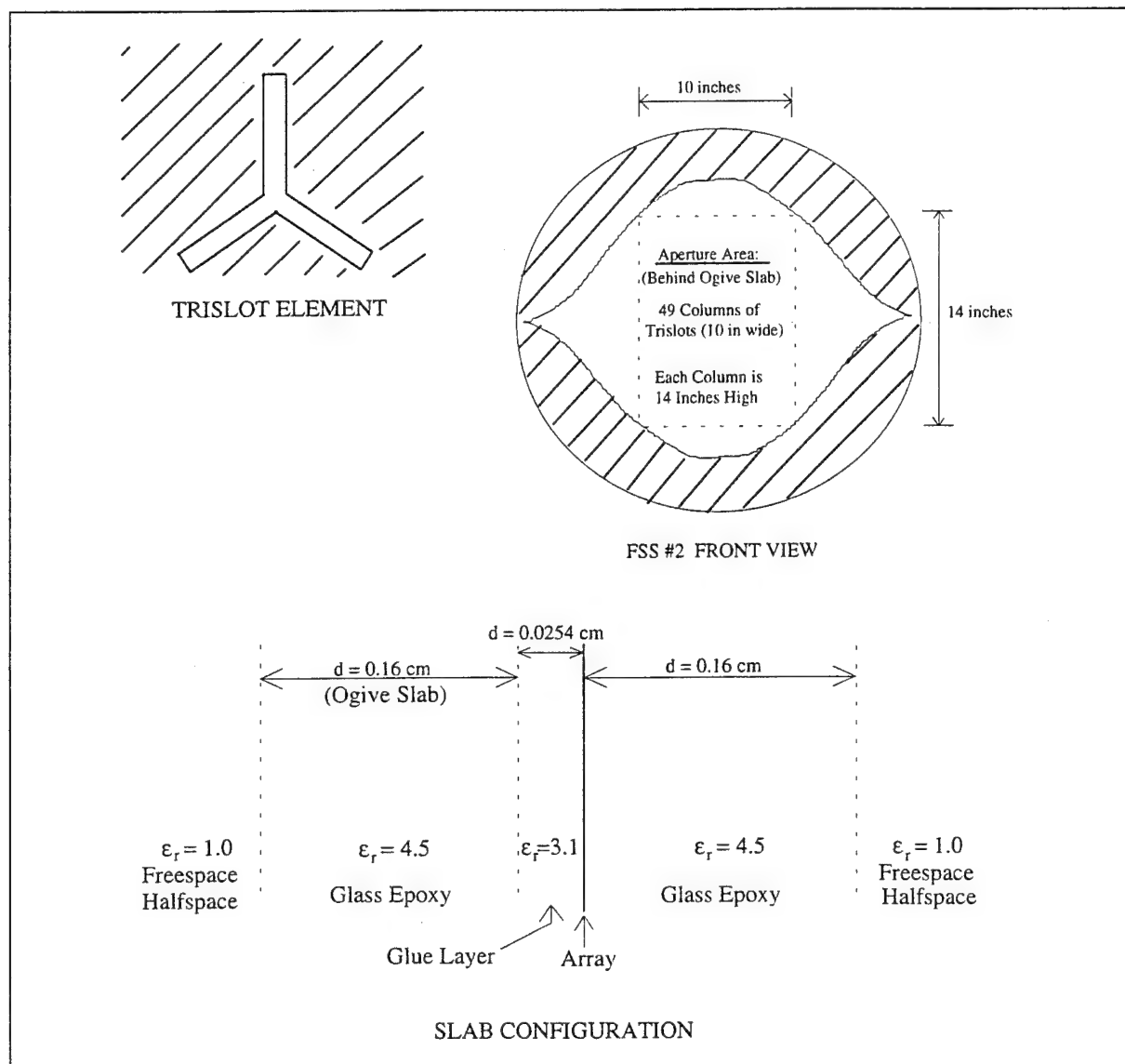


Figure 6.6 FSS #2 Configuration.

One other FSS sample was constructed to help validate the code, and it is referred to as FSS #2. FSS #2 was constructed and measured in the same manner as FSS #1, but with the following differences: The slot elements are trislots, there are 49 columns* of these slots, and 3 dielectric layers are now present as shown in Figure 6.6. The slab to the

* As will be described later, there are actually 47 columns of "full" elements, and 4 columns of partial elements. This is due to the etching stencil being off center during the fabrication process.

right of the array in the figure (in back of the array and inside the test body during measurements) is a circular disk. This slab was copper clad and the copper was chemically etched to form the slot columns. When mounted on the test body, the copper surface of the disk was flush with the copper surface of the test body, and copper tape was used to seal the seams. The outer slab was glued to the copper clad circular disk, and thus, it had a raised profile with respect to the surface of the test body. In an effort to minimize scattering due to the thickness of this outer slab (in order to better simulate the infinite slabs of the computer model), the slab was cut into the shape of an ogive and the edges of the slab were beveled to approximately 45 degrees. With respect to the slot columns, the inter-column spacing is $Dx=0.52$ centimeters, the inter-element spacing on a column is $Dz=0.60$ centimeters, and the grid is skewed. For the trislot elements, each of the three legs is 0.40 centimeters long, with a width of 0.05 centimeters.

To determine if the beveling could be improved upon, the edges of the ogive were taped with magnetic absorber material, and the data measurements were repeated. In the plots that follow, "Measured data_2" refers to data associated with the beveled edges, while "Measured data_3" refers to data associated with the taped beveled edges. As will be seen, this tape modification noticeably affected the results. From this difference, it can be reasonably speculated that the process of truncating infinite columns and slabs to finite configurations will also affect the results to a noticeable degree. In other words, some differences should be expected between the measured and modeled data because two different geometries are being represented. However, by understanding how such approximations affect results, an FSS designer can use a tool like FIFEE to accurately predict the performance of physical sample.

There is another note to be made with respect to differences between what was modeled and the physical sample. The etching stencil used to construct the slots was cut from a larger stencil (which had more than 49 columns), and as a result, instead of the 49

anticipated columns, there are only 47 full columns along with 4 partial columns. See Figure 6.7. It was predicted that the resulting effect of this difference would be minor. However, since FIFEE can model a slot array composed of columns of different element shapes (as long as the D_z spacing for all columns is the same), it was not necessary to rely on this prediction. The 47 full columns and the 4 partial columns were modeled by FIFEE, and the results were almost identical to that obtained from a 49 (full) column model. However, because the elements in the outermost columns were very small electrically, their radiation patterns were nearly isotropic in nature and caused the infinite sums to converge very slowly. Out of curiosity, the experiment was repeated again without the outermost columns of tiny elements. This time, practically identical results were obtained in half the cpu time. This case illustrates how FIFEE can be used to quickly compare two different methods of terminating an array.

The FSS #2 data measured for horizontal polarization at 6 GHz is shown in Figure 6.8, along with FIFEE's predictions. At the grazing angles of incidence (about 0° to 20°), surface wave phenomena can be observed in the measured data, which is due to the finite size of the test body. Around normal angles of incidence, the measured levels were expected to be higher than the modeled levels because of some reflections due to the interior of the test body. This was not expected to be an enormous difference since the test body interior was filled with absorber. The results obtained bear this out. Generally, there is an excellent correlation between the data. Notice that for some lobes, the two measured data do not have as high of a correlation as that between FIFEE and one of the measured data sets.

Figure 6.9 shows the results for vertical polarization at 6 GHz. Notice that for this polarization, as expected, the surface wave phenomena at grazing angles is not present. Again, the modeled data is in good agreement with the measured data.

Figures 6.10 and 6.11 show the 8 GHz results for horizontal and vertical polarizations, respectively. The obtained results for the horizontal polarization is excellent. For v-pol, although the correlation is very good, there is an unexplained drop of about 4 dB in the level of the lobes predicted by FIFEE, which gets progressively larger within the grazing angles. Still, the results could be used to accurately predict the peaks and nulls, and give a good estimate of the peak levels.

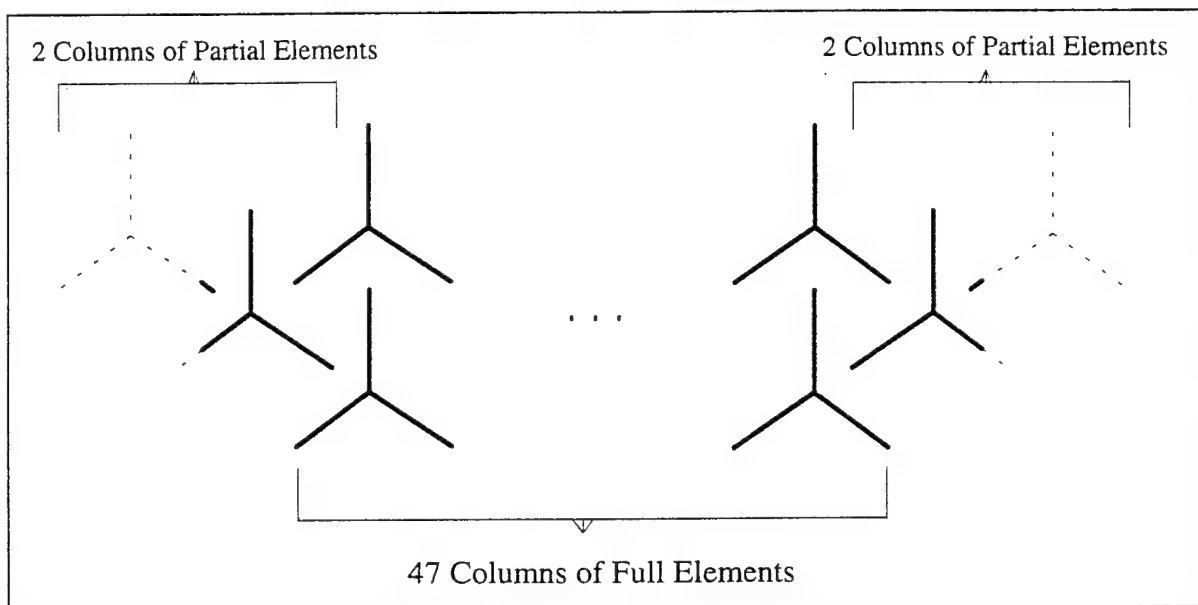


Figure 6.7 Illustration of Fabrication Anomaly in FSS #2.

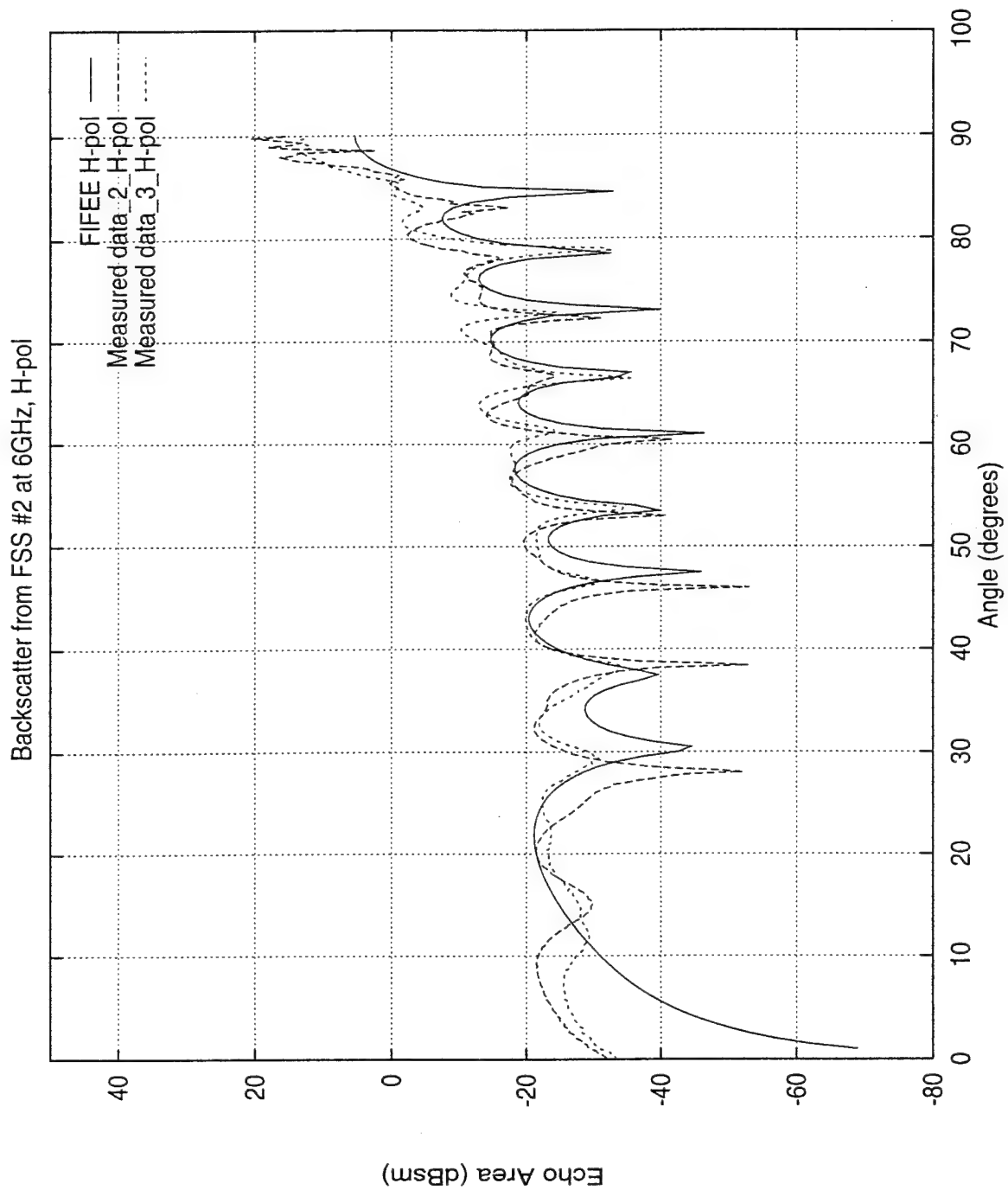


Figure 6.8 Comparison Between FIFEE and Measured Data for FSS #2 at 6GHz, H-pol: Geometry of 3 Dielectric Slabs, and 1 Array with 49 Slot Columns, Slot Length=0.4cm, Slot Width=0.05cm, Dx=0.52cm, Dz=0.6cm, Skewed Grid.

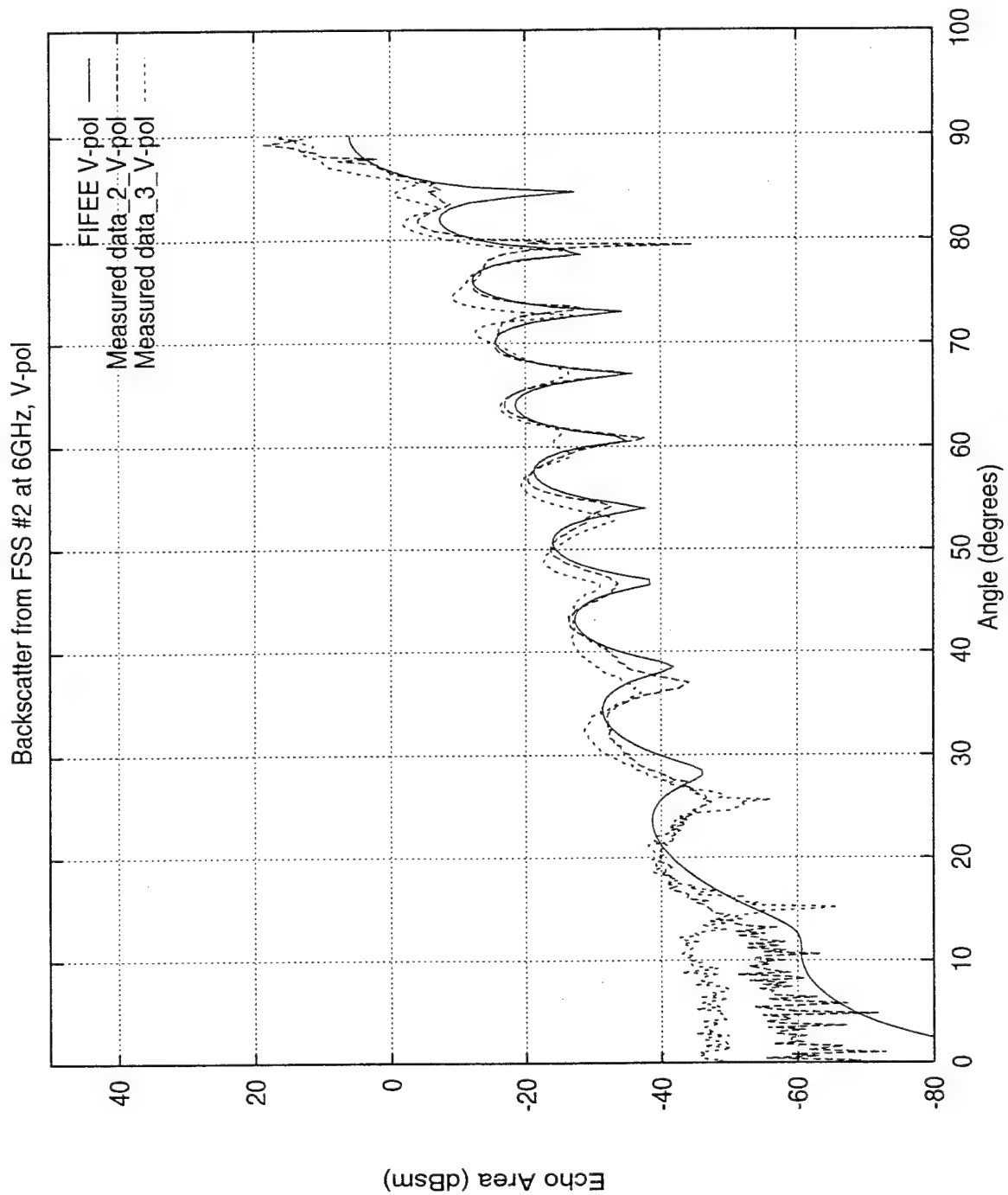


Figure 6.9 Comparison Between FIFEE and Measured Data for FSS #2 - 6GHz, Vertical Polarization.

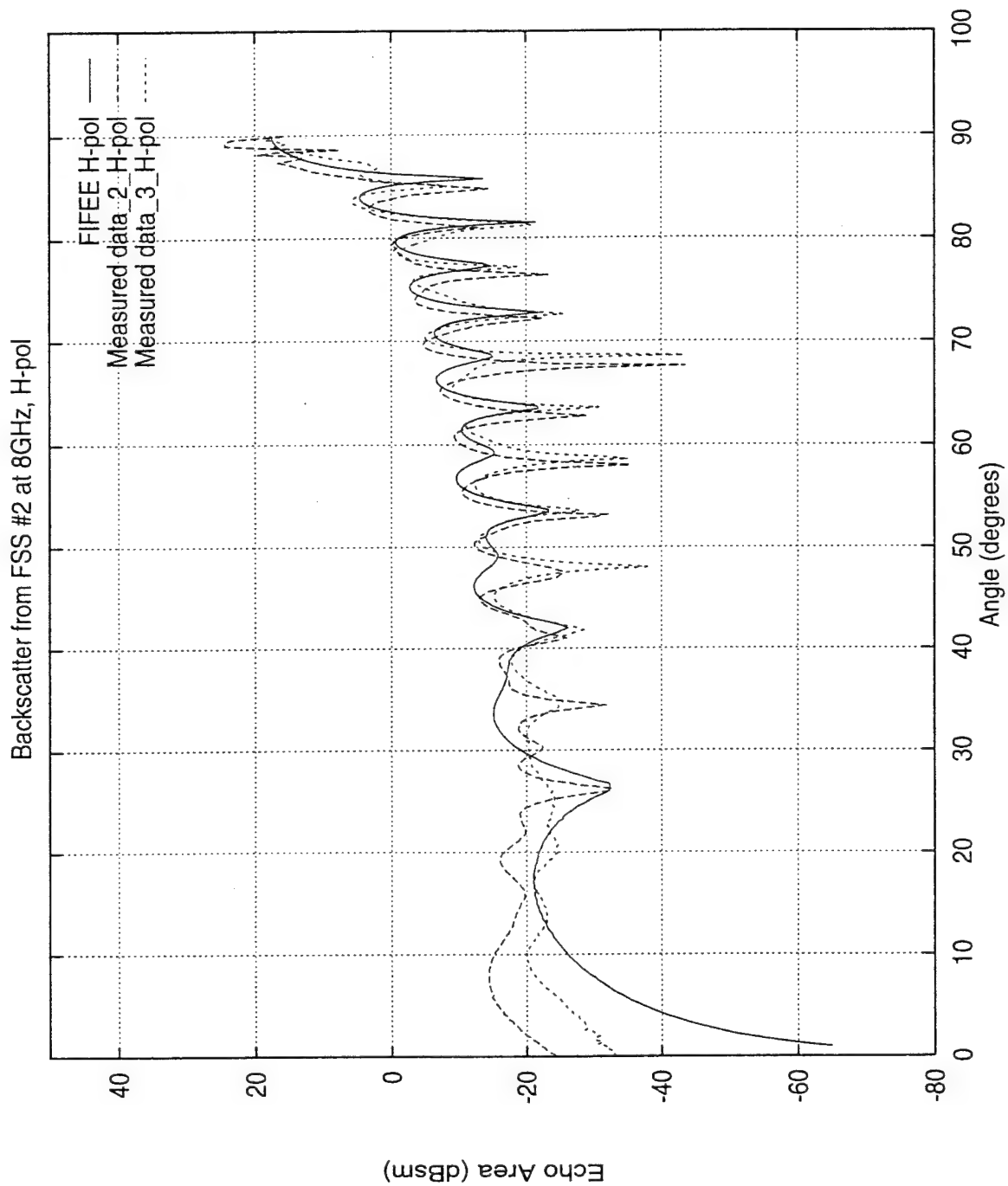


Figure 6.10 Comparison Between FIFEE and Measured Data for FSS #2 - 8GHz, Horizontal Polarization.

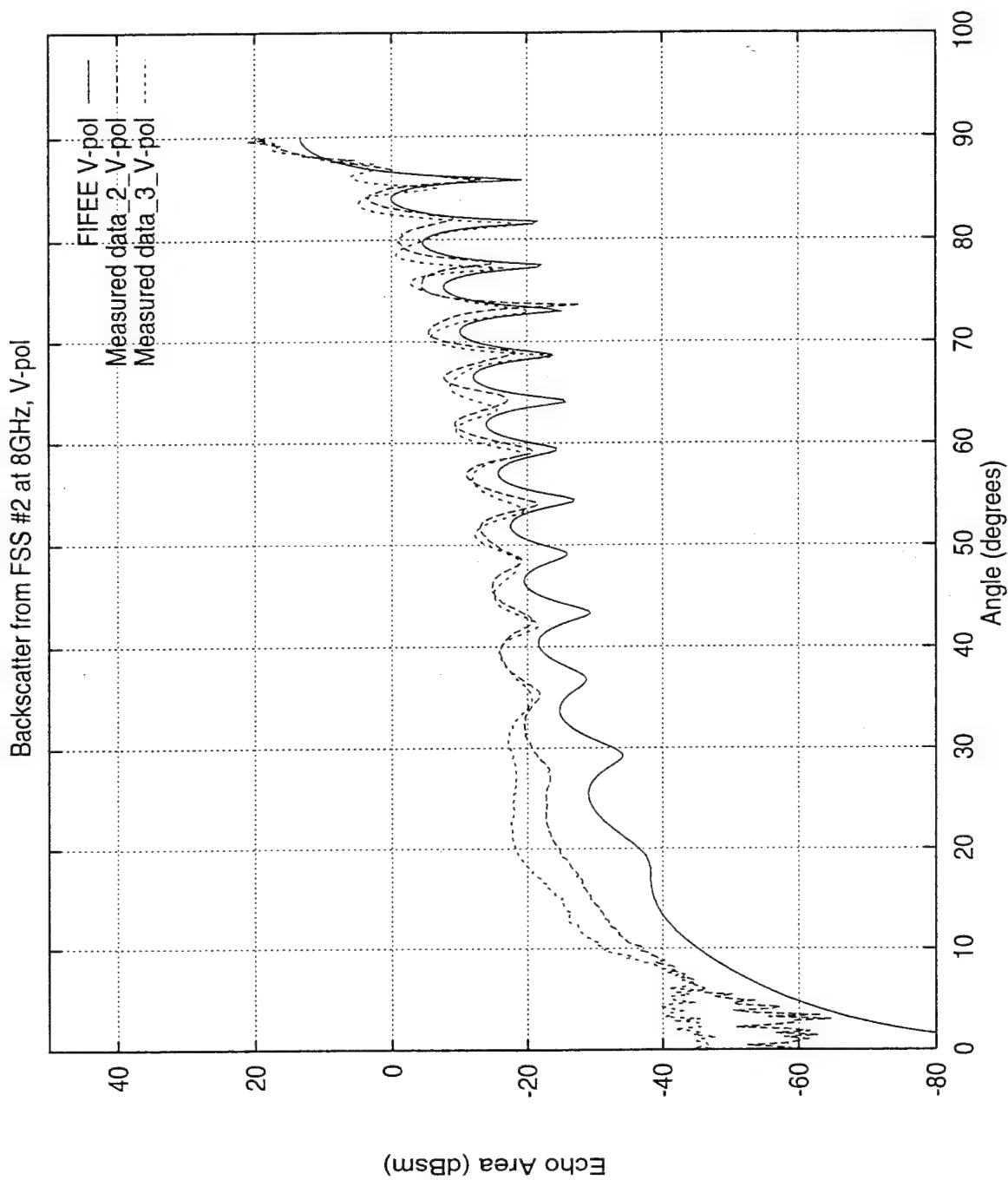


Figure 6.11 Comparison Between FIFEE and Measured Data for FSS #2 at 8GHz, Vertical Polarization.

VII. CONCLUSIONS

The computer model FIFEE has successfully implemented the analysis developed in this dissertation, and can handle a class of frequency selective surfaces that is best described as "planar and finite by infinite". More specifically, the model can handle an FSS that consists of an arbitrary number of planar dielectric slabs and of planar slot arrays; the slot elements in each array are composed of arbitrary, yet piecewise linear, thin slot segments. Also, a user friendly front end based on the PMM input language was incorporated into this model to facilitate the design process. Other features include the ability to conveniently place resistive loads on individual columns of slots (or on individual arrays as a whole), and the ability to define arrays that consist of different column structures. This dissertation has shown that the model, including the above mentioned features, has been implemented correctly, and can be successfully used as a tool in the design of frequency selective surfaces.

During the development of this model, most attention was given to functionality, not to optimizing the implementation. As a result, the model is sluggish. However, there were two major attempts at improving performance that showed promise, but they were not successfully integrated due to time constraints. If there is serious interest in using this model as a design tool, it is recommended that these two avenues towards improving performance be taken.

The first of these is to take advantage of Fourier flavor of the integral associated with the Array Scanning Method. An FFT can be used to efficiently solve the ASM integral at a set of equi-spaced points (where the set size is a power of two and is large

enough to satisfy resolution requirements). By taking advantage of the fact that the only difference between many of the mutual admittance geometries is the x -location of the columns, further performance gains can be realized using linear interpolation on the original set of answers. The problem encountered in this approach occurred when zero padding was placed on a function to be integrated. There were instances where zero padding needed to be placed on functions that did not taper off towards zero, creating a discontinuity in the data that resulted in unrealistic frequency components. Some attempts at windowing the data were tried, but none were successful; and in the interest of time, this approach was abandoned.

The second unsuccessful attempt at optimization was made by applying the *rho algorithm* (18) to accelerate the convergence of the infinite sums in the spectral domain (and using Shanks' algorithm to accelerate the convergence of these same sums when the separation distance associated with the mutual admittance was very small). This approach was successfully implemented to a degree: Performance was significantly improved for small problems (when the total number of modes was 20 or less), but due to the way in which the routine was implemented, larger problems were stifled by an exponential increase in memory requirements. A way was identified to optimize the implementation of this algorithm, but it involved re-writing the indexing scheme of the entire code.

If a project is undertaken to enhance the computational efficiency of this model, there are other items that would be desirable to address. Due to the repetitive nature of the internal calculations, this program would be a good candidate for implementation on a parallel computer. Also, ultra-fast routines could be created to handle special cases of simplified or symmetric geometries. For example, surface wave singularities (in the T factors of the ASM integrand) could be analytically removed for single, double, and triple slab geometries, removing the need to finely integrate functions associated with certain k -

n values. It would also be desirable to incorporate dipoles and lossy dielectrics into FIFEE's capabilities. As such tools are developed, new classes of radome and antenna designs can be investigated more thoroughly with respect to edge scattering effects; such investigations are severely limited when an FSS sample must be fabricated to explore its design potential.

APPENDIX A

USER'S GUIDE

The FIFEE Input Language

A.1 Introduction.

The input language for FIFEE is based on the input parser used in Henderson's *Periodic Moment Method (PMM)* program, which was designed under contract to the U.S. Air Force. The rationale behind using PMM's input structure is that many of the anticipated users of FIFEE will be familiar with this format and its associated documentation, thereby making it easier to learn and use this new program. Thus, the rest of this User's Guide is very similar in format to Chapter 3 of Henderson's *Introduction to PMM*. However, it should be noted that not all of PMM's commands are applicable, and that FIFEE introduces some new commands to the input structure.

This appendix will explain the syntax required to communicate with FIFEE. The input processor for this program is a language interpreter similar to BASIC, where the syntax of this language describes the concise format of the input file. This language allows the user to communicate with the program's number cruncher using simple English-like commands and arithmetic expressions. The arithmetic processor allows standard operations such as addition, subtraction, multiplication, division, and exponentiation, and also allows the grouping of sub expressions using parentheses. Further, it provides a library of mathematical functions such as sine, cosine, log, etc.. Whenever an input statement requires a numerical value, an expression can be inserted. The input processor will evaluate the expression and use the resulting value. This

alleviates the need for the user to pre compute such quantities as segment lengths, node coordinates, and slab widths. It also makes it possible to parameterize the input, thus making adjustments of the input data much easier. Upon program execution, the user will be requested to specify the input file containing the FIFEE language statements. At this time, the output filename is also requested, and the user is asked whether scattered field patterns should be in units of decibels per square meter (dBsm) or decibels per meter (dBm). All other communication is accomplished via commands (FIFEE language statements) in the input file.

A.2 Syntax.

There are five basic components of FIFEE language statements:

- Constants — fixed, self-describing values.
- Variables — symbolic names that represent stored values.
- Expressions — single constants, variables, function references or combinations of these components, plus operators that specify computations to be performed.
- Keywords — words recognized by FIFEE as having a specific meaning such as SHOW and SLOT ARRAY.
- Comments — comments can be inserted at the end of each statement. Anything following an exclamation point, !, is treated as a comment except when the exclamation point is used in a quoted string.

The input language is free formatted; a statement can begin in any column, and blanks can appear anywhere within a statement (except within variable names, constants, and keywords). Blank lines are treated as comments and are ignored.

There can only be one statement per line and there are no continuation lines. There are two main restrictions on the input file: **all KEYWORDS must be capitalized and tabs must not be used.**

A.3 Symbolic Names.

A symbolic name is a character string that has a maximum length of 16 and that is composed of letters, digits, or characters. However, only two types of characters are

allowed in a filename: these special characters are the dollar sign (\$) and the underscore (_). Further, the first character in a symbolic name must be a letter. The use of variable names which are the same as keywords is discouraged since it can cause confusion. Symbolic names are used to identify the variables within FIFEE. Examples of valid symbolic names are:

```
ALL$R_GOOD
X
SLOT_WIDTH
```

Examples of invalid symbolic names are:

NO BLANKS	(contains a blank)
5thMODE	(begins with a numeral and contains lower case)
NOT_GOOD:GO	(contains a special character other than _ or \$)
\$NO	(begins with a \$)

By convention, character strings beginning with FIF\$ are reserved variables in FIFEE. These types of variables are used to perform functions within FIFEE not normally allowed by the input language. To avoid possible conflicts, do not use symbolic names starting with the four characters FIF\$.

A.4 Data Types.

The FIFEE input processor only recognizes one data type — real. Integer constants can be specified, but they are treated as real numbers. All operations are performed using real arithmetic.

A.4.1 Constants.

A constant represents a fixed value. Integer constants are allowed but they are converted to real values by the input processor. A constant can have any one of the following forms:

```
n
sn
s.n
sn.n
sn.
```

where s is an optional sign, plus or minus, and n is a string of decimal digits. The decimal point can appear anywhere in the string, while leading and trailing zeroes are ignored.

A.4.2 Complex Numbers.

The input processor does not explicitly recognize complex numbers, nor will it perform complex arithmetic. However, some of the statements require a complex value and thus, a method for specifying a complex number is provided. A complex number is specified as an ordered pair of real numbers in one of two formats:

(real, imaginary)
or
(magnitude, phase)

where the phase angle of the complex number must be expressed in radians. Examples of valid complex numbers are:

(A,1.23)
(1.5,.44)
((A+B)/C,SIN(D/2.3))

Examples of invalid complex numbers are:

(A,) (second expression missing)
(1.3,(A+B) (unmatched parentheses).

A.4.3 Variables.

A variable is a symbolic name associated with a storage location. The number held in that storage location defines the variable's current value. A variable is redefined by assigning it a new value using the equality symbol, =. A variable is undefined until a value has been assigned to it. FIFEE implicitly assumes that all values are real, thus, there are no data-type declaration statements. For the following example:

$var = 0.5 + (1/2)$,

the value assigned to var is 1.0, not 0.5 as would be produced if integer division were applied to $(1/2)$.

A.5 Arithmetic Expressions.

An arithmetic expression represents a single numeric value. It can be a single basic component, such as a constant or variable, or a combination of basic components with one or more operators. Operators specify computations to be performed using the values of the basic components. An arithmetic element can be any one of the following:

- A numeric constant.
- A numeric variable.
- An expression enclosed in parentheses.
- An arithmetic function reference.

Arithmetic operators specify a computation to be performed using the values of the arithmetic elements, and they produce a value as a result. The operators and their meanings are:

OPERATOR	FUNCTION
**	Exponentiation
*	Multiplication
/	Division
+	Addition
-	Subtraction (and negation)

A variable element must be defined before it can be used in an arithmetic expression. Arithmetic expressions are evaluated from left to right with the same operator precedence as is used in the FORTRAN computer programming language. Parentheses can be used to force a particular order of evaluation, but nonessential parentheses, as in the following expression, do not affect evaluation of the expression:

$$3.+(1/2)$$

The arithmetic assignment statement assigns the value of an expression to a numeric variable. If the variable has not been previously referenced, it is defined by the act of assigning the value. The assignment statement has the form:

$$v=e$$

where v is a numeric variable, and e is an arithmetic expression.

A.6 Commands.

There are nine commands that must be in every input file in order to generate sensible results. These are:

[NON]SKEWED GRID

SLOT ARRAY

NODE

SEGMENT

MODE

END ARRAY

XEQ

EXIT, and either

AZSCAN or FREQSCAN.

The rest of the commands are used to more fully communicate the desired geometry to FIFEE and to tailor the resulting output.

The remainder of this chapter is devoted to describing the FIFEE input language. First, a quick reference for the entire language is given. Then, descriptions of the syntax for the keywords are presented, including examples of their use. The chapter concludes with an example input file and the resulting output.

FIFEE Commands

AZSCAN *etamin, etamax, delta_eta, freq*
 END ARRAY
 EXIT
 FREQSCAN *freqmin, freqmax, delta_freq, eta*
 GET ADMITTANCES
 * LEFT HALFSPACE *epsilon, mu*
 MODE *terminal, segment, segment [,segment]*
 MOVE *node*
 NODE *label, coordinate, coordinate*
 /NO/PLOTFILE *filename*
 * RIGHT HALFSPACE *epsilon, mu*
 ROTATE *angle*
 SAVE ADMITTANCES
 SCALE *factor*
 SEGMENT *label, node, node*
 SET COORDINATES *qualifier[, qualifier...]*
 qualifiers: RELATIVE, ABSOLUTE, CARTESIAN, POLAR
 SET MODE $\begin{Bmatrix} \text{sine} \\ \text{cosine} \end{Bmatrix}$
 /NO/SHOW *qualifier[, qualifier...]*
 qualifiers: ARRAYS, MATRIX, MODES, CURRENTS, VOLTAGES, SLABS,
 BWDFIELDS, FWDFIELDS, INPUT, VALUES, ALL
 /NON/SKEWED GRID *dx, DX=dz*
 * SLAB *thickness, epsilon, mu*
 * SLOT ARRAY *width, number_of_columns [,epsilon]*
 TITLE $\{ \cdot \} \text{title} \{ \cdot \}$
 TRANSLATE *x, z*
 XEQ
 ZLOAD *column_number, complex_lumped_impedance_loading*

Built in Functions

SIN	COS	TAN	ASIN	ACOS	ATAN	SINH	COSH
TANH	EXP	LOG10	LOG	SQRT	INT	NINT	ABS

Reserved Variables

FIF\$ACCURACY	FIF\$FIND_EQUIVALENT_PATTERNS
FIF\$POLAR_FORMAT	FIF\$PRINT_EQUIVALENT_PATTERNS
FIF\$PRINT_EQUIVALENT_ARRAYS	FIF\$FIND_EQUIVALENT_ARRAYS

* Assumes imaginary parts of *epsilon* and *mu* are zero.

Built in Functions

The following is a list of the functions which are recognized by FIFEE within arithmetic expressions, and should be familiar to most users. If more information is desired about a particular function, consult a reference manual for the FORTRAN computer programming language; all of these functions are described there.

SIN	trigonometric sine
COS	trigonometric cosine
TAN	trigonometric tangent
ASIN	trigonometric arc sine
ACOS	trigonometric arc cosine
ATAN	trigonometric arc tangent
EXP	e^x
LOG10	$\log_{10}(x)$
LOG	$\ln(x)$
SQRT	\sqrt{x}
INT	real number truncated to integer value, e.g. INT(3.9) = 3.
NINT	real number rounded to nearest integer, e.g. NINT(3.9) = 4.
ABS	$ x $
SINH	hyperbolic sine
COSH	hyperbolic cosine
TANH	hyperbolic tangent

Reserved Variables

FIFEE uses certain reserved variables to allow the user to exercise controls not normally allowed by the input language. When such a variable is recognized, FIFEE checks their values before performing any operations which would be affected. These functions are usually diagnostic in nature and thus, do not warrant inclusion in the main language. The first four characters of a reserved variable are always FIF\$. In order to avoid conflicts, the user should not define variables names which start with those same four characters.

FIF\$ACCURACY Default value = 10000.

The reciprocal of the value assigned to this variable determines the accuracy to which the double summation in k,n space is carried. Under normal circumstances, the default value will insure that the sum has adequately converged without incurring undue processing time. Values greater than the default will increase accuracy at the expense of computer time. For values greater than 1×10^8 , FIFEE should be compiled in double precision.

FIF\$FIND_EQUIVALENT_PATTERNS Default value = 1.

Possible values are zero and one. A value of zero disables this feature. When set to one, the pattern factors of all modes are checked to see if they are equal to that of any other mode. For a set of modes that have equal pattern factors, on all subsequent calculations, the pattern factor for only one mode in the set is calculated and its value is used for the whole set. Saves CPU time.

FIF\$FIND_EQUIVALENT_ARRAYS Default value = 1.

Possible values are zero and one. A value of zero disables this feature. When set to one, all modes on a slab boundary are compared to all modes on a different slab boundary to see if they will produce the same self admittance matrix for their respective boundary; that is, the coupling between all the slots on a given boundary is calculated for comparison. Coupling from one boundary to another is not included in this comparison. Save CPU time when equivalent arrays are found, since certain calculations will not have to be duplicated.

FIF\$PRINT_EQUIVALENT_PATTERNS Default value = 0.

Possible values are zero and one. A value of zero disables this feature. When set to one, a listing of equivalent patterns are included in the output file.

FIF\$PRINT_EQUIVALENT_ARRAYS Default value = 0.

Possible values are zero and one. A value of zero disables this feature. When set to one, a listing of equivalent arrays are included in the output file.

FIF\$POLAR_FORMAT Default value = 1.

Possible values are zero and one. When set to one, all complex quantities are printed in the output file in polar format. When set to zero, the real and imaginary components of all complex quantities are printed in the output file.

AZSCAN

Specifies the monostatic scattering angles and the frequency to be used for analysis.

FORMAT *AZSCAN etamin, etamax, delta_eta, freq*

where *etamin* is an expression which defines the starting angle in degrees.
 etamax is an expression which defines the ending angle in degrees.
 delta_eta is an expression which specifies the angle increment, $\Delta\eta$, in degrees.
 freq is an expression which defines the frequency in GHz.

restrictions A spherical coordinate system is used with the restriction that $\alpha = 0$, limiting the plane of incidence to the x,y plane. Because the plane of incidence would be undefined for $\eta = 0$, anytime an angle of zero degrees is specified for η , 0.01 degrees is used instead. Reference Figure A.12.

DESCRIPTION When the XEQ statement is encountered, the analysis of the specified system will be performed at the frequency *freq* for the angles *etamin*, *etamin* + $\Delta\eta$, *etamin* + $2\Delta\eta$, until *etamin* + $n\Delta\eta$ is greater than *etamax*. If *etamax* is less than *etamin* then no computations are performed. If *etamax* = *etamin* then the computations are performed only at that angle.

EXAMPLES

The statement

```
AZSCAN -8., 0., 2., 18.
```

would result in computations at 18 GHz for angles of -8, -6, -4, -2, and 0.01 degrees.

Note: Anytime an angle of zero degrees is specified, 0.01 degrees is used instead. This is because the plane of incidence would be undefined for $\eta = 0$.

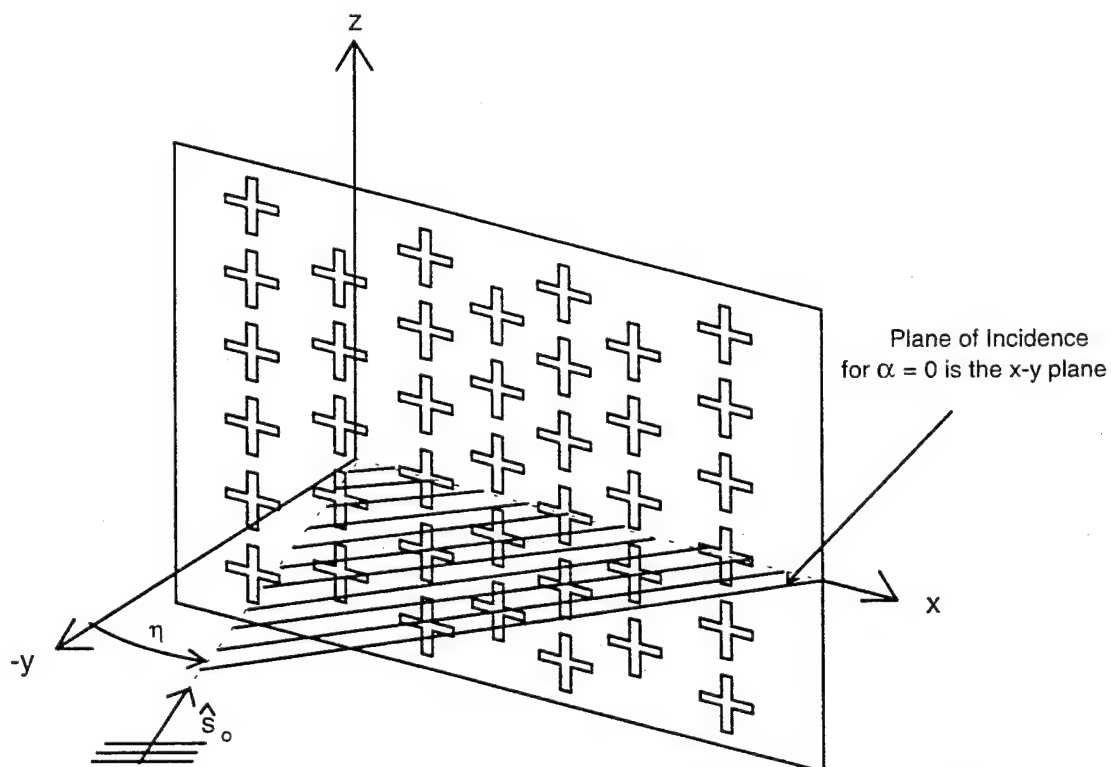
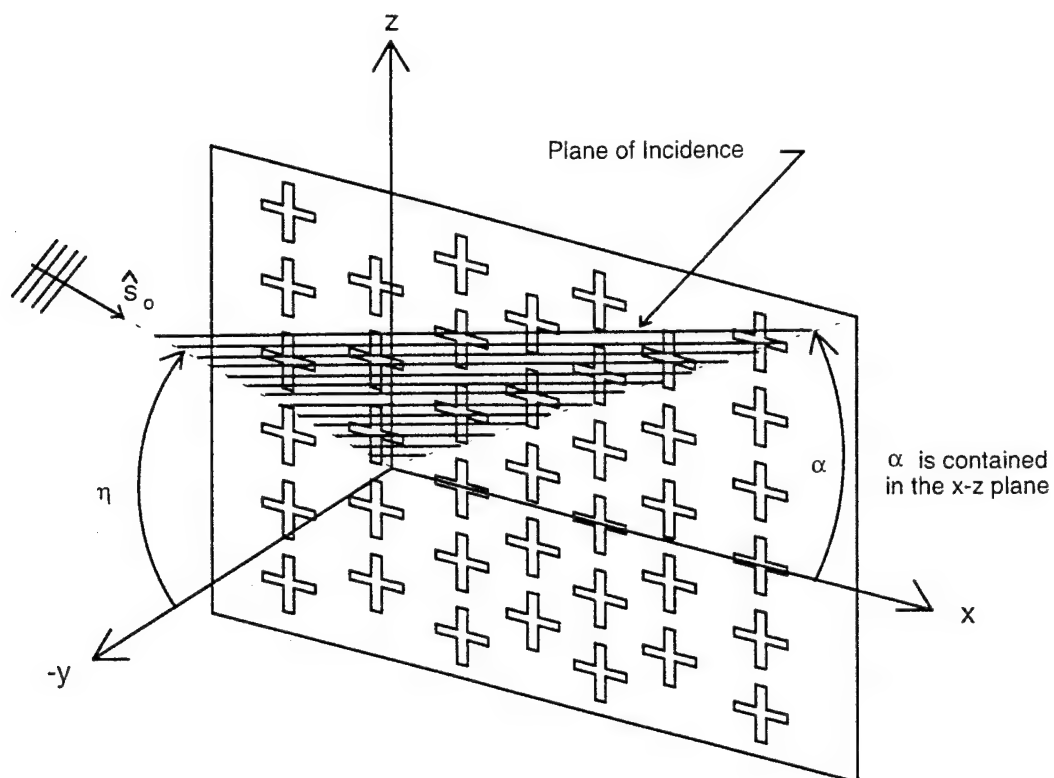


Figure A.12 The Spherical Coordinate System Used by FIFEE.

END ARRAY

Terminates an array definition block.

FORMAT	END ARRAY
--------	-----------

restrictions	Must occur within an array definition block.
--------------	--

DESCRIPTION	Terminates the definition of the current array. Once the array definition block has been closed by this statement, no more data can be added to that array; however, a new array can be started on the same boundary. Refer to the description for the SLOT ARRAY command for a further discussion on defining arrays.
-------------	--

EXIT

Terminates FIFEE.

FORMAT	EXIT
--------	------

restrictions	None.
--------------	-------

DESCRIPTION	Effects a graceful exit from FIFEE and should always be the last statement in the input file
-------------	--

FREQSCAN

Specifies the frequencies and the monostatic scattering angle to be used for analysis.

FORMAT

FREQSCAN *freqmin, freqmax, delta_freq, eta*

where

freqmin is an expression that defines the starting frequency in GHz.

freqmax is an expression that defines the ending frequency in GHz.

delta_freq is an expression that specifies the frequency increment, Δf , in GHz.

eta is an expression that defines the monostatic scattering angle in degrees.

restrictions

A spherical coordinate system is used with the restriction that $\alpha = 0$, limiting the plane of incidence to the x,y plane. Because the plane of incidence would be undefined for $\eta = 0$, anytime an angle of zero degrees is specified for η , 0.01 degrees is used instead. Reference Figure A.12.

DESCRIPTION

When the XEQ statement is encountered, the analysis of the specified system will be performed at the angle *eta* for the frequencies *freqmin*, *freqmin* + $\Delta\eta$, *freqmin* + $2\Delta\eta$, until *freqmin* + $n\Delta f$ is greater than *freqmax*. If *freqmax* is less than *freqmin* then no computations are performed. If *freqmax* = *freqmin* then the computations are performed only at that frequency.

EXAMPLES

The statement

FREQSCAN 8., 10., 2., 0.

would result in computations at 8 GHz and 10 GHz at an angle of 0.01 degrees. Note: Anytime an angle of zero degrees is specified, 0.01 degrees is used instead. This is because the plane of incidence would be undefined for $\eta = 0$.

GET ADMITTANCES

Reads a file created by the SAVE ADMITTANCES command.

FORMAT

GET ADMITTANCES

restrictions
for

Applicable when using AZSCAN, or for FREQSCAN if the scan is
only one frequency..

DESCRIPTION

Reads an existing file called *ymatrix* to obtain the values of a previously calculated admittance matrix. These values were saved to file using the command SAVE ADMITTANCES. Care must be taken to only use this feature when the geometry of the current input file is basically the same as that of the input file that issued the SAVE ADMITTANCES command. Note: the admittance matrix is recalculated for each new frequency, but not for new angles of incidence at the same frequency. This command is useful to obtain finer azscans without having to wait for the admittance matrix to be recalculated.

LEFT HALFSPACE

Sets μ_r and ϵ_r of the left halfspace.

FORMAT

LEFT HALFSPACE *epsilon, mu*

where

epsilon is an expression that defines ϵ_r , the complex relative permittivity. See section A.4.2 of this appendix for rules concerning complex numbers. Although defined as a complex number, the imaginary part of ϵ_r must equal zero (later versions of FIFEE will remove this lossless restriction).

mu is an expression that defines the complex relative permeability, μ_r , whose imaginary part must also equal zero.

restrictions

None.

DESCRIPTION

This statement allows the user to specify the constitutive parameters of the left semi-infinite halfspace. This halfspace is the region $y < 0$ as shown in Figure A.13. If not specified, it is assumed to be free space.

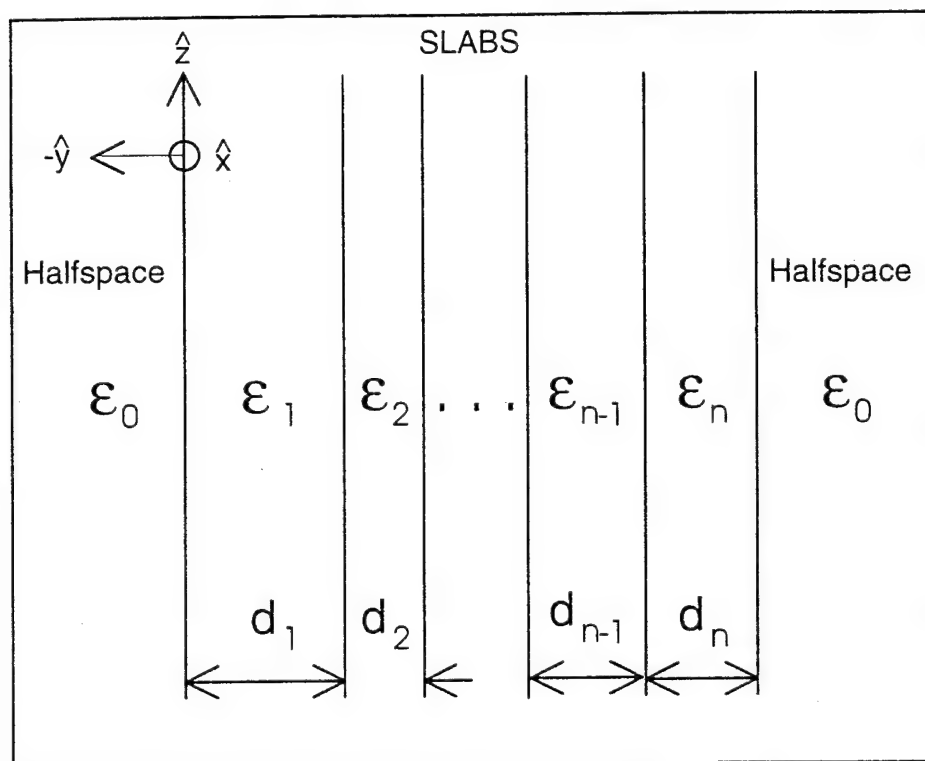


Figure A.13 An Example of a Stratified Dielectric Medium.

MODE

Defines a magnetic current mode.

FORMAT **MODE** *terminal, segment, segment [, segment...]*

where *terminal* is the label of the node which is at the terminals of the mode.

segment is the label of one of the segments which comprise the mode.

restrictions Only valid within an array definition block.

DESCRIPTION The list of segments must be able to form a continuous line with exactly two distinct endpoints but the segments do not need to be listed in any particular order — FIFEE will sort the list of segments into a suitable order. The colon delimiter, :, can be used between two segment labels (in place of the comma) to imply a list of segments. This feature is somewhat restrictive since it requires that the segment labels be in numerical sequence (1, 2, 3, 4, etc.).

EXAMPLES

The following three examples are all valid and all produce exactly the same mode (refer to Figure A.14):

```
MODE 2,6,7,8,9,10,1,2,3,4,5
MODE 2,1,2,3,4,5,6,7,8,9,10
MODE 2,1:4,5,6:10
```

The following four examples also refer to Figure A.14 and are invalid:

```
MODE 7,1,2,3        (the terminal is on the end)
MODE 2:1,2         (colon must delimit two segment labels)
MODE 1,1:          (colon must delimit two segment labels)
MODE 7,1:11        (the segments form a closed loop)
```

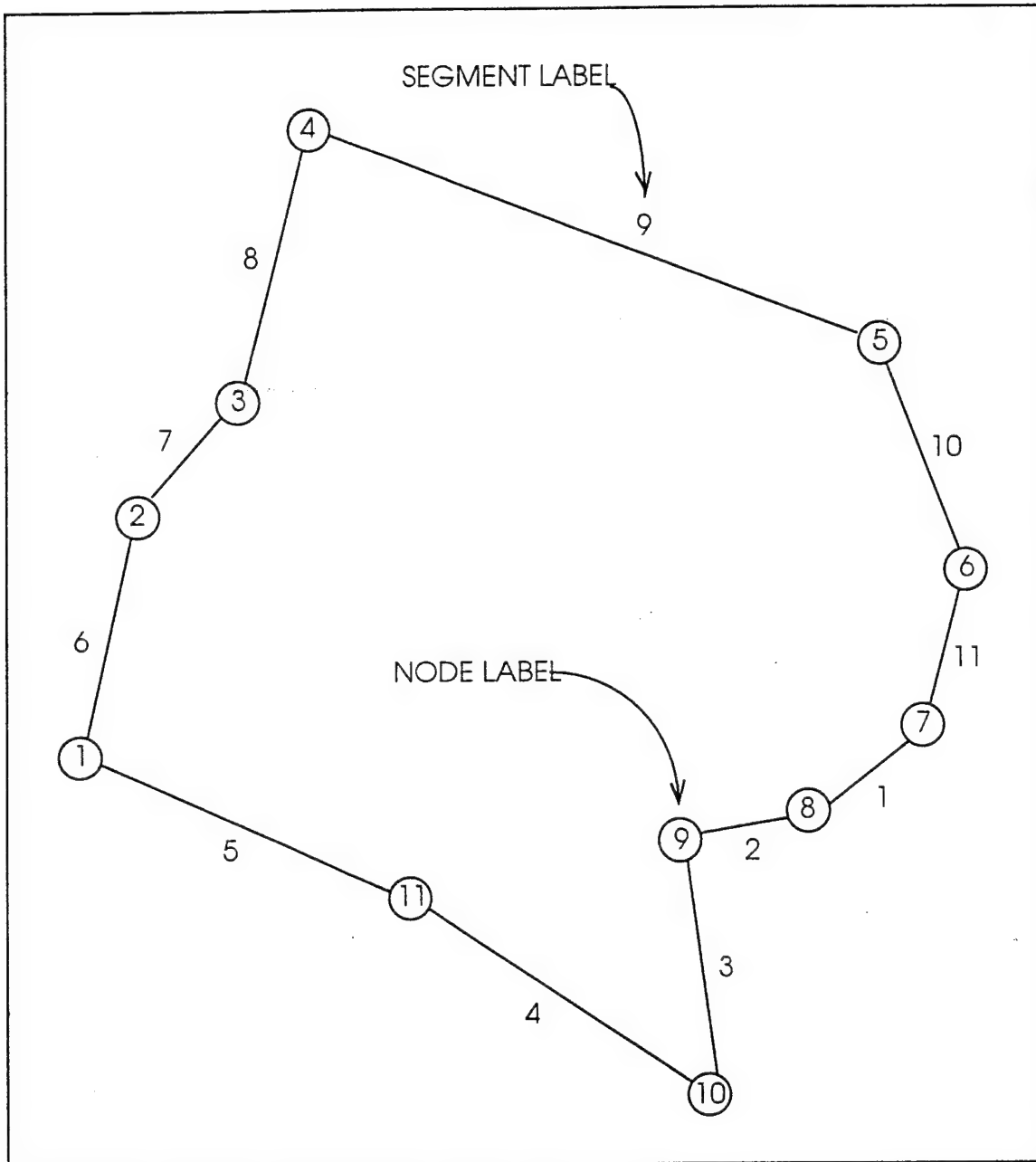


Figure A.14 A Loop Composed of 11 Segments and 11 Nodes.

MOVE

Resets the present position in relative coordinates.

FORMAT

MODE *node*

where

node is the label of the node which is to be the new reference point.
mode.

restrictions

Only valid within an array definition block.

DESCRIPTION

When relative coordinates are being used to define the node positions, the coordinates given in the NODE command are always interpreted as being relative to the previous node. This statement provides a mechanism for breaking that rule. It assigns as the new reference point the node being specified. This statement does not change any existing nodes or node coordinates; it merely sets the reference point for the next node to be defined. If absolute coordinates are in effect, then this statement does nothing.

EXAMPLES: This statement is best illustrated by the following example:

```
SET COORDINATES ABSOLUTE, CARTESIAN
NODE 10,0.,0.
SET COORDINATES RELATIVE
NODE 20,1.,0.
MOVE 10
NODE 30,-1.,0.
```

The nodes will be created with the coordinates shown in the table below. As the table shows, had the MOVE statement not been used, node 30 would have been created at (0.,0.), since it's specified coordinates would have been relative to node 20. The only effect of the MOVE command was to change the reference point for node 30 to node 10.

Node Label	Location with MOVE	Location without MOVE
10	(0.,0.)	(0.,0.)
20	(1.,0.)	(1.,0.)
30	(-1.,0.)	(0.,0.)

NODE

Creates a node for the present array.

FORMAT

NODE *label*, *coordinate_1*, *coordinate_2*

where

label is an expression that defines the node label.

coordinate_1 is an expression that defines the first coordinate in the coordinate pair.

coordinate_2 is an expression defining the 2nd coordinate in the pair.

restrictions

Only valid within an array definition block.

DESCRIPTION

This statement is used to define a node (a named coordinate point) for the array currently being defined. The reference element of an array is constructed by first specifying a set of nodes via the NODE statement. These nodes are then connected to form segments via the SEGMENT statement. Finally, the current modes are built by specifying which segments comprise each mode and at which node the terminals of the mode are to be located.

The integer portion of the value assigned to label is used as a unique name by which the node can be referred, much like the statement label used in FORTRAN programs. The label must be unique within the definition of the current array. If a node with the same label has already been defined, an error message is generated. The list of node labels is cleared by the END ARRAY statement, thus two nodes on different arrays can have the same label.

The interpretations of *coordinate_1* and *coordinate_2* are determined by which coordinate system is being used. If the system is Cartesian, then they correspond to *x* and *z*. If polar coordinates are being used, then they correspond to *r* and θ , where θ is in degrees. If any coordinate transformations have been specified (using the TRANSLATE, SCALE, and ROTATE commands), these transformations are applied to the coordinate pair to determine the actual coordinates. **The final coordinates used to define the node position are assumed to be in centimeters** See the ROTATE command for a description of coordinate transformations.

PLOTFILE

Open or close the file containing the calculated results of the forward or backward scattered fields.

FORMAT NOPLOTFILE
 PLOTFILE *filename*

where *filename* is a character string which specifies the name of the file.

restrictions None.

DESCRIPTION The plot file is intended to be used with a plotting program, such as GNUPLOT, to produce graphic images of the forward and/or backward scattered field patterns. The file is in ASCII format and consists of three columns of numbers. The first column contains the incident angle, η , while the second and third columns contain the real and imaginary parts of the requested scattered field, respectively.

The data is generated with generally formatted FORTRAN write statements in single precision. Therefore, an entry in this file will be either a pure decimal number or a decimal number with an extension in the E±i format, indicating a real exponent.

The NOPLOTFILE form of the above statement will cause an existing plot file to be closed. If no file is open, then no operation takes place and no error is generated.

The PLOTFILE form will cause either two or four files to be opened for output, depending on how the SHOW command is used in the input file. Two files are generated for the FWDFIELDS option, and two for the BWDFIELDS option. The default is that all four are generated. The root name of these files will be the specified filename, which is then appended with an extension indicating the data it contains. There are four possibilities:

plotfile_bo (containing the backscattered field's orthogonal component),
plotfile_bp (containing the backscattered field's parallel component),
plotfile_fo (containing the forwardscattered field's orthogonal component), *plotfile_fp* (containing the forwardscattered field's parallel component).

If a plot file is already open, it is closed and deleted, and a new file is opened in its place. The filename string must be delimited by a space

on the left and either a space, an end of line, or a comment (!) character on the right. There can be no spaces within the filename.

EXAMPLES:

Valid examples are:

PLOTFILE PLOT.DAT which can generate PLOT.DAT_BP, PLOT.DAT_BO,
PLOT.DAT_FP, and PLOT.DAT_FO.

PLOTFILE PLOT.DAT ! comment

PLOTFILE PLOT.DAT!comment

Invalid examples are:

PLOTFILEPLOT.DAT (No space after keyword)

PLOTFILE PLOT. DAT (Space within filename)

RIGHT HALFSPACE

Sets μ_r and ϵ_r of the right halfspace.

FORMAT

RIGHT HALFSPACE *epsilon, mu*

where

epsilon is an expression that defines ϵ_r , the complex relative permittivity. See section A.4.2 of this appendix for rules concerning complex numbers. Although defined as a complex number, the imaginary part of ϵ_r must equal zero (later versions of FIFEE will remove this lossless restriction).

mu is an expression that defines the complex relative permeability, μ_r , whose imaginary part must also equal zero.

restrictions

None.

DESCRIPTION

This statement allows the user to specify the constitutive parameters of the right-hand semi-infinite halfspace. This halfspace is the region from the last dielectric slab to $y = \infty$ as shown in Figure A.13. If not specified, it is assumed to be free space.

ROTATE

Specifies a rotation of coordinates.

FORMAT

ROTATE *angle*

where

angle is an expression that defines the rotation in degrees.

restrictions

Only valid within an array definition block.

DESCRIPTION

This command sets a rotational transformation to be applied to all subsequent nodes. **It does not affect existing nodes.** The angle is always measured counterclockwise from the \hat{x} axis.

All coordinate transformations are cleared by the ARRAY command when an array begins. The coordinate transformations are applied in the order, SCALE, ROTATE, TRANSLATE; irregardless of the order in which they were specified. When using absolute coordinates (either polar or Cartesian), the center of rotation is always at the origin (0,0) as shown in Figure A.15. When using relative coordinates the center of rotation is always the current node as shown in Figure A.16.

Note that in relative coordinates, the effect of translation is cumulative, which can be confusing. The very nature of relative coordinates provides a built in translation mechanism and thus this transformation is not particularly useful when using relative coordinates. The coordinate transformations are always specified as absolute quantities — specification of transformations is independent of coordinate system and existing transformations.

EXAMPLES:

To rotate all coordinates 45°, the following statement would be used:

```
ROTATE 45.
```

If it then became desirable to have no rotation, the following statement would be issued:

```
ROTATE 0.
```

The coordinate transformations only apply to nodes which are defined after the specified transformations. For example, the following sequence of statements:

```
SET COORDINATES ABSOLUTE, CARTESIAN
NODE 10,2.,2.
ROTATE -90.
NODE 20,2.,2.
ROTATE 90.
NODE 30,2.,2.
ROTATE 0.
NODE 40,3.,3.
```

would create the following nodes:

Node Label	Position (x,z)	Explanation
10	2.,2.	No transformation
20	2.,-2.	Rotate by -90°
30	-2.,2.	Rotate by 90°
40	3.,3.	Rotate by 0°

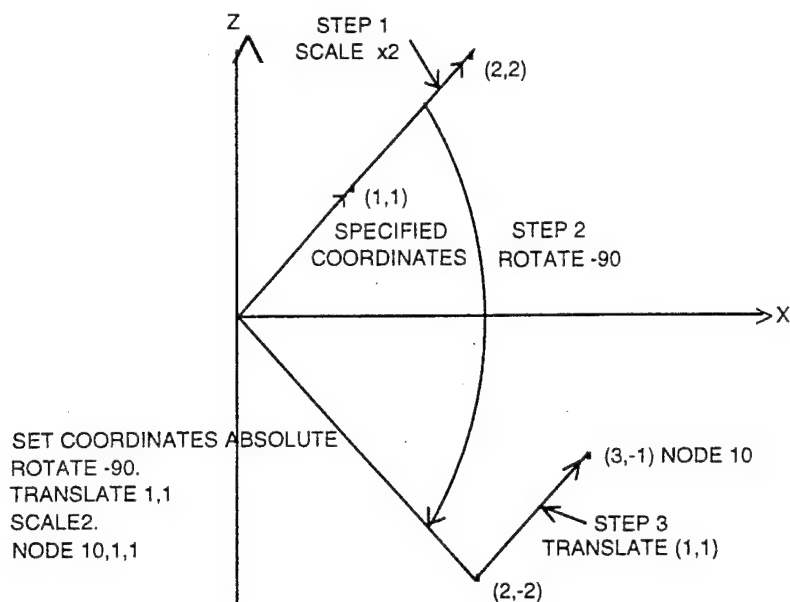


Figure A.15 Coordinate Transformations in Absolute Coordinates.

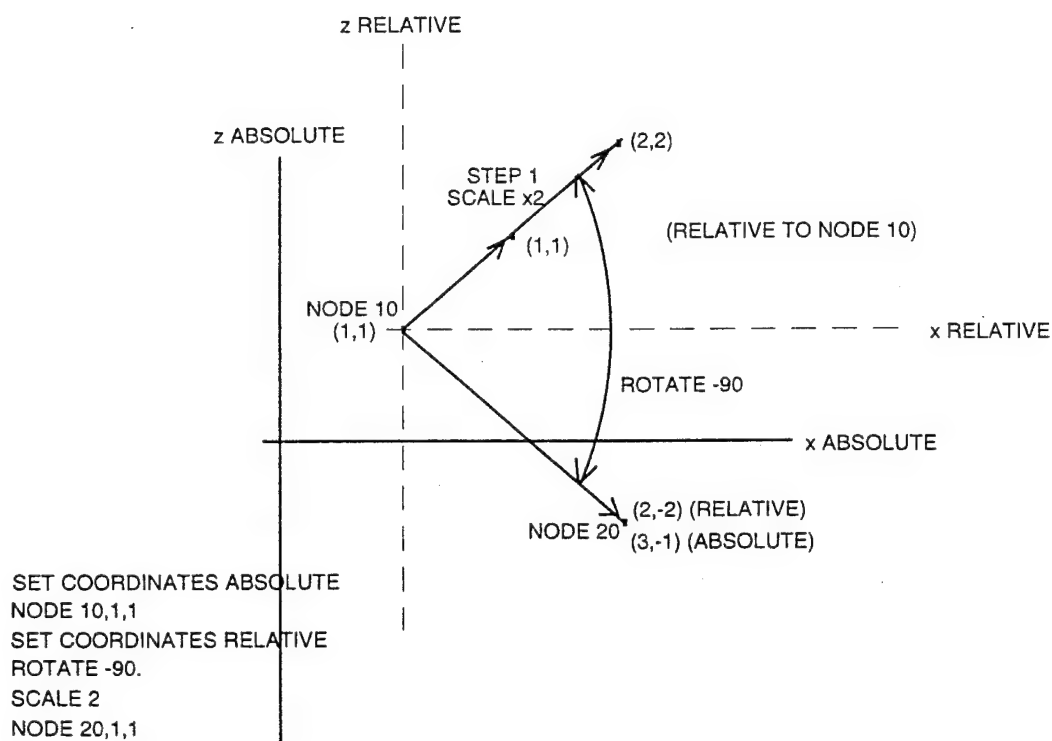


Figure A.16 Coordinate Transformations in Relative Coordinates. Note: node 20 is defined relative to node 10 and thus node 10 is the center of rotation for node 20.

SAVE ADMITTANCES

Saves the calculated admittance matrix to a file call "ymatrix" for later use.

FORMAT

SAVE ADMITTANCES

restrictions
the

Applicable when using AZSCAN, or when using FREQSCAN if scan is for only one frequency..

DESCRIPTION

Opens a file called *ymatrix* and writes to it the admittance matrix that

FIFEE calculates. These admittance values can be read into FIFEE at a later time by using the command GET ADMITTANCES. If the file *ymatrix* already exists, then the old contents will be overwritten; the new data is not appended. Note: the admittance matrix is recalculated for each new frequency, but not for new angles of incidence at the same frequency. This command can be useful to obtain finer azscans without having to wait for the admittance matrix to be recalculated.

SCALE

Sets the scaling factor.

FORMAT	SCALE <i>factor</i>
--------	---------------------

where	<i>factor</i> is an expression that defines the scale factor.
-------	---

restrictions	Only valid within an array definition block.
--------------	--

DESCRIPTION	This statement is used to provide a scale factor which is applied to all subsequent node coordinates. The scale factor does not modify any existing nodes and only applies to the current array. It is set to unity each time a new array is started. Refer to the explanation of the ROTATE command for a discussion on the coordinate transformations.
-------------	--

SEGMENT

Defines a new segment.

FORMAT `SEGMENT label, node_1, node_2`

where *label* is the segment label.
 node_1 is the label of the first endpoint node.
 node_2 is the label of the second endpoint node.

restrictions Only valid within an array definition block.

DESCRIPTION The integer portion of *label* is used as a unique name by which the segment can be referred. Segment labels function much like the node labels described in the NODE command. A segment label must be unique within the definition of the current array. If a segment with the same label has already been defined, an error message is generated. The list of segment labels is cleared by the END ARRAY command; thus two segments on different arrays can have the same label. The nodes given by *node_1* and *node_2* must have been previously defined via the NODE command.

SET COORDINATES

Specifies the coordinate system for defining nodes.

FORMAT SET COORDINATES *qualifier* [, *qualifier*]

where *qualifier* is one of the following keywords:
RELATIVE, ABSOLUTE, CARTESIAN, POLAR.

restrictions Only valid within an array definition block.

DESCRIPTION There are actually four possible coordinate systems available. They are:

- relative Cartesian
- absolute Cartesian
- relative polar
- absolute polar

The qualifiers RELATIVE and ABSOLUTE are mutually exclusive, as are the qualifiers CARTESIAN and POLAR. If two mutually exclusive qualifiers appear, then only the second is used as shown in the first example below.

EXAMPLES:

Valid examples are:

```
SET COORDINATES POLAR, CARTESIAN      (gives Cartesian)
SET COORDINATES CARTESIAN
SET COORDINATES RELATIVE, CARTESIAN
```

SET MODE

Defines the basis functions used for analysis.

FORMAT	SET MODE { sine cosine
--------	------------------------------

restrictions	None.
--------------	-------

DESCRIPTION	<p>This statement defines the shape of the current modes used for the basis functions. The keyword SINE will cause FIFEE to use the piecewise sinusoidal (PWS) modes, and COSINE will cause the piecewise cosinusoidal (PWC) modes to be used. If not specified, the PWC modes are used. The same type of modes are used for all arrays.</p> <p>The testing functions are always PWS modes.</p>
-------------	---

SHOW

Controls the format of the printed output produced by FIFEE.

FORMAT *[NO]SHOW qualifier [, qualifier...]*

where

qualifier is one or more of the following keywords:

ARRAYS[†], MATRIX[†], MODES[†], CURRENTS,
VOLTAGES, SLABS[†], BWDFIELDS, FWDFIELDS,
INPUT[†], VALUES[†], ALL

restrictions

None.

DESCRIPTION

This statement is used to select the type of information that is output by FIFEE. By selecting from the above list of *qualifiers*, the user can tailor the type of information that is included in the output file, and also decide which data files are generated, if any. However, indiscriminate use of the available options can produce huge output files, making them cumbersome to read. The default options, denoted by the symbol †, are option which are initially enabled by FIFEE.

The *qualifiers* in the NOSHOW version of this statement cause the corresponding options to be disabled.

The SHOW and NOSHOW statements are optional and can appear any number of times, thus allowing the output listing to be tailored to meet specific needs and minimize the amount of extraneous data printed.

The data associated with each of the *qualifiers* is described as follows:

ALL — causes all options to be enabled.

ARRAYS — causes the structure of arrays, nodes, and segments to be included in the output file.

BWDFIELDS — directs FIFEE to produce two backscatter data files (plot files) for the FSS with respect to the plane of incidence: one for the orthogonal components of the backscattered fields and one for the parallel components backscattered fields. The file contains four columns of numbers: 1. the frequency, 2. the angle of incidence, 3. the real field components, and 4. the imaginary field components.

† Indicates default values.

CURRENTS — causes the electric currents induced in the slots by the incident plane wave to be included in the output file. These currents describe the forcing functions in the equivalent problem.

FWDFIELDS — directs FIFEE to produce two forwardscatter data files in the same format generated by BWDFIELDS.

INPUT — causes the data in the input file to be echoed in the output file.

MATRIX — while enabled, causes all calculated admittance matrices to be included in the output file. An admittance matrix is calculated for each frequency of interest, and each admittance matrix is $N \times N$, with N being the number of modes. Since there is at least one mode per column of slots, this data can become extremely lengthy.

MODES — causes the mode structure of all the electric scattering voltages in the slots (the mode structure of the magnetic scattering currents in the equivalent problem*) to be included in the output file.

SLABS — causes the structure of the stratified dielectric medium, consisting of a list of slabs and their dielectric properties, to be included in the output file.

VALUES — causes the value generated by each arithmetic assignment statement in the input file to be displayed. Since there is no print statement for displaying the values assigned to variables, this is the only means for retrieving the data.

VOLTAGES — causes the solutions of the electric scattering voltages in the slots (magnetic scattering currents in the equivalent problem*) to be included in the output file.

EXAMPLES:

Valid examples are:

```
SHOW ALL
SHOW VALUES, FWDFIELDS, INPUT
NOSHOW MATRIX
```

* For a problem based on a slotted ground plane, an equivalent problem can be constructed using a solid ground plane loaded with magnetic scattering currents at the former slot locations.

SKEWED GRID

Create a dielectric slab.

FORMAT /NON/SKEWED GRID dx , $DZ = dz$

where

dx is an expression that defines the spacing between adjacent columns of elements.

dz is an expression that defines the spacing between elements in the same column.

restrictions

None.

DESCRIPTION This statement is used to define the grid structure (inter-element spacing) of all of the arrays. An example is shown in Figure A.17. Since the use of Floquet's theorem requires that all of the columns of elements have the same periodicity, the inter-element spacings defined by dz must be the same for all arrays. This statement should be used to define different column (dx) spacings for different arrays, and thus can appear more than once; but a fatal error is generated if different dz values are used. This statement can be used to change the parameters for a subsequent XEQ statement.

If a nonskewed grid is specified, then $\Delta z = 0$. If a skewed grid is specified, then $\Delta z = dz / 2$. No other values are possible, and all arrays should have the same Δz value, else a fatal error is generated.

EXAMPLES:

Valid examples are:

SKEWED GRID 1.5, $DZ = 1.5$

NONSKEWED GRID 1.5, $DZ = 1.5$

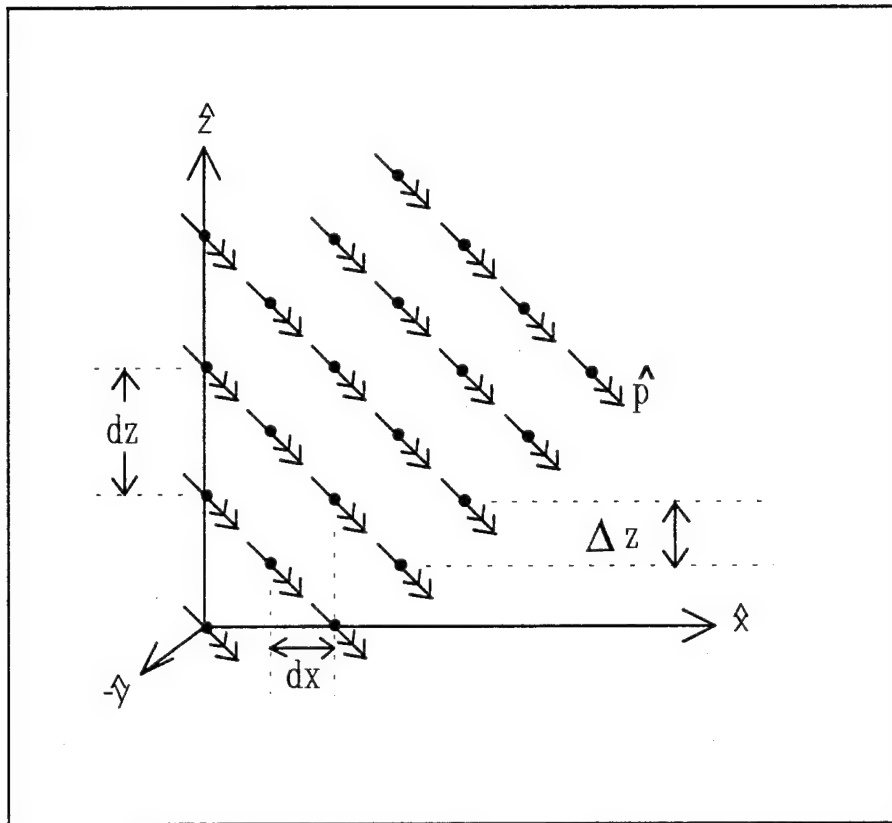


Figure A.17 The Grid Structure used by FIFEE.

SLAB

Create a dielectric slab.

FORMAT SLAB *thickness, epsilon, mu*

where *thickness* is an expression that defines the thickness of the slab in centimeters.

epsilon is an expression that defines the complex relative permittivity, ϵ_r . See section A.4.2 for rules concerning complex numbers.

mu is an expression that defines the complex relative permeability, μ_r . See section A.4.2 for rules concerning complex numbers.

restrictions Not valid within an array definition block.

DESCRIPTION This statement is used to define a dielectric slab of material. As shown in Figure A.13, the stratified medium used by FIFEE consists of multiple slabs of material which are infinite in the $\pm\hat{x}$ and $\pm\hat{z}$ directions, and have a finite thickness in the \hat{y} direction. An array can be defined only in the boundary between two slabs. If an array is to be imbedded within a single slab, it must be defined on the boundary between two slabs of identical characteristics. Mathematically this is the same as placing the array within a single slab. **All of the slabs and arrays are defined in sequence beginning at the $y = 0$ plane and moving in the $+y$ direction.** After a given slab i is defined, any arrays to be placed between slab i and slab $i + 1$ must be defined using the ARRAY statement before slab $i + 1$ is defined.

EXAMPLES:

Valid examples are:

SLAB 1., (A,B), (C,D)

SLAB THICK+2.3, (2.,0.), (1.,0.)

Invalid examples are:

SLAB THICK+1., (1.,0.) (No mu specified)

SLAB THICK+1.,1.,2. (epsilon and mu must be complex)

SLOT ARRAY

Begins the definition of an array of slots..

FORMAT **SLOT ARRAY** *width, number_of_columns* [, *epsilon*]

where *width* is an expression that defines the width of the array segments in centimeters.

number_of_columns is an expression which, if greater than one, causes multiple array columns to be defined and centered around the reference element location specified in the array definition block. The dx value for the array, which was specified in the *[non]skewed grid* statement determines the spacing between these infinite columns.

epsilon is an expression that defines the effective epsilon, ϵ_d , in which the array resides.

restrictions This statement must not appear within the context of an array definition block.

DESCRIPTION This statement begins the definition of an array of slots in a ground plane. All of the statements after a SLOT ARRAY statement up to and including an END ARRAY statement are said to exist within the array definition block. Most statements concerning arrays such as NODE, SEGMENT, MODE etc. are only valid within an array definition block. The array is placed at the boundary between the last dielectric slab specified via a SLAB statement and the next dielectric slab specified. The left and right halfspaces can be considered slabs which are automatically specified, thus an array can be put on the first boundary (between free space and the first slab) by defining it before the first slab, and an array can be put on the last boundary (between the last slab and the right halfspace) by specifying it after the last slab. If no slabs are specified (the SLAB statement is never used) then the array is placed on the $y = 0$ plane between the left and right halfspaces. More than one array can be defined on a boundary, thus several SLOT ARRAY, END ARRAY pairs can occur between two SLAB statements. All segments on an array are assumed to be the same width and exist in the same

medium ϵ_d . The quantity ϵ_d is used to compute the shape of the piecewise sinusoidal and piecewise cosinusoidal current modes; its primary purpose is to reduce the number of modes needed for accurate results. The default value is generally adequate, but, when in doubt, its effect can be nullified by adding more modes. If not specified by the user, then $\epsilon_d = (\epsilon_n + \epsilon_{n+1})/2$, where ϵ_n and ϵ_{n+1} are the dielectric constants of the adjacent slabs.

Multiple arrays can be defined on the same boundary. This feature can be used to define an array with columns of different element shapes and/or columns with different impedance loads. Arrays defined on the same boundary must have the same dz value, the same element width, and the same ϵ_d .

TITLE

Specifies a title for the output file and plots.

FORMAT TITLE "*title*"
 TITLE '*title*'

where *title* is a character string of up to 64 characters enclosed in single or double quotes.

restrictions None.

DESCRIPTION This statement is used to provide an identifying title for the output listings. It is an optional statement, but is very useful for cataloguing results. Only the last title specified before each XEQ statement is used, and any previous titles are lost. Whether the title is enclosed in single or double quotes is a matter of choice, but the choice must be consistent; a title cannot be enclosed on the left with a single quote and then on the right with a double quote, or vice versa. If the title is enclosed with single quotes then it may contain double quotes and vice versa.

EXAMPLES:

Valid examples are:

```
TITLE 'This is the title'
TITLE "This is the title"
TITLE "It's the title"
```

Invalid examples are:

```
TITLE 'This is the title        (No closing quote)
TITLE 'This is the title"       (Mixed quotes)
```

TRANSLATE

Specify a coordinate translation.

FORMAT TRANSLATE x, z

where x is an expression that defines the amount of translation in the \hat{x} direction.

z is an expression that defines the amount of translation in the \hat{z} direction.

restrictions Only valid within an array definition block.

DESCRIPTION This statement is used to provide an automatic translation to be applied to all subsequent nodes. **It does not affect existing nodes.**

The x, z coordinates specified with this command are unaffected by the coordinate system. They are always specified in absolute Cartesian coordinates, and are always applied after any scaling and rotation. Any desired translation must be specified separately for each array that is to be translated, otherwise the default value of "no translation" is used. Refer to the explanation of the ROTATE command for a discussion on coordinate transformations.

XEQ

Starts the actual analysis.

FORMAT

XEQ

restrictions

Must not occur within an array definition block, and must be preceded by the /NON/SKEWED GRID statement and either the AZSCAN or FREQSCAN statement.

DESCRIPTION

This statement is used to actually perform the scattering computations based on the preceding input data. When the XEQ statement is encountered, all arrays, slabs, frequencies, angles, etc., that are needed for analysis must have already been specified. If the NON/SKEWED GRID statement and either the AZSCAN or FREQSCAN statement does not precede the XEQ statement, then a divide by zero error will occur when computation begins. More than one XEQ statement can appear, allowing several sets of data to be obtained. The XEQ statement does not make any changes to the existing system (slabs, arrays, etc.). If several different sets of data are to be generated, changes must be made before a subsequent XEQ statement.

ZLOAD

Specifies the lumped impedance loading for a slot column's reference modes.

FORMAT *ZLOAD column_number, complex_impedance_load*

where *column_number* is an expression that specifies the column number of a particular array, counting from right to left (-x to x).

 complex_impedance_load is an expression defining the lumped impedance load (in ohms) to be placed at the center of each mode that composes the reference element for the specified column.

restrictions Only valid within an array definition block.

DESCRIPTION This statement is used to place a lumped impedance load at the terminal nodes of all the modes that compose the reference element of the specified slot column. An error is generated if the specified column number is less than zero or if the specified column number is greater than the number of columns defined for the array. If the column number is input as zero, then all columns of the specified array, that is, all modes of the array, will be loaded.

EXAMPLES:

Valid examples are:

```
ZLOAD 0., (187.5, 0.0)
ZLOAD 1., (187.5, 0.59)
ZLOAD 49., (93., 3.3)
```

Invalid examples are:

```
ZLOAD 0., 187.5            (Impedance load not in complex format)
ZLOAD -1., (93., 3.3)      (Negative value entered for column number)
```

An Example.

Two types of reference elements are defined in the following input file example, and are shown graphically in the following figure:

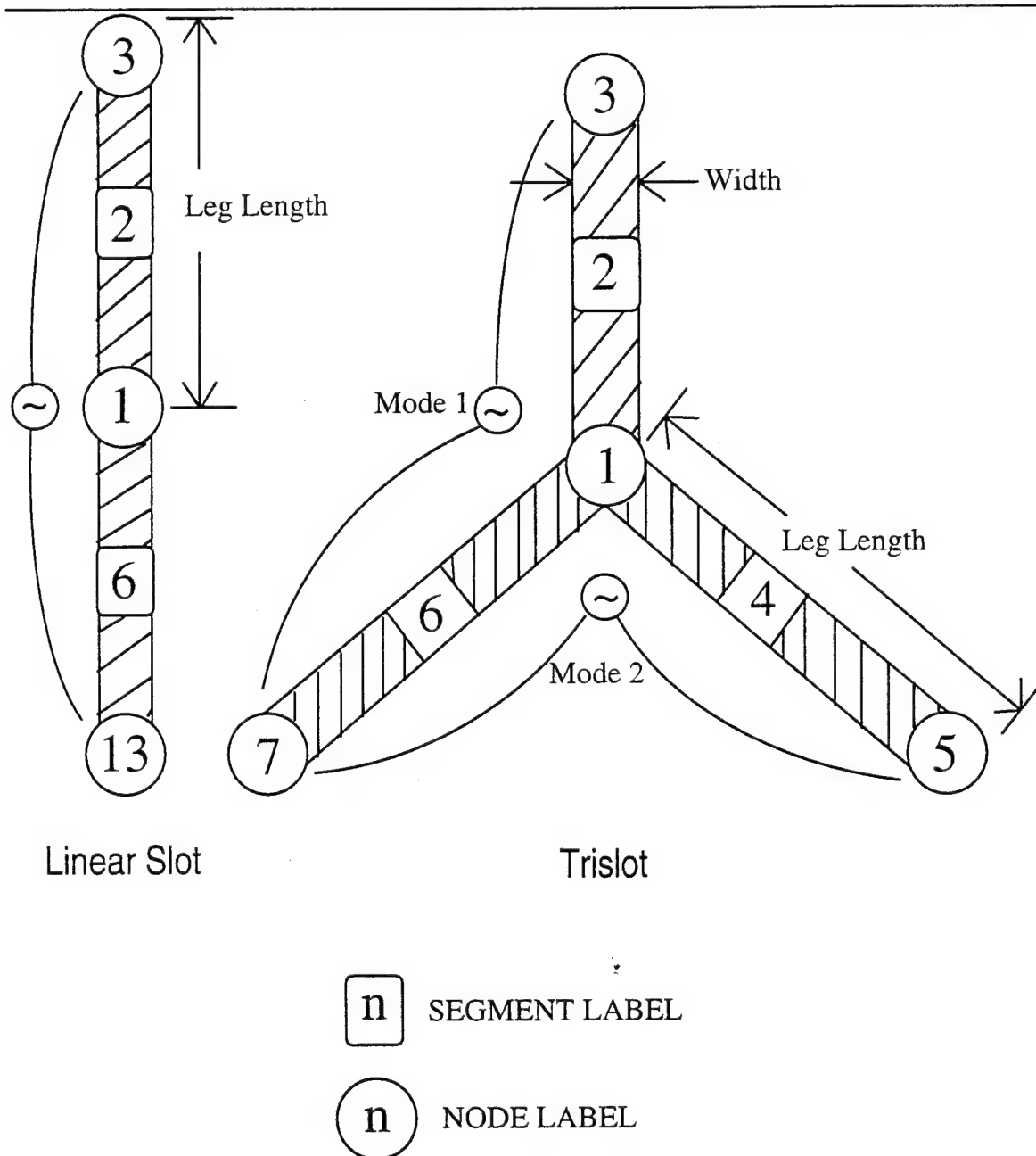


Figure A.18 Reference Elements for the Arrays in the FIFEE Example.

The Input File

```

TITLE 'FIFEE Example'
PLOTFILE ex.dat          ! NOSHOW FWDFIELDS selected below: 2 plot files generated: ex.dat_bp & ex.dat_bo
SHOW ALL                 ! Enables all output options
NOSHOW FWDFIELDS         ! Disables the 'forward scattered fields' option
!GET ADMITTANCES — would read file 'ymatrix' for admittance matrix values vice calculating them
!SAVE ADMITTANCES — would save calculated admittance matrix to a file called 'ymatrix' for later use
SET MODE SINE             ! The receiving (scattering) modes will be represented by PWS basis functions
AZSCAN -45.,-41.,3.0,10. ! A 10 GHz plane wave incident at -45 and -42 degrees
!FREQSCAN 10.,10.,1.0,45. — would initiate a 10 GHz plane wave at 45 degrees (statement commented out)
DX=.1                    ! Intercolumn spacing assigned to be 0.48 centimeters
WVL1=1.5                 ! Initializes variable WVL1 with a constant, 1.5 centimeters
WVL2=2.12132
DZ=0.75*WVL1             ! Variable DZ initialized using an arithmetic expression
D1=0.2*WVL1
D2=0.2*WVL2
LEG_LENGTH=WVL1/6.
SLOT_WIDTH=LEG_LENGTH/10.
NONSKEWED GRID DX,DZ=DZ ! The inter-column spacing & spacing of column elements are defined for next array
DZ=.36 ! The variable DZ is redefined. This does not redefine the spacing for column elements of array #1
SLAB D2,(2.0,0.),(1.,0.) ! Define slab #2. Slab #1 is the left halfspace (freespace in this case).
SLAB D1,(4.0,0.),(1.,0.) ! Slab #3 is defined. It's (0.2x1.5) cm thick, with a relative epsilon of 4.0
NUM_OF_COL=2.
  SLOT ARRAY SLOT_WIDTH,NUM_OF_COL ! Array #1 is defined in the boundary between slabs 3 and 4
  ZLOAD 1,(99.9,0.0) ! Column one slot modes are resistively loaded with 99.9 ohms
  ZLOAD 2,(199.9,0.0) ! Column two slot modes are resistively loaded with 199.9 ohms
  TRANSLATE -0.65,0.0 ! Provides a coordinate translation for all nodes in this array block.
  NODE 1,0.,0.
  NODE 3,0.,LEG_LENGTH*(3/4)
  NODE 13,0.,-LEG_LENGTH*(3/4)
  SEGMENT 2,1,3
  SEGMENT 6,1,13
  MODE 1,2,6          ! Linear slot element in the z direction is defined
END ARRAY             ! Terminate definition of array #1
NUM_OF_COL=2.
DX=.5                 ! Each array can have a different DX
DZ=0.75*WVL1          ! DZ redefined because all arrays must have same column spacing (DZ & Δz)
NONSKEWED GRID DX,DZ=DZ ! The spacings for an array are redefined.
  SLOT ARRAY SLOT_WIDTH,NUM_OF_COL ! Array #2 on same boundary as array #1
  TRANSLATE 0.0,0.0 ! This statement redefines the translation set up by the previous TRANSLATE
  NODE 1,0.,0.
  NODE 3,0.,LEG_LENGTH
  ROTATE -120.         ! -120 degree coordinate rotation
  NODE 5,0.,LEG_LENGTH
  ROTATE 120.
  NODE 7,0.,LEG_LENGTH
  SEGMENT 2,1,3
  SEGMENT 4,1,5
  SEGMENT 6,1,7

```

```

MODE 1,2,6      ! First mode of a trislot is defined
MODE 1,6,4      ! Second mode of a trislot is defined
END ARRAY      ! Terminate definition of array #2
NUM_OF_COL=2.
DX=.1
NONSKEWED GRID DX,DZ=DZ ! Spacings for array #3 are defined. Arrays 1, 2, and 3, since on same boundary,
! will be combined by FIFEE and labeled as array #1 in the output file.
  SLOT ARRAY SLOT_WIDTH,NUM_OF_COL      ! Array #3 on same boundary as arrays #1 and #2
  TRANSLATE 0.65,0.0 ! Node translation once again redefined
  NODE 1,0.,0.
  NODE 3,0.,LEG_LENGTH*(3/4)
  NODE 13,0.,-LEG_LENGTH*(3/4)
  SEGMENT 2,1,3
  SEGMENT 6,1,13
  MODE 1,2,6
  ZLOAD 1,(199.9,0.0) ! This type of statement can appear anywhere in an array definition block
  ZLOAD 2,(99.9,0.0) ! Ditto
END ARRAY      ! Terminate definition of array #3
SLAB D1,(4,0,0.),(1.,0.) ! Slab #4 is defined
SLAB D2,(2,0,0.),(1.,0.)
SLAB D1,(4,0,0.),(1.,0.) ! Slab #6 is defined
NONSKEWED GRID .5,DZ=DZ ! Spacings for array #4 are defined. This array will be re-labeled as array #2 in the
output
! file since arrays 1, 2, and 3 were on the same boundary and thus combined. If a SKEWED GRID was specified here,
a
! fatal error would be generated since arrays would not all have same  $\Delta z$ .
NUM_OF_COL=3.
SLOT ARRAY SLOT_WIDTH,NUM_OF_COL
  ZLOAD 0,(199.9,0.01)
  NODE 1,0.,0.
  NODE 3,0.,LEG_LENGTH*(3/4)
  NODE 13,0.,-LEG_LENGTH*(3/4)
  SEGMENT 2,1,3
  SEGMENT 6,1,13
  MODE 1,2,6
END ARRAY
SLAB D1,(4,0,0.),(1.,0.)
SLAB D2,(2,0,0.),(1.,0.) ! Slab #8 defined. Slab #9 will be the right halfspace, freespace in this case
FIF$POLAR_FORMAT=0. ! Requests that complex numbers in the output file be in the (real, imag) format.
FIF$ACCURACY=10000. ! This statement does nothing since 10000 is the default value for the reserved variable
! FIF$ACCURACY, which is the accuracy parameter for the double summation in the
! Array Scanning Method.
FIF$PRINT_EQUIVALENT_ARRAYS=1.
FIF$PRINT_EQUIVALENT_ARRAYS=1.
XEQ ! Compute the results
EXIT ! Finished

```

The Output File

```

TITLE 'FIFEE Example'
PLOTFILE ex.dat
SHOW ALL
NOSHOW FWDFIELDS
!GET ADMITTANCES
!SAVE ADMITTANCES
SET MODE SINE
AZSCAN -45.,-41.,3.0,10.
!FREQSCAN 10.,10.,1.0,45.
DX=.1
::: DX = 1.00000E-01
WVL1=1.5
::: WVL1 = 1.50000
WVL2=2.12132
::: WVL2 = 2.12132
DZ=0.75*WVL1
::: DZ = 1.12500
D1=0.2*WVL1
::: D1 = 0.300000
D2=0.2*WVL2
::: D2 = 0.424264
SLOT_LENGTH=0.5*WVL1
::: SLOT_LENGTH = 0.750000
SLOT_WIDTH=SLOT_LENGTH/10.
::: SLOT_WIDTH = 7.50000E-02
NONSKEWED GRID DX,DZ=DZ
DZ=.36
::: DZ = 0.360000
SLAB D2,(2.0,0.),(1.,0.)
SLAB D1,(4.0,0.),(1.,0.)
NUM_OF_COL=2.
::: NUM_OF_COL = 2.00000
    SLOT ARRAY SLOT_WIDTH,NUM_OF_COL
        ZLOAD 1,(99.9,0.0)
        ZLOAD 2,(199.9,0.0)
        TRANSLATE -0.65,0.0
        NODE 1,0.,0.
        NODE 3,0.,SLOT_LENGTH/4.
        NODE 13,0.,-SLOT_LENGTH/4.
        SEGMENT 2,1,3
        SEGMENT 6,1,13
        MODE 1,2,6
    END ARRAY
NUM_OF_COL=2.
::: NUM_OF_COL = 2.00000
DX=.5
::: DX = 0.500000
DZ=0.75*WVL1
::: DZ = 1.12500

```

```

NONSKEWED GRID DX,DZ=DZ
  SLOT ARRAY SLOT_WIDTH,NUM_OF_COL
    TRANSLATE 0.0,0.0
    NODE 1,0.,0.
    NODE 3,0.,SLOT_LENGTH/3.
    ROTATE -120.
    NODE 5,0.,SLOT_LENGTH/3.
    ROTATE 120.
    NODE 7,0.,SLOT_LENGTH/3.
    SEGMENT 2,1,3
    SEGMENT 4,1,5
    SEGMENT 6,1,7
    MODE 1,2,6
    MODE 1,6,4
  END ARRAY
NUM_OF_COL=2.
  ::: NUM_OF_COL                      =      2.00000
DX=.1
  ::: DX                              =      1.00000E-01
NONSKEWED GRID DX,DZ=DZ
  SLOT ARRAY SLOT_WIDTH,NUM_OF_COL
    TRANSLATE 0.65,0.0
    NODE 1,0.,0.
    NODE 3,0.,SLOT_LENGTH/4.
    NODE 13,0.,-SLOT_LENGTH/4.
    SEGMENT 2,1,3
    SEGMENT 6,1,13
    MODE 1,2,6
    ZLOAD 1,(199.9,0.0)
    ZLOAD 2,(99.9,0.0)
  END ARRAY
SLAB D1,(4.0,0.), (1.,0.)
SLAB D2,(2.0,0.), (1.,0.)
SLAB D1,(4.0,0.), (1.,0.)
NONSKEWED GRID .5,DZ=DZ
NUM_OF_COL=3.
  ::: NUM_OF_COL                      =      3.00000
SLOT ARRAY SLOT_WIDTH,NUM_OF_COL
  ZLOAD 0,(199.9,0.01)
  NODE 1,0.,0.
  NODE 3,0.,SLOT_LENGTH/4.
  NODE 13,0.,-SLOT_LENGTH/4.
  SEGMENT 2,1,3
  SEGMENT 6,1,13
  MODE 1,2,6
END ARRAY
SLAB D1,(4.0,0.), (1.,0.)
SLAB D2,(2.0,0.), (1.,0.)
ORB$POLAR_FORMAT=0.
  ::: ORB$POLAR_FORMAT                =      0.
ORB$ACCURACY=10000.
  ::: ORB$ACCURACY                    =      10000.00

```

ORBS\$PRINT_EQUIVALENT_ARRAYS=1.

::: ORBS\$PRINT_EQUIVALENT_ARRAYS = 1.00000

ORBS\$PRINT_EQUIVALENT_ARRAYS=1.

::: ORBS\$PRINT_EQUIVALENT_ARRAYS = 1.00000

XEQ

Output will be in dB-m.

```
*****
*
* Title      : FIFEE Example
* Date       : 15 Dec 94  03:54
* Input File  : ex.in
* Output File : ex.out
* Plot File   : ex.dat
*
*****
```

```
*****
*
* DIELECTRIC LAYERS
*
* layer  thickness      permittivity      permeability
* 1      0.0000      ( 1.00000, 0.00000) ( 1.00000, 0.00000) *
* 2      0.4243      ( 2.00000, 0.00000) ( 1.00000, 0.00000) *
* 3      0.3000      ( 4.00000, 0.00000) ( 1.00000, 0.00000) *
* 4      0.3000      ( 4.00000, 0.00000) ( 1.00000, 0.00000) *
* 5      0.4243      ( 2.00000, 0.00000) ( 1.00000, 0.00000) *
* 6      0.3000      ( 4.00000, 0.00000) ( 1.00000, 0.00000) *
* 7      0.3000      ( 4.00000, 0.00000) ( 1.00000, 0.00000) *
* 8      0.4243      ( 2.00000, 0.00000) ( 1.00000, 0.00000) *
* 9      0.0000      ( 1.00000, 0.00000) ( 1.00000, 0.00000) *
*
*****
```

ARRAY CONFIGURATIONS: DZ = 1.125000 delta_dz = 0.000000

SLOT ARRAY 1 ON BOUNDARY 3:

Slot Width = 0.075000 Number of Array Columns = 6

node	label	x	z	column
1	1	-0.700000	0.000000	1
2	3	-0.700000	0.187500	1
3	13	-0.700000	-0.187500	1
4	1	-0.600000	0.000000	2
5	3	-0.600000	0.187500	2
6	13	-0.600000	-0.187500	2
7	1	-0.250000	0.000000	3
8	3	-0.250000	0.250000	3
9	5	-0.033494	-0.125000	3

10	7	-0.466506	-0.125000	3
11	1	0.250000	0.000000	4
12	3	0.250000	0.250000	4
13	5	0.466506	-0.125000	4
14	7	0.033494	-0.125000	4
15	1	0.600000	0.000000	5
16	3	0.600000	0.187500	5
17	13	0.600000	-0.187500	5
18	1	0.700000	0.000000	6
19	3	0.700000	0.187500	6
20	13	0.700000	-0.187500	6

segment	label	ia	ib	column
1	2	1	2	1
2	6	1	3	1
3	2	4	5	2
4	6	4	6	2
5	2	7	8	3
6	4	7	9	3
7	6	7	10	3
8	2	11	12	4
9	4	11	13	4
10	6	11	14	4
11	2	15	16	5
12	6	15	17	5
13	2	18	19	6
14	6	18	20	6

SLOT ARRAY 2 ON BOUNDARY 6:

Slot Width = 0.075000 Number of Array Columns = 3

node	label	x	z	column
21	1	-0.500000	0.000000	7
22	3	-0.500000	0.187500	7
23	13	-0.500000	-0.187500	7
24	1	0.000000	0.000000	8
25	3	0.000000	0.187500	8
26	13	0.000000	-0.187500	8
27	1	0.500000	0.000000	9
28	3	0.500000	0.187500	9
29	13	0.500000	-0.187500	9

segment	label	ia	ib	column
15	2	21	22	7
16	6	21	23	7
17	2	24	25	8
18	6	24	26	8
19	2	27	28	9

	1	2	3	4	5	6	7	8	9
1	!0.11056!	0.10177!	0.61789!	-.97319!	-.29432!	-.54978!	-.44677!	-.41255!	-.41128!
	! e -1 !	e -2 !	e -3 !	e -4 !	e -3 !	e -4 !	e -3 !	e -3 !	e -3 !
	!-.92928!	-.19025!	-.85276!	0.90160!	-.64469!	0.66305!	-.14939!	-.52660!	0.14194!
	! e -2 !	e -2 !	e -3 !	e -4 !	e -3 !	e -4 !	e -3 !	e -4 !	e -3 !
2	!0.10177!	0.60485!	0.79764!	-.85348!	-.15493!	-.73809!	-.45417!	-.44677!	-.41301!

```

! e -2 ! e -2 ! e -3 ! e -4 ! e -3 ! e -4 ! e -3 ! e -3 ! e -3 !
! -.19025! -.92928! -.96305! 0.28761! -.74954! 0.57148! -.26822! -.14939! 0.12079!
! e -2 ! e -2 ! e -3 ! e -3 ! e -3 ! e -4 ! e -3 ! e -3 ! e -3 !

```


	1	2	3	4	5	6	7	8	9
3	!0.61789!	0.79764!	0.91974!	0.40862!	0.33142!	0.17897!	-.22874!	-.34930!	-.42874!
	! e -3 !	e -3 !	e -3 !	e -3 !	e -3 !	e -3 !	e -3 !	e -3 !	e -3 !
	!-.85276!	-.96305!	-.60469!	0.28610!	-.69545!	-.21864!	-.69233!	-.57888!	0.15759!
	! e -3 !	e -3 !	e -2 !	e -2 !	e -3 !	e -3 !	e -3 !	e -3 !	e -3 !
4	!-.97319!	-.85348!	0.40862!	-.81719!	0.44540!	-.62440!	0.73809!	0.54977!	0.28982!
	! e -4 !	e -4 !	e -3 !	e -3 !	e -3 !	e -3 !	e -4 !	e -4 !	e -5 !
	!0.90160!	0.28761!	0.28610!	-.56758!	-.88270!	0.11004!	-.57149!	-.66305!	0.18352!
	! e -4 !	e -3 !	e -2 !	e -2 !	e -3 !	e -2 !	e -4 !	e -4 !	e -4 !
5	!-.29432!	-.15493!	0.33142!	0.44540!	0.91974!	0.40862!	0.71229!	0.52057!	-.29076!
	! e -3 !	e -3 !	e -3 !	e -3 !	e -3 !	e -3 !	e -3 !	e -3 !	e -3 !
	!-.64469!	-.74954!	-.69545!	-.88270!	-.60469!	0.28610!	-.67550!	-.76248!	0.43336!
	! e -3 !	e -3 !	e -3 !	e -3 !	e -2 !	e -2 !	e -3 !	e -3 !	e -3 !
6	!-.54978!	-.73809!	0.17897!	-.62440!	0.40862!	-.81719!	0.85347!	0.97319!	0.33414!
	! e -4 !	e -4 !	e -3 !	e -3 !	e -3 !	e -3 !	e -4 !	e -4 !	e -4 !
	!0.66305!	0.57148!	-.21864!	0.11004!	0.28610!	-.56758!	-.28761!	-.90159!	0.30347!
	! e -4 !	e -4 !	e -3 !	e -2 !	e -2 !	e -2 !	e -3 !	e -4 !	e -4 !
7	!-.44677!	-.45417!	-.22874!	0.73809!	0.71229!	0.85347!	0.60485!	0.10177!	0.48357!
	! e -3 !	e -3 !	e -3 !	e -4 !	e -3 !	e -4 !	e -2 !	e -2 !	e -4 !
	!-.14939!	-.26822!	-.69233!	-.57149!	-.67550!	-.28761!	-.92928!	-.19025!	0.55435!
	! e -3 !	e -3 !	e -3 !	e -4 !	e -3 !	e -3 !	e -2 !	e -2 !	e -3 !
8	!-.41255!	-.44677!	-.34930!	0.54977!	0.52057!	0.97319!	0.10177!	0.11056!	0.15789!
	! e -3 !	e -3 !	e -3 !	e -4 !	e -3 !	e -4 !	e -2 !	e -1 !	e -3 !
	!-.52660!	-.14939!	-.57888!	-.66305!	-.76248!	-.90159!	-.19025!	-.92928!	0.54516!
	! e -4 !	e -3 !	e -3 !	e -4 !	e -3 !	e -4 !	e -2 !	e -2 !	e -3 !
9	!-.41128!	-.41301!	-.42874!	0.28982!	-.29076!	0.33414!	0.48357!	0.15789!	0.60485!
	! e -3 !	e -3 !	e -3 !	e -5 !	e -3 !	e -4 !	e -4 !	e -3 !	e -2 !
	!0.14194!	0.12079!	0.15759!	0.18352!	0.43336!	0.30347!	0.55435!	0.54516!	-.92930!
	! e -3 !	e -3 !	e -3 !	e -4 !	e -3 !	e -4 !	e -3 !	e -3 !	e -2 !
10	!-.29433!	-.34209!	-.42584!	-.28982!	-.42874!	0.28982!	-.34209!	-.29433!	0.44997!
	! e -3 !	e -3 !	e -3 !	e -5 !	e -3 !	e -5 !	e -3 !	e -3 !	e -3 !
	!0.40006!	0.33804!	0.17594!	-.18352!	0.15759!	0.18352!	0.33803!	0.40006!	-.77334!
	! e -3 !	e -3 !	e -3 !	e -4 !	e -3 !	e -4 !	e -3 !	e -3 !	e -3 !
11	!0.15789!	0.48357!	-.25735!	-.33414!	-.42584!	-.28982!	-.41301!	-.41128!	-.36121!
	! e -3 !	e -4 !	e -3 !	e -4 !	e -3 !	e -5 !	e -3 !	e -3 !	e -3 !
	!0.54516!	0.55435!	0.46370!	-.30347!	0.17594!	-.18352!	0.12079!	0.14194!	-.52459!
	! e -3 !	e -3 !	e -3 !	e -4 !	e -3 !	e -4 !	e -3 !	e -3 !	e -3 !

	10	11
1	!-.29433!0.15789!	
	! e -3 ! e -3 !	
	!0.40006!0.54516!	
	! e -3 ! e -3 !	
2	!-.34209!0.48357!	
	! e -3 ! e -4 !	
	!0.33804!0.55435!	
	! e -3 ! e -3 !	
3	!-.42584!-.25735!	
	! e -3 ! e -3 !	
	!0.17594!0.46370!	
	! e -3 ! e -3 !	
4	!-.28982!-.33414!	
	! e -5 ! e -4 !	
	!-.18352!-.30347!	
	! e -4 ! e -4 !	
5	!-.42874!-.42584!	
	! e -3 ! e -3 !	
	!0.15759!0.17594!	
	! e -3 ! e -3 !	
6	!0.28982!-.28982!	
	! e -5 ! e -5 !	
	!0.18352!-.18352!	
	! e -4 ! e -4 !	
7	!-.34209!-.41301!	
	! e -3 ! e -3 !	
	!0.33803!0.12079!	
	! e -3 ! e -3 !	
8	!-.29433!-.41128!	
	! e -3 ! e -3 !	
	!0.40006!0.14194!	
	! e -3 ! e -3 !	
9	!0.44997!-.36121!	
	! e -3 ! e -3 !	
	!-.77334!-.52459!	
	! e -3 ! e -3 !	
10	!0.60485!0.44997!	
	! e -2 ! e -3 !	
	!-.92930!-.77334!	
	! e -2 ! e -3 !	

```

      10      11
-----+-----
11 !0.44997!0.60485!
   ! e -3 ! e -2 !
   !-.77334!-.92930!
   ! e -3 ! e -2 !
-----+-----

```

FORCING VECTORS (MAGNETIC VOLTAGES / ELECTRIC CURRENTS):

[alpha = 0.00 (deg) eta = -45.00 (deg) freq = 10.00 (Ghz)]

Mode	Orthogonal	Parallel
1	(0. , 0.)	(0.53225E-03,-0.13353E-02)
2	(0. , 0.)	(0.32925E-03,-0.13993E-02)
3	(-0.26321E-03,-0.84268E-03)	(-0.37194E-03,-0.14525E-02)
4	(0.70549E-03, 0.16067E-02)	(-0.10610E-03, 0.31386E-04)
5	(-0.76303E-03,-0.44406E-03)	(-0.12549E-02,-0.82055E-03)
6	(0.16051E-02, 0.70923E-03)	(-0.57098E-04, 0.94779E-04)
7	(0. , 0.)	(-0.14371E-02,-0.33790E-04)
8	(0. , 0.)	(-0.14263E-02, 0.17878E-03)
9	(0. , 0.)	(0. , 0.)
10	(0. , 0.)	(0. , 0.)
11	(0. , 0.)	(0. , 0.)

SOLUTION VECTORS (MAGNETIC SCATTERING CURRENTS/ ELEC SCAT V):

[alpha = 0.00 (deg) eta = -45.00 (deg) freq = 10.00 (Ghz)]

Mode	Orthogonal	Parallel
1	(-0.28362E-02, 0.11545E-02)	(0.72584E-01,-0.28161E-01)
2	(-0.10366E-01, 0.60878E-02)	(0.96769E-01,-0.24704E-01)
3	(-0.17408E-01, 0.31387E-01)	(0.24072 , -0.11471)
4	(-0.38010 , 0.10311)	(0.11745 , -0.60787E-01)
5	(0.53218E-01,-0.30156E-02)	(0.40657E-01,-0.23818)
6	(-0.21452 , 0.22453)	(0.26564E-01,-0.12451)
7	(0.14092E-02,-0.10376E-01)	(-0.63510E-01,-0.61081E-01)
8	(-0.51031E-03,-0.17204E-02)	(-0.61254E-01,-0.18248E-01)
9	(0.55019E-03, 0.13789E-02)	(0.11108E-01,-0.32193E-02)
10	(0.21887E-03, 0.13711E-02)	(0.18449E-01,-0.81123E-02)
11	(0.96585E-03, 0.85401E-03)	(0.19458E-01,-0.24567E-01)

FORCING VECTORS (MAGNETIC VOLTAGES / ELECTRIC CURRENTS):

[alpha = 0.00 (deg) eta = -42.00 (deg) freq = 10.00 (Ghz)]

Mode	Orthogonal	Parallel
1	(0. , 0.)	(0.40933E-03,-0.14164E-02)
2	(0. , 0.)	(0.20733E-03,-0.14597E-02)
3	(-0.30723E-03,-0.83832E-03)	(-0.47627E-03,-0.14626E-02)
4	(0.78252E-03, 0.15942E-02)	(-0.10095E-03, 0.36819E-04)
5	(-0.77557E-03,-0.44233E-03)	(-0.13074E-02,-0.81024E-03)
6	(0.16263E-02, 0.71322E-03)	(-0.53377E-04, 0.93256E-04)
7	(0. , 0.)	(-0.14737E-02,-0.42772E-04)
8	(0. , 0.)	(-0.14652E-02, 0.16365E-03)
9	(0. , 0.)	(0. , 0.)
10	(0. , 0.)	(0. , 0.)
11	(0. , 0.)	(0. , 0.)

SOLUTION VECTORS (MAGNETIC SCATTERING CURRENTS/ ELEC SCAT V):

[alpha = 0.00 (deg) eta = -42.00 (deg) freq = 10.00 (Ghz)]

Mode	Orthogonal	Parallel
1	(-0.28163E-02, 0.12784E-02)	(0.71065E-01,-0.35929E-01)
2	(-0.10238E-01, 0.65558E-02)	(0.96387E-01,-0.33821E-01)
3	(-0.17452E-01, 0.30827E-01)	(0.23695 , -0.13108)
4	(-0.38125 , 0.11712)	(0.11492 , -0.68552E-01)
5	(0.52451E-01,-0.41893E-02)	(0.37566E-01,-0.24185)
6	(-0.21825 , 0.22983)	(0.25377E-01,-0.12677)
7	(0.15436E-02,-0.10501E-01)	(-0.62607E-01,-0.63205E-01)
8	(-0.41820E-03,-0.17591E-02)	(-0.61244E-01,-0.20749E-01)
9	(0.55684E-03, 0.13532E-02)	(0.11524E-01,-0.46606E-02)
10	(0.23569E-03, 0.13151E-02)	(0.18819E-01,-0.96559E-02)
11	(0.94232E-03, 0.76886E-03)	(0.18777E-01,-0.26024E-01)

```

+++++
+          FORWARD SCATTERED FIELDS FOR ORTHOGONAL POLARIZATION:          +
+                                                                           +
+ PHI-SCAT      ECHO WIDTH      MAGNITUDE      PHASE      FREQ      +
+   (deg)        (dB-m)          E Scat (V)      (deg)      (GHz)      +
+                                                                           +
+ -45.00        -100.000         0.0000E+00      0.00      10.00      +
+ -42.00        -100.000         0.0000E+00      0.00      10.00      +
+                                                                           +
+++++

```

```

+++++
+          BACK SCATTERED FIELDS FOR ORTHOGONAL POLARIZATION:          +
+                                                                           +
+ PHI-SCAT      ECHO WIDTH      MAGNITUDE      PHASE      FREQ      +
+   (deg)        (dB-m)          E Scat (V)      (deg)      (GHz)      +
+                                                                           +
+ -45.00        -32.330         0.9648E-01     -103.60      10.00      +
+ -42.00        -31.869         0.1017E+00     -103.42      10.00      +
+                                                                           +
+++++

```

```

+++++
+          FORWARD SCATTERED FIELDS FOR PARALLEL POLARIZATION:          +
+                                                                           +
+ PHI-SCAT      ECHO WIDTH      MAGNITUDE      PHASE      FREQ      +
+   (deg)        (dB-m)          E Scat (V)      (deg)      (GHz)      +
+                                                                           +
+ -45.00        -56.458         0.5998E-02      55.92      10.00      +
+ -42.00        -55.524         0.6679E-02      55.57      10.00      +
+                                                                           +
+++++

```

```

+++++
+          BACK SCATTERED FIELDS FOR PARALLEL POLARIZATION:          +
+                                                                           +
+ PHI-SCAT      ECHO WIDTH      MAGNITUDE      PHASE      FREQ      +
+   (deg)        (dB-m)          E Scat (V)      (deg)      (GHz)      +
+                                                                           +
+ -45.00        -41.057         0.3532E-01      83.86      10.00      +
+ -42.00        -39.585         0.4185E-01      75.69      10.00      +
+                                                                           +
+++++

```

EXIT

The Plotfiles

Since NOSHOW FWDFIELDS was specified in the input file, only two data files were generated and these were for the backscattered fields. One was for components orthogonal to the plane of incidence and the other for components parallel to the plane of incidence. These two files are presented below; the units of the quantities are shown in the above table in the output listing.

File "ex.dat_bp":

inc angle	echo width	magnitude	phase	frequency
-45.0000	-41.0574	3.53216E-02	83.8644	10.00000
-42.0000	-39.5852	4.18457E-02	75.6866	10.00000

File "ex.dat_bo":

inc angle	echo width	magnitude	phase	frequency
-45.0000	-32.3297	9.64768E-02	-103.6031	10.00000
-42.0000	-31.8691	1.01732E-01	-103.4156	10.00000

APPENDIX B

PATTERN FACTORS

FIFEE (Finite by Infinite: Fss with Edge Effects) is the name given to the computer model that implements the theory described in the main body of this text. As introduced in Chapter 3, if a periodic slot mode is composed of more than one piecewise linear segment, then FIFEE calculates the pattern factor integral for each segment associated with the mode, and then the results of these integrations are added to obtain the total pattern factor solution. The mathematical approach used to obtain this total solution, a solution which can be referred to as the *composite* pattern factor, is described in this appendix.

Consider the arbitrary bent mode shown in Figure B.1. In general, a mode is composed of a terminal node and two legs. The two legs are connected by the terminal node, and each leg is composed of one or more segments. The calculations begin at the terminal node and move outward along leg 1. In doing so, the pattern factor integration is performed over each segment that composes leg 1. The vector $\bar{\mathbf{P}}^{(1,n)}$ is used to point to that end of a segment, the n th mode segment of leg 1, which corresponds to the lower limit of the integration. Leg 2 is then calculated in the same manner. For the n th mode segment of leg 1,

$$\ell_{n-1} < \ell < \ell_n \quad (\text{B-1})$$

and the position vector is given by

$$\bar{\mathbf{R}}' = \bar{\mathbf{R}} + \ell_1 \hat{\mathbf{p}}^{(1,1)} + (\ell_2 - \ell_1) \hat{\mathbf{p}}^{(1,2)} + \dots + (\ell_{n-1} - \ell_{n-2}) \hat{\mathbf{p}}^{(1,n-1)} + (\ell - \ell_{n-1}) \hat{\mathbf{p}}^{(1,n)}. \quad (\text{B-2})$$

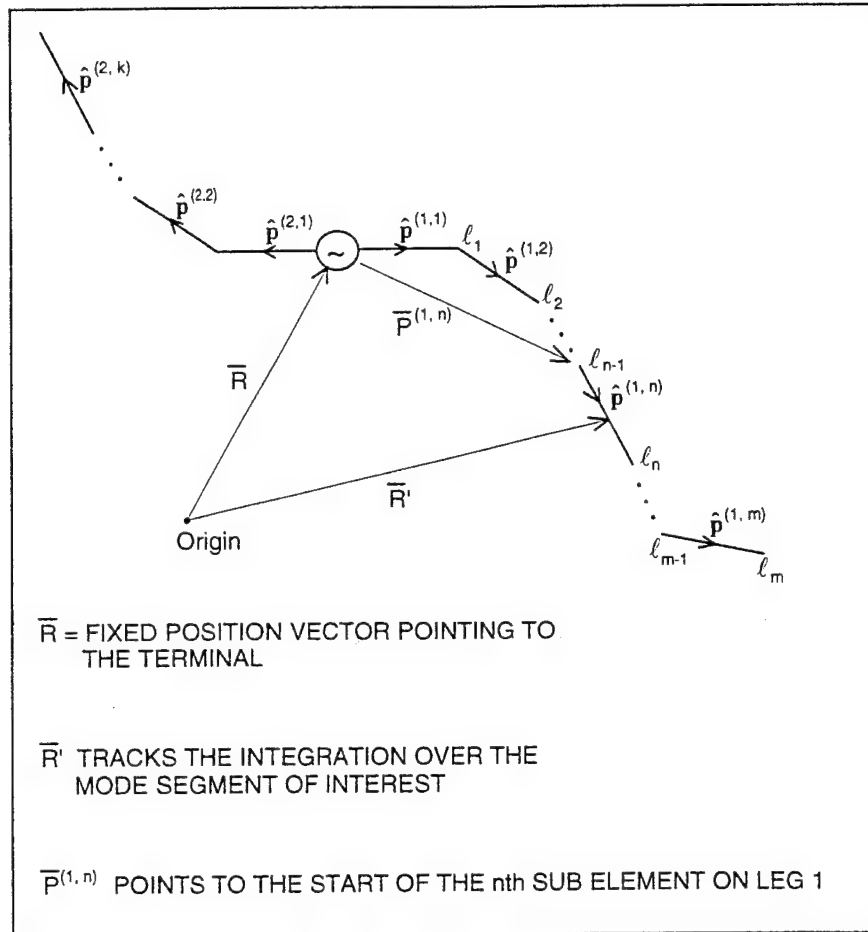


Figure B.1 An Arbitrary Piecewise Linear Current Mode That Contains m Sub Elements on Leg 1 and k Sub Elements on Leg 2

Letting $d_n = \ell_n - \ell_{n-1}$, the position vector can then be written as

$$\bar{R}' = \bar{R} + \sum_{i=1}^{n-1} d_i \hat{p}^{(1,i)} + (\ell - \ell_{n-1}) \hat{p}^{(1,n)} \quad (B-3)$$

or equivalently as

$$\bar{R}' = \bar{R} + \bar{P}^{(1,n)} + (\ell - \ell_{n-1}) \hat{p}^{(1,n)}. \quad (B-4)$$

In chapter 3, the general pattern factor equation for a sub element in slab v was given in its *receive* form (indicated by the superscript r) as

$$P_v^r = \int_a^b I(\ell) e^{-j\beta_v \ell \hat{\mathbf{p}} \cdot \hat{\mathbf{r}}_v} d\ell, \quad (\text{B-5})$$

where $\hat{\mathbf{r}}_v$ gives the direction of propagation of the incident wave in slab v . The transmitting form of this equation is obtained by changing the sign on the exponential term:

$$P_v^t = \int_a^b I(\ell) e^{+j\beta_v \ell \hat{\mathbf{p}} \cdot \hat{\mathbf{r}}_v} d\ell. \quad (\text{B-6})$$

Let $\varsigma = \pm 1$ be used to indicate whether the pattern factor is of the receiving type or of the transmitting type. Using ς to combine Equations (B-5) and (B-6), and substituting Equation (B-4) into this pattern factor definition yields the following equation for the basic pattern factor (of the n th sub element of leg 1 in slab v):

$$\begin{aligned} P_{v,n} &= \int_{\ell_{n-1}}^{\ell_n} I(\ell) e^{-\varsigma j\beta_v \left(\bar{\mathbf{p}}^{(1,n)} + (\ell - \ell_{n-1}) \hat{\mathbf{p}}^{(1,n)} \right) \cdot \hat{\mathbf{r}}_v} d\ell \\ &= e^{-\varsigma j\beta_v \left(\bar{\mathbf{p}}^{(1,n)} - \ell_{n-1} \hat{\mathbf{p}}^{(1,n)} \right) \cdot \hat{\mathbf{r}}_v} \int_{\ell_{n-1}}^{\ell_n} I(\ell) e^{-\varsigma j\beta_v \ell \hat{\mathbf{p}}^{(1,n)} \cdot \hat{\mathbf{r}}_v} d\ell \end{aligned} \quad (\text{B-7})$$

The function $I(\ell)$ represents the chosen basis or testing function, which in the case of this work is either a piecewise sinusoid (PWS) or a piecewise cosinusoid (PWC). For both of these functions, the integral in Equation (B-7) can be evaluated in closed form.

B.1 Piecewise Sinusoidal.

For a piecewise sinusoidal current

$$I(\ell) = \sinh[j\beta_v(\ell_m - \ell)], \quad (\text{B-8})$$

where ℓ_m represents the total length of one of the mode's legs (in this case, leg 1). Let

$$c_{1,n} = -\zeta\beta_v \hat{\mathbf{p}}^{(1,n)} \cdot \hat{\mathbf{r}}. \quad (\text{B-9})$$

Suppress the leg subscript such that $c_{1,n} = c_n$. Substituting Equations (B-8) and (B-9)

into Equation (B-7) yields

$$P_{v,n} = e^{-\zeta j\beta_v (\bar{\mathbf{p}}^{(1,n)} - \ell_{n-1} \hat{\mathbf{p}}^{(1,n)}) \cdot \hat{\mathbf{r}}_v} \int_{\ell_{n-1}}^{\ell_n} \sinh[j\beta_v(\ell_m - \ell)] e^{\ell c_n} d\ell. \quad (\text{B-10})$$

Define μ and ν such that

$$\mu = \frac{-1}{[2(c_n + j\beta_v)]}, \quad (\text{B-11})$$

and

$$\nu = \frac{1}{[2(c_n - j\beta_v)]}. \quad (\text{B-12})$$

Then, Equation (B-10) becomes:

$$P_{v,n} = e^{-\zeta j\beta_v (\bar{\mathbf{p}}^{(1,n)} - \ell_{n-1} \hat{\mathbf{p}}^{(1,n)}) \cdot \hat{\mathbf{r}}_v} \left[\mu \left[\cosh(-j\beta_v(\ell_m - \ell) + c_n \ell) + \sinh(-j\beta_v(\ell_m - \ell) + c_n \ell) \right] \right]_{\ell_{n-1}}^{\ell_n} + \nu \left[\cosh(j\beta_v(\ell_m - \ell) + c_n \ell) + \sinh(j\beta_v(\ell_m - \ell) + c_n \ell) \right]_{\ell_{n-1}}^{\ell_n} \quad (\text{B-13})$$

which simplifies to

$$P_{v,n} = e^{-\zeta j\beta_v (\bar{\mathbf{p}}^{(1,n)} - \ell_{n-1} \hat{\mathbf{p}}^{(1,n)}) \cdot \hat{\mathbf{r}}_v} \left[\mu \left[e^{j\beta_v(\ell_n - \ell_m) + c_n(\ell_n - \ell_{n-1})} - e^{j\beta_v(\ell_{n-1} - \ell_m)} \right] + \nu \left[e^{j\beta_v(\ell_m - \ell_n) + c_n(\ell_n - \ell_{n-1})} - e^{j\beta_v(\ell_m - \ell_{n-1})} \right] \right] \quad (\text{B-14})$$

B.2 Piecewise Cosinusoidal.

For a piecewise cosinusoidal current

$$I(\ell) = \frac{\cosh[j\beta_v \ell] - \cosh[j\beta_v \ell_m]}{1 - \cosh[j\beta_v \ell_m]}. \quad (\text{B-15})$$

Substituting Equations (B-9) and (B-15) into Equation (B-7) yields:

$$P_{v,n} = \frac{e^{-\zeta j\beta_v (\bar{\mathbf{p}}^{(1,n)} - \ell_{n-1} \hat{\mathbf{p}}^{(1,n)}) \hat{\mathbf{r}}_v}}{1 - \cosh[j\beta_v \ell_m]} \int_{\ell_{n-1}}^{\ell_n} [\cosh(j\beta_v \ell) - \cosh(j\beta_v \ell_m)] e^{\ell c_n} d\ell \quad (\text{B-16})$$

and performing the integration results in:

$$P_{v,n} = \frac{e^{-\zeta j\beta_v (\bar{\mathbf{p}}^{(1,n)} - \ell_{n-1} \hat{\mathbf{p}}^{(1,n)}) \hat{\mathbf{r}}_v}}{2(1 - \cosh[j\beta_v \ell_m])} [A + B - C] \quad (\text{B-17})$$

where

$$A = \frac{e^{j\beta_v \ell_n + c_n(\ell_n - \ell_{n-1})} - e^{j\beta_v \ell_{n-1}}}{c_n + j\beta_v} \quad (\text{B-18})$$

$$B = \frac{e^{-j\beta_v \ell_n + c_n(\ell_n - \ell_{n-1})} - e^{-j\beta_v \ell_{n-1}}}{c_n - j\beta_v} \quad (\text{B-19})$$

$$C = \frac{2 \cosh[j\beta_v \ell_m]}{c_n} \left(e^{c_n(\ell_n - \ell_{n-1})} - 1 \right) \quad (\text{B-20})$$

NOTE: In implementing the moment method, FIFEE always uses PWS shapes to define the testing functions. The basis functions have a default of PWC shapes, although the user can elect to use PWS shapes instead.

B.3 Composite Pattern Factor.

The PWS and PWC pattern factors derived above are for a sub segment of one of the legs of a mode. The composite pattern factor, the pattern factor for the entire mode, is computed as the sum of the pattern factors of all the sub segments of the mode (both legs). Ultimately, however, it is the polarized pattern factors that are desired. Using the notation already introduced (Chapter 3 and Appendix B), the polarized composite pattern factors are expressed as follows, where the first summation on the right hand side represents leg 1, where the second summation on the right hand side represents leg 2, and where the polarizing vectors $\hat{\mathbf{n}}$ (as shown in Figure B.2) are perpendicular and parallel to the plane of incidence with respect to slab v :

$$P_{\parallel,v} = \sum_{n=1}^m P_{v,n} \hat{\mathbf{p}}_n \cdot \hat{\mathbf{n}}_{\parallel,v} + \sum_{n'=1}^{m'} P_{v,n'} \hat{\mathbf{p}}_{n'} \cdot \hat{\mathbf{n}}_{\parallel,v} \quad (\text{B-21})$$

$$P_{\perp,v} = \sum_{n=1}^m P_{v,n} \hat{\mathbf{p}}_n \cdot \hat{\mathbf{n}}_{\perp,v} + \sum_{n'=1}^{m'} P_{v,n'} \hat{\mathbf{p}}_{n'} \cdot \hat{\mathbf{n}}_{\perp,v}. \quad (\text{B-22})$$

The plane of incidence is defined as the plane containing the $\hat{\mathbf{y}}$ axis and the vector $\hat{\mathbf{r}}_v^+$, and the polarizing vectors are defined mathematically as

$$\hat{\mathbf{n}}_{\perp,v}^{\pm} = -\frac{\hat{\mathbf{y}} \times \hat{\mathbf{r}}_v^{\pm}}{|\hat{\mathbf{y}} \times \hat{\mathbf{r}}_v^{\pm}|} = \frac{-r_{z_v} \hat{\mathbf{x}} + r_{x_v} \hat{\mathbf{z}}}{\sqrt{r_{x_v}^2 + r_{z_v}^2}} \quad (\text{B-23})$$

$$\text{and} \quad \hat{\mathbf{n}}_{\parallel,v}^{\pm} = \frac{\hat{\mathbf{n}}_{\perp,v}^{\pm} \times \hat{\mathbf{r}}_v^{\pm}}{|\hat{\mathbf{n}}_{\perp,v}^{\pm} \times \hat{\mathbf{r}}_v^{\pm}|} \quad (\text{B-24})$$

$$\text{where} \quad \hat{\mathbf{r}}_v^{\pm} = r_{x_v} \hat{\mathbf{x}} \pm r_{y_v} \hat{\mathbf{y}} + r_{z_v} \hat{\mathbf{z}}. \quad (\text{B-25})$$

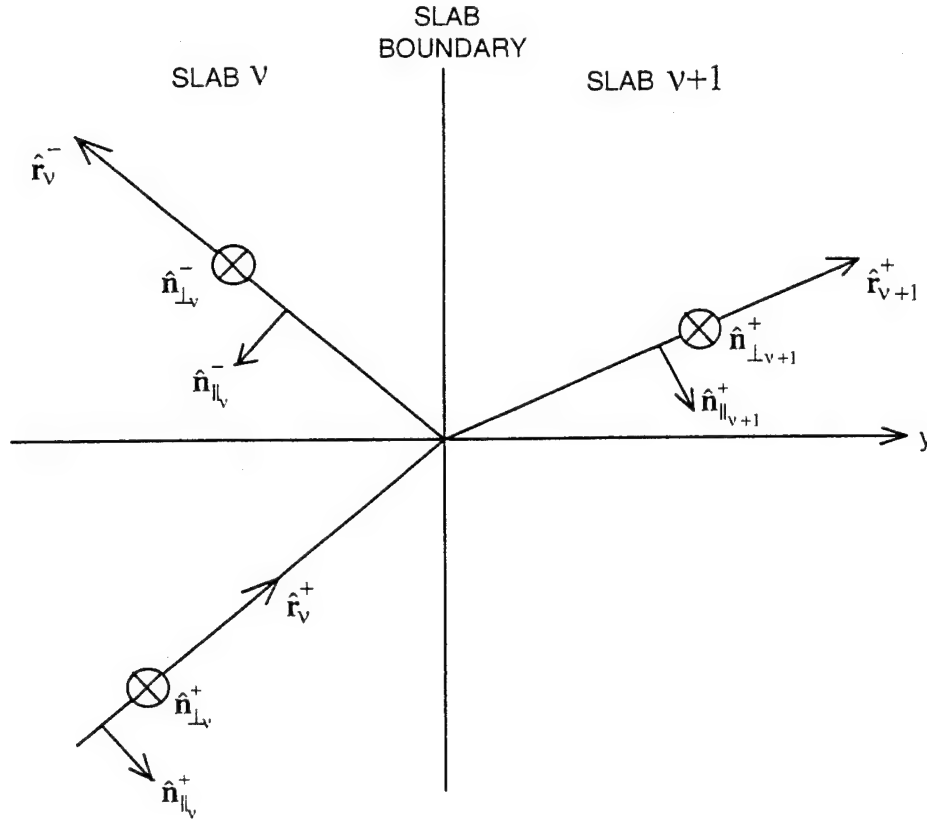


Figure B.2 Graphical Definitions of the Polarizing Vectors \hat{n}_{\parallel} and \hat{n}_{\perp} .

As the incident wave propagates through the dielectric boundary, its propagation direction refracts. By matching the phases of the fields at the boundary (using Snell's Law), the direction of propagation in medium $v+1$ can be related to the direction of propagation in medium v as follows:

$$r_{x_{v+1}} = r_{x_v} \frac{\beta_v}{\beta_{v+1}}, \quad (\text{B-26})$$

$$r_{z_{v+1}} = r_{z_v} \frac{\beta_v}{\beta_{v+1}}, \quad (\text{B-27})$$

and since r is a unit vector

$$r_{y_{v+1}} = \sqrt{1 - r_{x_{v+1}}^2 - r_{z_{v+1}}^2}. \quad (\text{B-28})$$

Bibliography

1. B. A. Munk, T. W. Kornbau, and R. D. Fulton, *Scan Independent Phase Arrays*, Radio Science, Vol. 14, No. 6, pp. 979-990, Nov-Dec 1979.
2. Lee Webb Henderson. *The Scattering of Planar Arrays of Arbitrarily Shaped Slot and/or Wire Elements in a Stratified Dielectric Medium*, PhD thesis, The Ohio State University, 1983.
3. P. M. Morse and H. Feshbach, *Methods of Theoretical Physics*, McGraw-Hill Book Company, 1953.
4. B. A. Munk and G. A. Burrell and T. W. Kornbau. *A General Theory of Periodic Surfaces in Stratified Dielectric Media*. Technical Report #784346-1, ElectroScience Laboratory, The Ohio State University, November 1977. Generated under contract F33615-76-C-1024, for Avionics Laboratory, Air Force Wright Aeronautical Laboratories, Wright-Patterson AFB, Ohio.
5. R. F. Harrington. *Field Computations by Moment Methods*, Krieger Publishing Co., 1968.
6. J. Paul Skinner. *Scattering From a Finite Collection of Transverse Dipole and Axial Slot Arrays With Edge Effects*. PhD thesis, The Ohio State University, 1991.
7. Travis E. Pepler. *Experimental Verification of Frequency Selective Surface Truncation Scattering and Treatment*. Master's Thesis, The Air Force Institute of Technology, December 1992.
8. B. A. Munk and G. A. Burrell. "Plane-Wave Expansion for Arrays of Arbitrarily Oriented Piecewise Linear Elements and Its Application in Determining the Impedance of a Single Linear Antenna in a Lossy Half-Space", *IEEE Transactions on Antennas and Propagation*, AP-27(3:331-343), May 1979.

9. Constantine A. Balanis. *Advanced Engineering Electromagnetics*, John Wiley & Sons, 1989.
10. S. A. Schelkunoff and H. T. Friis. *Antenna Theory and Practice*. John Wiley and Sons, 1952.
11. Constantine A. Balanis. *Antenna Theory, Analysis, and Design*, John Wiley and Sons, 1982.
12. T. Cwik, R. Mittra, K. C. Lang, and T. K. Wu, "Frequency Selective Screens", *feature article for the IEEE Antennas and Propagation Society Newsletter*, 29(2), April 1987.
13. J. A. Hughes. *Impedance Properties of Cylindrical Arrays and Finite Planar Arrays*. Master's thesis, The Ohio State University, 1988.
14. R. Kastner and R. Mittra. "A Combination of the Spectral-Iterative Technique and the Conjugate gradient Method for Analyzing Finite-Sized Frequency Selective Surfaces with Rectangular Patches," *IEEE Antennas and Propagation Soc. Int. Symp. Dig., Boston, Massachusetts*, pages 925-928, June 1984.
15. B. A. Munk. *A General Theory of Periodic Surfaces in a Stratified Dielectric Medium*. Technical Report #715582-4, ElectroScience Laboratory, The Ohio State University, February 1986. Generated under contract F33615--83--C-1013, for Avionics Laboratory, Air Force Wright Aeronautical Laboratories, Wright-Patterson AFB, Ohio.
16. Robert W. Scharstein. "Mutual Coupling in a Slotted Phased Array, Infinite in E-Plane and Finite in H-Plane," *IEEE Transactions on Antennas and Propagation*, 38(8):1186-1191, August 1990.
17. K. A. Shubert. *Immittance Properties of Large Finite Dielectric Covered Phased Arrays*. PhD thesis, The Ohio State University, 1980.

18. Surendra Singh and Ritu Singh. "On the Use of Rho-Algorithm in Series Acceleration," *IEEE Transactions on Antennas and Propagation*, 39(10), October 1991.
19. K. A. Strickler. *Impedance Properties of Singly Infinite Periodic Surfaces Composed of AzHxially Oriented Dipoles*, Master's Thesis, The Ohio State University, 1989.
20. Johnson Wang. *Generalized Moment Methods in Electromagnetics: Formulation and Computer Solution of Integral Equations*. John Wiley & Sons, Inc., 1991.
21. D. A. McNamara, C. W. I Pistorius, and J. A. G. Malherbe. *Introduction to the Uniform Geometrical Theory of Diffraction*, Artech House, 1990.
22. L. W. Henderson, *Introduction to PMM, Version 4.0*, Technical Report #725347-1, ElectroScience Laboratory, The Ohio State University, July 1993. Generated under contract SC--SP18--91--0001.

VITA

August 5, 1961 Born in New Orleans, Louisiana

November 1984 B.S.E.E., Summa Cum Laude
Ohio University,
Athens, Ohio

26 November 1984 Commissioned as a 2nd Lieutenant
in the U.S. Air Force

August 1988 M.S.E.E.
Ohio University,
Athens, Ohio

June 1986 - June 1991 Research and Development Engineer
New Technologies Division
HQ Electronic Security Command
Kelly Air Force Base, San Antonio, TX

13 December 1988 Promotion to Captain, U.S. Air Force

8 July 1991 Entered Electrical Engr. Ph.D. Program
Air Force Institute of Technology
Wright-Patterson Air Force Base, Ohio

8 June 1993 Admission to Candidacy, Ph.D. Degree
Air Force Institute of Technology
Wright-Patterson Air Force Base, Ohio

REPORT DOCUMENTATION PAGE

Form Approved
OMB No. 0704-0188

Public reporting burden for this collection of information is estimated to average 1 hour per response, including the time for reviewing instructions, searching existing data sources, gathering and maintaining the data needed, and completing and reviewing the collection of information. Send comments regarding this burden estimate or any other aspect of this collection of information, including suggestions for reducing this burden, to Washington Headquarters Services, Directorate for Information Operations and Reports, 1215 Jefferson Davis Highway, Suite 1204, Arlington, VA 22202-4302, and to the Office of Management and Budget, Paperwork Reduction Project (0704-0188), Washington, DC 20503.

1. AGENCY USE ONLY (Leave blank)		2. REPORT DATE JUN 95	3. REPORT TYPE AND DATES COVERED FINAL	
4. TITLE AND SUBTITLE Scattering from Finite by Infinite Periodic Arrays with Arbitrary Piecewise-Linear Slot Elements			5. FUNDING NUMBERS	
6. AUTHOR(S) Paul R. Barre'				
7. PERFORMING ORGANIZATION NAME(S) AND ADDRESS(ES) AFIT/ENG WPAFB OH 45433			8. PERFORMING ORGANIZATION REPORT NUMBER	
9. SPONSORING/MONITORING AGENCY NAME(S) AND ADDRESS(ES)			10. SPONSORING/MONITORING AGENCY REPORT NUMBER	
11. SUPPLEMENTARY NOTES				
12a. DISTRIBUTION / AVAILABILITY STATEMENT Distribution Unlimited			12b. DISTRIBUTION CODE	
13. ABSTRACT (Maximum 200 words) A numerical model for analyzing electromagnetic scattering from a planar Frequency Selective Surface (FSS) is developed. The model can represent an FSS with multiple arrays of arbitrary piecewise-linear scatterers in a stratified dielectric medium. The FSS's arrays are finite by infinite, accounting for edge effects, where a periodic array element is formed from the piecewise-linear connection of thin slots in a groundplane. The stratified dielectric medium is defined as an arbitrary stack of lossless dielectric slabs that sandwich the user defined arrays, simulating an FSS. The Surface Equivalence theorem is used to construct an equivalent problem based on groundplanes and magnetic current sources. Integral equations based on the equivalent magnetic scattering currents are solved via the moment method. These unknown currents are expanded such that independent modes are defined for each infinite column of an array, where the current fluctuations along each column are defined in terms of a reference element and Floquet's theorem. Individual column contributions are determined using the Array Scanning Method, preserving the plane wave form of the solution. The model has been implemented in a user-friendly computer program, and admittance calculations and scattering predictions have been validated against measured data and appropriately similar FSS codes.				
14. SUBJECT TERMS Frequency Selective Surfaces, Array Scanning Method, Moment Method			15. NUMBER OF PAGES 181	
			16. PRICE CODE	
17. SECURITY CLASSIFICATION OF REPORT UNCLASSIFIED	18. SECURITY CLASSIFICATION OF THIS PAGE UNCLASSIFIED	19. SECURITY CLASSIFICATION OF ABSTRACT UNCLASSIFIED	20. LIMITATION OF ABSTRACT UL	